QC
1
U56
v.54
no.6

Journal of Research

of the

National Bureau of Standards

JUNE 1955

VOLUME 54 NUMBER 6

UNIVERSITY OF MICHIGAN
GENERAL LIBRARY

UNIVERSITY OF MICHIGAN LIBRARIES

UNITED STATES OF AMERICA

U. S. DEPARTMENT OF COMMERCE
Sinclair Weeks, Secretary
NATIONAL BUREAU OF STANDARDS
A. V. Astin, Director

JUNE • 1953
VOLUME • 50
NUMBER • 6

JOURNAL OF RESEARCH
of the
NATIONAL BUREAU OF STANDARDS

PERIODICALS OF THE NATIONAL BUREAU OF STANDARDS
(Published monthly)

The National Bureau of Standards is engaged in fundamental and applied research in physics, chemistry, mathematics, and engineering. Projects are conducted in fifteen fields: electricity and electronics, optics and metrology, heat and power, atomic and radiation physics, chemistry, mechanics, organic and fibrous materials, metallurgy, mineral products, building technology, applied mathematics, data processing systems, cryogenic engineering, radio propagation, and radio standards. The Bureau has custody of the national standards of measurement and conducts research leading to the improvement of scientific and engineering standards and of techniques and methods of measurement. Testing methods and instruments are developed; physical constants and properties of materials are determined; and technical processes are investigated.

JOURNAL OF RESEARCH

The Journal presents research papers by authorities in the specialized fields of physics, mathematics, chemistry, and engineering. Complete details of the work are presented, including laboratory data, experimental procedures, and theoretical and mathematical analyses. Annual subscription: domestic, $4.00; foreign, $5.25.

TECHNICAL NEWS BULLETIN

Summaries of current research at the National Bureau of Standards are published each month in the Technical News Bulletin. The articles are brief, with emphasis on the results of research, chosen on the basis of their scientific or technologic importance. Lists of all Bureau publications during the preceding month are given, including Research Papers, Handbooks, Applied Mathematics Series, Building Materials and Structures Reports, Miscellaneous Publications, and Circulars. Each issue contains 12 or more two-column pages; illustrated. Annual subscription: domestic, $1.00; foreign, $1.35.

BASIC RADIO PROPAGATION PREDICTIONS

The Predictions provide the information necessary for calculating the best frequencies for communication between any two points in the world at any time during the given month. The data are important to all users of long-range radio communications and navigation, including broadcasting, airline, steamship, and wireless services, as well as to investigators of radio propagation and ionosphere. Each issue, covering a period of one month, is released three months in advance and contains 16 large pages, including pertinent charts, drawings, and tables. Annual subscription: domestic, $1.00; foreign, $1.25.

Order all publications from the Superintendent of Documents
U. S. Government Printing Office, Washington 25, D. C.

The printing of this publication has been approved by the Director of the Bureau of the Budget, May 12, 1953.

UNITED STATES OF AMERICA

Journal of Research of the National Bureau of Standards Vol. 54, No. 6, June 1955 Research Paper 2593

Titrations of Bases with Diphenyl Phosphate in Some Aqueous and Nonaqueous Solvents[1]

Marion Maclean Davis and Hannah B. Hetzer

Successful titrations of various bases with diphenyl phosphate in benzene, methanol, water, and mixtures of these solvents have been performed, in some cases potentiometrically (using the glass, saturated calomel electrode-system) and in other cases using indicator dyes. Several of the dyes (bromophthalein magenta E, 5-phenyl-9-diethyl Nile blue, and the anhydro-base of tamarack green and Victoria blue B) have not been used elsewhere as acid-base indicators. Diphenyl phosphate is shown to be a strong acid which is easily obtained and maintained as anhydrous crystals. It is not strong enough, however, to serve as a replacement for perchloric acid in titrations in acetic acid. Attention is called to the differing behavior of benzoic acid and diphenyl phosphate when the solvent is changed from water to methanol. Using a "nonleveling" solvent in place of water makes it possible to obtain separate, sharp end-points in titrating a mixture of two such acids. Other pertinent information about diphenyl phosphate is summarized.

1. Introduction

As previously explained [1][2], we are engaged in developing methods for measuring acidity and basicity in organic solvents, with special emphasis on so-called "inert" solvents. Two essential parts of this research are (1) locating or preparing new chemical tools—indicator dyes and materials suitable for use as standard acids or bases in such solvents; and (2) finding out, by systematic studies, the behavior of different types of acids and bases in various nonaqueous solvents. This paper deals with a study of some of the properties of diphenyl phosphate, $(C_6H_5O)_2P(O)OH$, with particular attention to its use in titrations with bases in several aqueous and nonaqueous solvents.

Interest in diphenyl phosphate first arose upon noticing in a catalog of chemicals available for experimental purposes [2] that, besides giving a strongly acid solution in water, it is easily soluble in a variety of organic solvents, including benzene and carbon tetrachloride. The interest increased after finding that the acid can be obtained and maintained as pure, anhydrous crystals without difficulty. Very few studies have been made of the comparative effects of aqueous and nonaqueous solvents on the behavior of strong acids, and diphenyl phosphate appeared suitable for such studies, as well as a potentially useful standard acid for nonaqueous titrations. Hitherto, picric acid and a few arylsulfonic acids have been the only commonly available strong, crystalline acids soluble in both water and a variety of organic solvents, and these acids possess certain shortcomings. For instance, picric acid is somewhat hazardous to handle unless 10 percent or so of water has been added, and the yellow color of its salts is sometimes objectionable. A further incentive to studying diphenyl phosphate is the meagerness of the existing knowledge of the acidic behavior of this compound and of various related diaryl phosphates, even though they were first synthesized about 100 years ago and scattered articles have appeared dealing with such topics as their preparation, physical properties, and possible uses.

2. Apparatus and Miscellaneous Materials

2.1. Apparatus

A titration apparatus similar to the one described in [3], employing a glass and a sleeve-type saturated calomel electrode, was used in the potentiometric titrations. During titrations the temperature was usually within the range 25° ± 2° C. In most cases 10-ml burets having 0.05-ml graduations were used.

Melting points were determined by the capillary-tube method, using an automatically-stirred, electrically-heated, high-boiling silicone oil and an ASTM thermometer maintained at 3-inch immersion.

2.2. Solvents

The organic solvents were all of a grade that was claimed to meet ACS specifications. Acetic acid and methanol were said to contain approximately 0.5 percent of water. Distilled water was boiled shortly before use, to remove carbon dioxide.

2.3. Bases

1,3-Diphenylguanidine was recrystallized twice from toluene and once from benzene-cyclohexane; the melting point was 149.0° to 149.8° C. Titration with perchloric acid in glacial acetic acid indicated a purity of at least 99.5 percent. *Di-o-tolylguanidine* was recrystallized twice from 95-percent ethanol; melting point, 175.8° to 176.3° C. Titration in aqueous alcohol with 0.1 *N* hydrochloric acid indicated its purity to be 99.9 percent; titration in glacial acetic acid gave the value 99.6 percent. A commercial high grade of *guanidine acetate* was used without further treatment. Commercial high grad

[1] This research was supported in part by the United States Air Force, through the Office of Scientific Research of the Air Research and Development Command.
[2] Figures in brackets indicate the literature references at the end of this paper

UNIVERSITY OF MICHIGAN LIBRARIES

tribenzylamine was recrystallized from ethanol; melting point, 92.8° to 93.2° C. A good grade of *triethylamine* was distilled from sodium hydroxide immediately before use; the middle fraction was used. *Tris(hydroxymethyl)aminomethane* was part of a purified sample that had been used in the determination of the aqueous dissociation constant [4].

Potassium acid phthalate was NBS Standard Sample for acidimetry. *Sodium acetate* in glacial acetic acid was prepared by dissolving anhydrous sodium carbonate of analytical grade. The solutions containing *sodium methylate* were prepared from the solid compound.

2.4. Indicator Dyes

Both acidic and basic dyes were used in the titrations. *Bromophthalein magenta E* (fig. 1, formula I, $X=COOC_2H_5$) was prepared at the Bureau; its application in some nonaqueous acid-base titrations was described previously [1].[3] The other acidic indicator dyes—*phenolphthalein*, *p-naphtholbenzein* (α-naphtholbenzein), and the various *sulfonephthaleins* were all commercial materials; the sulfonephthaleins were used as their sodium salts.

Most basic indicator dyes are supplied commercially as a salt (generally, the chloride). Azo dyes, however, are often available only as the free base, though sometimes also available as a salt. For reasons of solubility, the salt is more convenient for aqueous titrations, and the free base is necessary for titrations in benzene and similar solvents. Either form of the dye dissolves readily in alcohols. In the work described here all basic dyes were used as the free bases with the exception of *α-Naphthyl red* (4-phenylazo-1-naphthylamine hydrochloride) and the three Nile blues.

p-Ethoxychrysoidin, 4-(*p*-ethoxyphenylazo)-*m*-phenylenediamine, was isolated by adding an excess of 10-percent sodium hydroxide to a hot solution of the commercial hydrochloride in 95-percent ethanol, then pouring the ethanolic solution into water; the base, consisting of fluffy yellow needles, was washed with water and dried at room temperature, first in the air and then in a vacuum desiccator containing anhydrous alumina.

For part of the work the indicator dyes commercially available were not suitable, and three new basic indicators were used. These call for some additional comment.

a. Tamarack Green Anhydro-Base

Tamarack green anhydro-base (fig. 1, formula II, X=Cl) has not been described previously, although the parent compound (X=H) has been known for many years. Both compounds belong to a class of derivatives of triphenylmethane, known as "Homolka bases" or "anhydro-bases", the first one of which was prepared by Homolka; later this class of compounds was studied by other workers, notably by Baeyer and Villiger [5,6].[4] The parent compound was first prepared by Meldola, who prepared its hydrochloride by the reaction of diphenylamine with benzotrichloride in the presence of anhydrous, powdered zinc chloride and named it "diphenylamine green" [7]. An impure specimen of the hydrochloride which he had prepared earlier by the oxidizing action of air on a mixture of diphenylamine and benzyl chloride had been introduced into commerce under the name "viridine." Meldola did not isolate the pure anhydro-base, although he observed the red-brown color, due to its presence, which resulted when a solution of the salt was shaken with benzene and sodium hydroxide solution. In later, more complete studies, Baeyer and Villiger obtained the anhydro-base in an analytically pure condition; they applied the name "viridine" to the *pure* dye [5].[5]

Tamarack green hydrochloride was prepared with the substitution of *o*-chlorobenzotrichloride for benzotrichloride, but otherwise essentially as described by Meldola [7].[6] The hydrochloride was converted to the picrate which, in turn, was converted to the anhydro-base, as outlined in [5], except for the use of benzene in place of ether. The properties of tamarack green (both hydrochloride and free base) resemble closely those described for the parent compounds [5, 7, 8].

[3] This indicator is now obtainable from Distillation Products Industries, listed as Eastman Organic Chemical No. 6810 (tetrabromophenolphthalein ethyl ester).

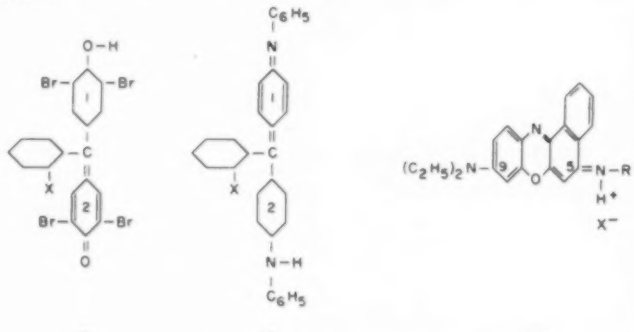

I II III

FIGURE 1. *Formulas of indicators.*

I. Bromophthalein magenta E (tetrabromophenolphthalein ethyl ester); $X=COOC_2H_5$.
II. Tamarack green anhydro-base (anhydro-N,N'-diphenyl-*p,p'*-diamino-*o''*-chlorotriphenylcarbinol); X=Cl.
III. 5-Phenyl-9-diethyl Nile blue (5-phenylimino-9-diethylaminobenzo[a]-phenoxazonium chloride); X=Cl.

[4] These seldom-mentioned compounds give yellow to red solutions in solvents like benzene. The nitrogen atom attached to ring 1 (see formula II) is rather strongly basic, and on the addition of a proton forms a resonant cation that is deeply colored (red to green, depending on the substituents on the nitrogens and in the rings). (This is a simplified discussion; it is probably not correct to assume that in solvents like benzene the proton is completely detached from the anion of the acid molecule of which it was originally a part.) Anhydro-bases tend to add water to form the well-known colorless compounds called "carbinol bases" or "color bases." Alcohols, ammonia, and primary or secondary amines give similar colorless compounds, H adding to the nitrogen of ring 1, and the rest of the molecule (—OH, —OR, or $—NR_2$) becoming linked to the methane carbon atom. A similar tendency is responsible for the fading by alkali of fabrics dyed with triphenylmethane dyes, but it has been reduced by introducing a bulky substituent (for instance, Cl, NO_2, or SO_3H) in an *o''*-position [6]. The *o''*-Cl in tamarack green was introduced with such an objective in mind.

[5] Hill, Branch, and Patapoff have also prepared and studied the anhydro-base and called it "viridine" [8].

[6] The dye was prepared almost 10 years ago by M. M. Davis and P. J. Schubmann, for exploratory studies. The base was not analyzed and may have contained a little carbinol. Since preparation, its behavior as an indicator has not visibly changed.

b. Victoria Blue Anhydro-Base

Comparison of the formula of Victoria blue B anhydro-base, $C_6H_5N=C_{10}H_6=C[C_3H_4N(CH_3)_2]_2$, with that of tamarack green anhydro-base reveals several differences in their structures, but it can be seen that they should function similarly when used as acid-base indicators. Victoria blue B anhydro-base was first prepared by Nathansohn and Müller [9], who erroneously believed it to be the carbinol. Noelting and Saas, after later studies [10], reported that the anhydro-base cannot be converted into the carbinol or to a carbinol ether or corresponding amino derivative.[7]

To prepare the anhydro-base, 4 g of the commercial salt (Color Index No. 729) was dissolved in about 800 ml of hot water, the solution was filtered to remove insoluble material, and the filtrate was stirred mechanically while 2 to 3 ml of 6 *N* sodium hydroxide was added. The dark brown precipitate was filtered and washed with the aid of suction, air-dried, and then recrystallized from benzene.

c. 5-Phenyl-9-diethyl Nile Blue (5-Phenylimino-9-diethylaminobenzo[a]phenoxazonium Chloride, $C_{28}H_{24}ClN_3O\cdot H_2O$)

The general structure of the three Nile blues used in the work is shown as formula III in figure 1. The only important difference among them is in the group R, which is *hydrogen* in Nile blue A (CI No. 913), *benzyl* in Nile blue 2B (CI No. 914), and *phenyl* in 5-phenyl-9-diethyl Nile blue. All of the salts give blue solutions which turn red (pink, if dilute) when the free base is liberated. As would be expected, the free base is strongest when R equals H and weakest when R equals phenyl.[8]

Phenyl diethyl Nile blue was a very pure material prepared in the research laboratories of American Cyanamid Company [12].[9]

3. Diphenyl Phosphate

3.1. General Discussion

Diphenyl phosphate has been studied intermittently since 1866. It was first detected by Hlasiwetz and Grabowski in a mixture formed by the reaction of phenol with phosphorus pentoxide [13], and was first isolated, as a brown oil, by Glutz, after treatment of phenol with phosphorus pentachloride [14]. Next, Jacobsen studied the stepwise reaction of phenol with phosphorus oxychloride, followed by hydrolysis of the intermediate products, and thus obtained crystalline monophenyl and triphenyl phosphates; diphenyl phosphate was obtained only as a colorless, viscous oil that would not solidify in a freezing mixture [15].

Rapp, repeating Jacobsen's procedure, succeeded in obtaining crystalline diphenyl phosphate by seeding an aqueous solution with a little sodium diphenyl phosphate, and reported the melting point of the acid as 56° C [16]. Autenrieth used a slight modification of the Jacobsen procedure and reported that diphenyl phosphate is easily obtained in the crystalline state if not contaminated with phenol; his final product, obtained from an aqueous solution as shimmering leaflets, had the melting point 61° to 63°—a value several degrees higher than that of Rapp [17]. The mystery of the divergent melting points was cleared up by Hoeflake's observation that diphenyl phosphate has two crystalline forms, one being anhydrous and the other, a dihydrate [18]. The products of Rapp and Autenrieth were presumably different mixtures of the two forms. Hoeflake's anhydrous diphenyl phosphate was obtained by heating the crude acid (prepared by Jacobsen's method) in vacuo to 60° to 80° to remove water of hydration, followed by solution of the acid in cold chloroform, then reprecipitation with ligroin. She described the anhydrous acid as fine needles melting at 70°. The dihydrate was obtained as small leaflets, melting at 51°, by recrystallizing the anhydrous acid from water. Hoeflake furthermore stated that anhydrous diphenyl phosphate takes up two molecules of water in the air, but loses this water again at 30°, also over sulfuric acid. Bernton [19] concurred in Hoeflake's description of the two crystalline modifications of diphenyl phosphate, but reported that the hydrate is very stable in the air.

Various practical applications have been suggested for diphenyl phosphate. Bernton found that it combines in 1:1 ratio with different types of bases (ammonia, methylamine, diethylamine, aniline, amino acids), forming well-crystallized salts [19]. Diphenyl phosphate, together with other diaryl and monoaryl phosphates, has been tested as a possible reagent for the determination of iron; aryl phosphates of various metals were prepared [20]. Potassium diphenyl phosphate, like the potassium salts of some related acids, increases the solubilities of various organic compounds in water [21]. Diphenyl phosphate has been used as a substrate in studies of enzyme action, and potassium salts of closely related acids have been reported to destroy certain kinds of bacteria. In industrial applications, diphenyl phosphate has been reported to retard the corrosion of steel sheets, improve lubricating oil for steel-light metal bearings, and excel dibutyl phthalate in reducing the permeability of ethylcellulose to water.

There is no evidence in the literature, or from our experience in using diphenyl phosphate, that it is toxic. However, considering that certain commercial esters of phosphoric acid and pyrophosphoric acid, as well as some related compounds, are known to interfere with normal physiological reactions, it seems prudent to avoid contact of diphenyl phosphate with the skin and inhalation of fine particles.

[7] Evidently a naphthyl group, like an *o*''-substituted phenyl group, impedes the addition of a fourth group to the methane carbon atom of triphenylmethane dyes.

[8] See figure 5 and related discussion. The *p*H range of the commercial Nile blue A used is given as about 10.2 (blue) to 13.1 (purple), and that of the commercial Nile blue 2B, as about 7.2 to 8.6. (However, Kolthoff reported the *p*H range of Nile blue A to be 9.0 (blue) to 10.4 (red) [11].)

[9] Phenyl diethyl Nile blue is one of a series of benzophenoxazine dyes prepared for possible chemotherapeutic applications and was made available, through the courtesy of J. J. Denton, for investigations of its utility as an acid-base indicator in nonaqueous media. As Dr. Denton has pointed out in correspondence, the compounds known commercially as Nile blue dyes are dye mixtures, whereas the specimen of 5-phenyl-9-diethyl Nile blue supplied was analytically pure, and is therefore properly referred to by its strict chemical name. However, a shorter name is needed for common usage, and the name used in this paper was agreed on. For ordinary titrations a less pure material should, of course, be satisfactory.

UNIVERSITY OF MICHIGAN LIBRARIES

3.2. Purification

a. Anhydrous Diphenyl Phosphate

"Anhydrous" diphenyl phosphate was supplied by the Dow Chemical Company, through the kindness of C. W. Robertson. The material as received contained a little water of hydration, was slightly tinged with pink, and had a faint odor of phenol. Diphenyl phosphate is fairly soluble in hot cyclohexane; the amount of cyclohexane needed can be reduced a good deal by adding 10 percent or so of benzene. Any water present in the sample is removed if the cyclohexane or cyclohexane-benzene solution is boiled for a while. The pink material goes into solution and tends to remain with the diphenyl phosphate, but it can be removed by repeated digestions with decolorizing carbon. A good way to remove most of the pink contaminant is to add less than the amount of hot solvent needed for complete solution of the acid; the bulk of the solution is then nearly colorless, the undissolved acid forming a pink oil which adheres to the bottom of the vessel when the colorless portion is decanted off. When the cooled solution is seeded, the acid quickly crystallizes in colorless needles; without seeding, it usually separates first as an oil. The purified acid has no odor. The purest product obtained in our work melted to a colorless liquid at 68.5° to 69.0° C, with slight softening from about 68.0°; the untreated acid melted about a degree lower, yielding a pale pink liquid. Titrations in water (see section 4.1) indicated that the best anhydrous acid was about 99.9 percent pure (see also section 4.5).

The crystals of anhydrous diphenyl phosphate showed no tendency to pick up water at room temperature (which was usually in the range 20° to 25° C). In one experiment a gram was exposed to the laboratory atmosphere for 36 days, during which the relative humidity probably averaged about 30 percent; the sample was reweighed at various intervals, 7 times in all, and no change in the weight could be detected. In a second experiment a 0.4-g sample showed no gain in weight during a total exposure of 7 days to about 60-percent relative humidity at 25° C, or during a subsequent 8 days' exposure to about 80-percent relative humidity.[10] These experiments do not support Hoeflake's assertion [18] that anhydrous diphenyl phosphate takes up two molecules of water in the air. It was not possible to repeat the experiments by which Hoeflake reached her conclusion, as they were not described. Our experiments indicate that no difficulty should be experienced in maintaining diphenyl phosphate as anhydrous crystals under usual laboratory conditions.

However, when in the *fused* condition anhydrous diphenyl phosphate was found to gain weight *temporarily* in a moist atmosphere. About a gram of the acid was placed in a porcelain boat in an Abderhalden drying apparatus which was open to the air, and the sample was heated to fusion by allowing ethyl acetate to reflux in the apparatus. Over a period of 9 days the sample was repeatedly heated, cooled, and reweighed. During this time the weight fluctuated; the greatest gain, which occurred during rainy weather, was 2.2 percent. Water was then placed in the absorption bulb of the Abderhalden, the bulb was attached to the apparatus with partial evacuation, and the sample was remelted. In 3 days it gained more than 10 percent in weight; for complete conversion to the dihydrate a 14.4-percent gain in weight would have been necessary. An accurate measurement of the total gain was impossible as the sample rapidly lost weight while on the balance; the loss became less rapid after the weight had dropped to about a 5-percent increase over the original weight. During 3-days' storage in the Abderhalden apparatus over phosphorus pentoxide at room temperature the sample became crystalline once more and regained its initial weight.

b. Diphenyl Phosphate Dihydrate

Some anhydrous diphenyl phosphate was dissolved in hot water and, after cooling in a refrigerator, the solution was seeded. Leaflets immediately started to form. After filtration these were partly dried between filter papers, then kept in a desiccator at 60-percent relative humidity (see footnote 10). After 12 days at 25° C, during which the weight of the crystals decreased about 1.6 percent, the molecular weight found by titration corresponded closely to the theoretical molecular weight of the dihydrate (286.2). The same result, within the limits of error, was obtained after further exposure of the material to 60-percent relative humidity for 25 days. On the assumption of an inert impurity (most likely, occluded water) the titrations indicated the dihydrate to be approximately 99.8 percent pure. A sample quickly liquefied when the tube containing it was placed in the melting-point bath at 49° to 50° C; bubbles formed, but they soon disappeared, leaving a clear, colorless liquid. However, the dihydrate did not melt sharply when heated gradually from a lower temperature. For example, a sample placed in the bath at 40° showed noticeable softening at about 41.5° and gradually liquefied, mostly at about 49° to 50°.

As mentioned in section 2.2.a, a sample of fused, anhydrous diphenyl phosphate that had gained weight in a moist atmosphere returned to its original weight within 3 days when stored over phosphorus pentoxide. Slightly moist crystals of the dihydrate (about 2 g) likewise lost weight when stored in a desiccator over anhydrous calcium sulfate. Within 100 days, while kept at a temperature that was automatically maintained close to 25° C, the sample lost 13.2 percent in weight; if the sample had been completely air-dry the loss during conversion to the anhydrous acid should have been 12.6 percent. The molecular weight (by titration) of the dried acid was the same as that of anhydrous diphenyl phosphate, within the limits of error.

[10] Approximately 60-percent relative humidity was achieved by keeping the sample in a desiccator containing saturated aqueous sodium bromide in contact with sodium bromide dihydrate. For 80-percent relative humidity, saturated aqueous ammonium chloride in contact with the solid salt was used.

Further study of the interconversion of anhydrous and dihydrated diphenyl phosphate would be of interest. However, the evidence seems sufficient to justify the conclusion that the anhydrous form of the acid can be maintained at constant composition more conveniently and reliably than the dihydrated form.

3.3. Solubilities in Various Solvents

In studies being made at the Bureau it is useful to know the approximate solubilities of anhydrous diphenyl phosphate in benzene, cyclohexane, and water. The results of some measurements are summarized in table 1. Other available information

TABLE 1. *Approximate solubilities of diphenyl phosphate in various solvents at 25° C*

Solvent	g of solute per 100 g of solvent
Acetone	100 [a]
Benzene	170 [b, c]
Carbon tetrachloride	4 [a]
Cyclohexane	1.5 [b, d, e]
Ether	100 [a]
Water	3 [a, b, d]

[a] This value, given in [2], was evidently obtained using *hydrated* diphenyl phosphate.
[b] Determined in this laboratory by a titration procedure, using *anhydrous* diphenyl phosphate.
[c] The value given in [2] is 10; see footnote a.
[d] The same value was obtained by weighing the residue left after evaporation of solvent.
[e] Infrared measurements by James Stewart of the Bureau indicated a benzene content less than 0.01 percent.

on solubilities is included in the table. Early investigators reported that diphenyl phosphate is easily soluble in alcohol, benzene, chloroform, and ether [14 to 17].

The solubility of diphenyl phosphate in benzene is difficult to measure because supersaturation tends to occur and a slight change in the temperature has a marked effect. However, good agreement was obtained in duplicate experiments. Partial hydration of the sample used may account for the much lower solubility reported in [2].

The earliest investigators [14 to 16] stated that diphenyl phosphate is practically insoluble in water, but later [17] 1 part of the acid was reported to be soluble in 35 parts of water. This value is close to the one measured at the Bureau and also reported in [2]. Crystals of anhydrous diphenyl phosphate liquefy as soon as they are brought in contact with a little water. On shaking, the liquid separates into minute, scarcely visible drops. As a result of this behavior, in some early aqueous titrations of diphenyl phosphate incomplete solution of the samples occurred without detection, even when the quantity used was much below the amount required for a saturated solution. It proved advantageous to dissolve the crystals in a little ethanol, then dilute to the desired volume with water.

3.4. Acidic Strength

Some years ago Morton [22] concluded from comparative potentiometric titrations of orthophosphoric acid and monophenyl phosphate in water at 18° C. that replacing one of the hydrogen atoms of orthophosphoric acid by a phenyl group increases the acidity. Subsequently, Kumler and Eiler [23] measured the relative acidic strengths of four monoalkyl esters (methyl, ethyl, *n*-propyl, and *n*-butyl) and the corresponding dialkyl esters of orthophosphoric acid in water at 25° C. Their data showed that the monoalkyl esters are stronger acids than phosphoric acid, and that the dialkyl esters are stronger still. Morton's data indicate that monophenyl phosphate is stronger than the monoalkyl phosphates investigated by Kumler and Eiler, although the experimental conditions used in the two sets of investigations were too different to permit a numerical comparison.

It was therefore to be expected that diphenyl phosphate would show strongly acidic behavior in water, and this proved to be the case. In fact, the curves obtained from potentiometric titrations with 0.1 *N* alkali in water were practically identical with curves obtained for hydrochloric acid of equivalent strength. Moreover, the measured *p*H values of several aqueous solutions [11] of diphenyl phosphate having concentrations in the range from about 0.005 *M* to 0.1 *M* were in very good agreement with the *p*H values calculated on the assumption of complete ionization.

As will be shown in section 4, diphenyl phosphate also behaves as a strong acid in benzene, and appears to be stronger in methanol than in water. However, in acetic acid it behaves like a rather weak acid.

3.5. Stability in Aqueous and Alcoholic Solutions

Experiments to be described in section 4 showed that diphenyl phosphate can be titrated with bases very successfully in benzene, methanol, water, and mixtures of these solvents, and therefore merits attention as a possible acidimetric standard in some or all of these solvents. However, if it underwent rapid chemical change in solution, such as hydrolysis or alcoholysis, its usefulness would be limited.

The literature contains fragmentary and partially conflicting statements about the stability of diphenyl phosphate and closely related esters in aqueous and alcoholic solutions. Glutz [14] stated that only one phenyl group is split off when triphenyl phosphate is treated with strong potash, and Autenrieth [17] reported the same result from heating various triaryl phosphates with an equivalent of alcoholic potash. As further evidence of the stability of diaryl phosphates, Autenrieth claimed that they are not much saponified in dilute aqueous acidic or alkaline solutions, even on long heating.

However, Plimmer and Burch [24] concluded that all three phenyl esters of orthophosphoric acid are completely hydrolyzed on heating with acid or alkali to 85° for periods as long as a week; 5-percent solutions of the esters in 1 *N* hydrochloric acid or sodium hydroxide were used, and at appropriate intervals analyses for phenol and inorganic phosphate were made. The comparative behavior of some alkyl

[11] Each solution contained about 10 percent of ethanol by volume.

UNIVERSITY OF MICHIGAN LIBRARIES

phosphates was also studied. The general conclusions were as follows: (1) All three phenyl esters of orthophosphoric acid can be completely hydrolyzed by dilute alkali, though a trialkyl phosphate is not hydrolyzed beyond the dialkyl ester; (2) all phenyl and alkyl esters can be completely hydrolyzed in dilute acid. Plimmer and Burch also mentioned that at 40° diphenyl phosphate was appreciably hydrolyzed by alkali in 24 hours.

Smith and Stohlman [25] found that 1-percent triphenyl phosphate in half-saturated aqueous sodium hydroxide is completely hydrolyzed to phenol and inorganic phosphate after about 5 hours' refluxing; the three isomeric tricresyl phosphates behaved analogously, except that they seemed to be more resistant to hydrolysis. In absolute ethanol tri-*o*-cresyl phosphate was hydrolyzed to di-*o*-cresyl phosphate at 25° C to an extent that was proportional to the concentration of potassium hydroxide present, but no removal of *o*-cresol from either di-*o*-cresyl phosphate or mono-*o*-cresyl phosphate was detected, even when the concentration of alkali was as high as 2.5 *N* and the experiment lasted 9 days.

The conclusions of Breusch and Keskin [26] are partially in conflict with those of Plimmer and Burch. Their results from refluxing various triaryl phosphates (0.01 *M*) in aqueous sulfuric acid or sodium hydroxide, with periodic analysis of small samples for inorganic phosphate, may be summarized as follows: (1) Triaryl phosphates are easily saponified in hot 1 *N* alkali, but are stable toward sulfuric acid (1 to 5 *N*), even on heating for hours; (2) tribenzyl phosphate is saponified by both acid and alkali. In explanation of the results, the authors suggested that tribenzyl phosphate is a true ester, but triaryl phosphates are rather to be regarded as acid anhydrides.

Enzymatic hydrolysis of diphenyl phosphate and other esters of phosphoric acid has been studied, mostly in Japan; the extent of hydrolysis reportedly varies with the nature of the phosphatase and the substrate and also with the *p*H. An interesting study has been made of the mechanism of hydrolysis of tri*methyl* phosphate in alkaline, acidic, and initially neutral aqueous solutions, with the use of water containing an excess of O^{18} [27]. The data indicate that in alkaline solution hydrolysis proceeds entirely through rupture of the P—O linkage, whereas in acid solution rupture involves mainly, if not exclusively, the O—CH_3 bond.

While recrystallizing diphenyl phosphate from water we observed that protracted boiling of an aqueous solution produces a slight milkiness and an odor of phenol. On the other hand, no change in the acidity of an essentially aqueous (see footnote 11) 0.1 *M* solution was observed during 156 days' storage at 25° C (see table 2). It seems clear that, while high temperatures must be avoided, diphenyl phosphate is sufficiently stable in neutral aqueous or alcoholic solutions to warrant further investigations of its utility as an acidimetric standard at room temperature. More rigorous tests, including intercomparisons with other acidimetric standards, will of course be necessary before it can be recommended for highly accurate measurements.

TABLE 2. *Stability of 0.1 M diphenyl phosphate in water at 25° C* [a]

Time elapsed since preparation	Molarity by titration with 0.1 *N* alkali
Days	
0	0.0987, 0.0989.
12	0.0985, 0.0986, 0.0985.
98	0.0989, 0.0989.
156	0.0988, 0.0988.

[a] The acid was dissolved with the aid of 20 ml of 95-percent ethanol, the final volume being 200 ml.

4. Use of Diphenyl Phosphate in Acid-Base Titrations in Various Aqueous and Nonaqueous Solvents

4.1. Titrations of Diphenyl Phosphate With Sodium Hydroxide in Water

The results of some titrations of two different lots of purified diphenyl phosphate are presented in table 3.[12] According to the results shown in the table, both lots of diphenyl phosphate were approximately 99.9 percent pure.

TABLE 3. *Titrations of diphenyl phosphate in water* [a]

Weight of sample	NaOH [b]		Purity
	Calculated	Found	
Titrations using phenolphthalein			
g	*ml*	*ml*	%
[c] 1.0025	35.68	35.69	100.03
[c] 0.9898	35.23	35.18	99.86
[c] 1.0437	37.15	37.12	99.92
[c] 1.0510	37.41	37.36	99.87
[c] 1.0966	39.03	39.00	99.92
[c] 1.0307	36.68	36.59	99.75
[c] 1.0193	36.28	36.23	99.86
Average			99.89
Potentiometric titrations			
[c] 0.3576	12.75	12.74	99.92
[c] .3222	11.49	11.47	99.83
[d] .3962	14.13	14.15	100.14
[d] .4213	15.02	15.01	99.93
[d] .4858	17.25	17.24	99.94

[a] In titrations with phenolphthalein, the samples were dissolved in 15 ml of 95-percent ethanol and 85 ml of water; in the potentiometric titrations, the respective amounts of ethanol and water were 10 and 90 ml.

[b] The normality (about 0.1 *N*) was determined by standardization against NBS Standard Sample of potassium acid phthalate.

[c, d] The superscripts c and d indicate two different lots of purified diphenyl phosphate.

4.2. Titrations of Bases With Diphenyl Phosphate in Glacial Acetic Acid

At the present time 70-percent perchloric acid is the only generally satisfactory reagent for preparing standard acid solutions for titrations of bases in glacial acetic acid. Acetic anhydride must be added to destroy water introduced with the reagent, and the concentration of the solution must always be deter-

[12] See also table 2 and section 4.3. As was pointed out in section 3.3 it is advisable to add a little alcohol to ensure complete solution of samples of diphenyl phosphate used in aqueous titrations.

mined by titration against a primary basic standard, such as diphenylguanidine, potassium acid phthalate, or sodium carbonate. Clearly, it would be very gratifying to find a solid, anhydrous acid, comparable in strength with perchloric acid. Diphenyl phosphate would not be expected to equal perchloric acid in strength, but it was desirable to ascertain the comparative behavior of the two acids in glacial acetic acid.

The titration curves presented in figure 2 show that diphenyl phosphate was not satisfactory as a replacement for perchloric acid in the potentiometric titration of di-*o*-tolylguanidine and guanidine acetate in glacial acetic acid. Curves obtained in the titration of potassium acid phthalate and tribenzylamine with diphenyl phosphate were very similar to those shown.[13] There is a recognizable break in all of the titration curves in the expected region (8.4 ml), but in the titrations with diphenyl phosphate the break is not steep enough for any but crude analytical procedures.[14] Dyes (for example, crystal violet) which are commonly used as indicators for titrations in glacial acetic acid change color in the emf region −450 to −550 mv, and plainly would be completely useless in titrations with diphenyl phosphate.

In a few miscellaneous titrations of sodium acetate with diphenyl phosphate in glacial acetic acid mixed with other solvents—benzene, dioxane, ethanol, water—the results were much the same. In general, the microvoltmeter readings were very steady except for mixtures containing a high proportion of benzene.[15]

[13] The two bases referred to in figure 2 did not give a precipitate with either diphenyl phosphate or perchloric acid; the perchlorates, but not diphenyl phosphates, produced upon titrating potassium acid phthalate and tribenzylamine precipitate under the conditions used.

[14] It should be noted that the titrations were only of an exploratory character, and the results with diphenyl phosphate would probably have been a little better if the solutions had been completely anhydrous. The solutions were estimated to contain about 0.6 percent of water.

[15] It is not unlikely that diphenyl phosphate associates with acetic acid through hydrogen bonding. No one seems to have made any studies of aryl phosphates which throw any direct light on their tendency to undergo self-association or otherwise participate in hydrogen bonding, but tributyl phosphate has been found useful for extracting acetic acid from aqueous mixtures with hydrochloric acid [28], and several other studies indicate that oxygen attached to phosphorus is sometimes a very effective electron donor and that some acids of phosphorus show a tendency to form aggregates in benzene [1(a) (p. 257), 29 to 32].

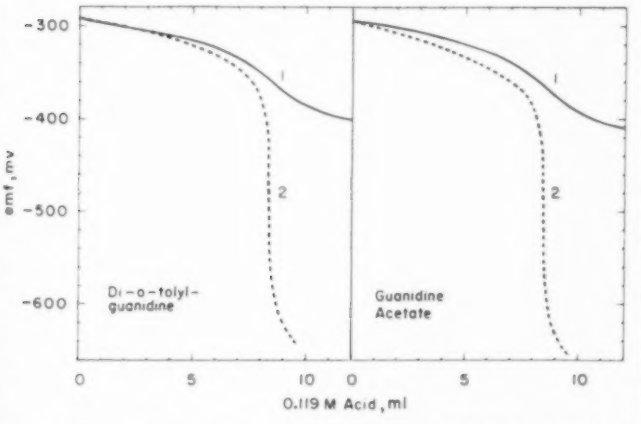

FIGURE 2. *Comparative behavior of (1) diphenyl phosphate and (2) perchloric acid in the potentiometric titration of di-o-tolylguanidine and of guanidine acetate in glacial acetic acid.*

Electrodes: glass, saturated calomel. Initial solutions contained 0.001 mole of the base in 30 ml.

4.3. Comparative Titrations of Diphenyl Phosphate and Carboxylic Acids With Sodium Methylate in Solvents of Various Compositions

a. Potentiometric Titrations

In preliminary potentiometric titrations of 5- or 10-ml portions of 0.1-*M* diphenyl phosphate with sodium methylate (approx 0.115-*M*) in methanol, the precision was very good (usually ±0.01 ml), even though the temperature of the laboratory was subject to fluctuations (mostly in the range 25° ±2° C) and methanol has a rather high coefficient of thermal expansivity. Carboxylic acids, of which acetic, benzoic, and palmitic acids are typical, are often dealt with in nonaqueous titrations. Solutions of these three acids were also titrated with sodium methylate in methanol, under conditions paralleling those used in titrations of diphenyl phosphate. The titration curves indicated that diphenyl phosphate is a much stronger acid than the three carboxylic acids, in harmony with the evidence that diphenyl phosphate is a strong acid in water.

The ready solubility of both diphenyl phosphate and benzoic acid in benzene, methanol, and water suggested the possibility of observing what alterations in the titration curves would result from changing the solvent gradually from *methanol* toward *benzene*, on the one hand, and toward *water*, on the other. For this, 5-ml samples of 0.1 *M* acid in methanol were diluted to approximately 50 ml with various proportions of methanol and benzene or methanol and water. The samples were then titrated with sodium methylate, dissolved in a solvent of approximately the same composition as that of the solution being titrated. The results are shown in figure 3.[16]

It is evident from the figure that for an *aqueous* solution of either acid a negative value on the emf scale would correspond to a low *p*H value, and an increasingly positive emf value would indicate a gradual increase in the *p*H of the solution. In the case of diphenyl phosphate, the *initial* acidity—as registered by the emf reading—was decidedly reduced when the solvent was changed from nearly pure methanol to predominantly water. Hardly any initial effect on the acidity was observable on changing from methanol to 17:3 benzene-methanol. In the case of benzoic acid, changing the solvent from nearly pure methanol to 9:1 water-methanol again produced a striking effect on the initial acidity, this time a decided *increase* in the acidity. As with diphenyl phosphate, comparatively little change in the initial acidity resulted from changing from methanol to 17:3 benzene-methanol.

[16] The titrant was prepared by diluting 1.15 *M* sodium methylate in methanol to 0.115 *M* in a volumetric flask, first adding any methanol and then diluting to volume with either benzene or water. The samples of 0.1 *M* acid in methanol were transferred to the titration beakers by means of a volumetric pipet; the added solvents, totalling 45 ml in volume before mixing, were measured in graduated cylinders. The solvents containing the sample and the titrant were thus similar, although not identical, in composition. A little water was, of course, introduced into each solution with the methanol, and a minute quantity could also enter through the sleeve-type connection of the calomel electrode with the solution. The quantities of water thus introduced were adequate for proper functioning of the glass electrode. The solutions that yielded curves 5 had such a high water content as to be practically the same as aqueous solutions.

UNIVERSITY OF MICHIGAN LIBRARIES

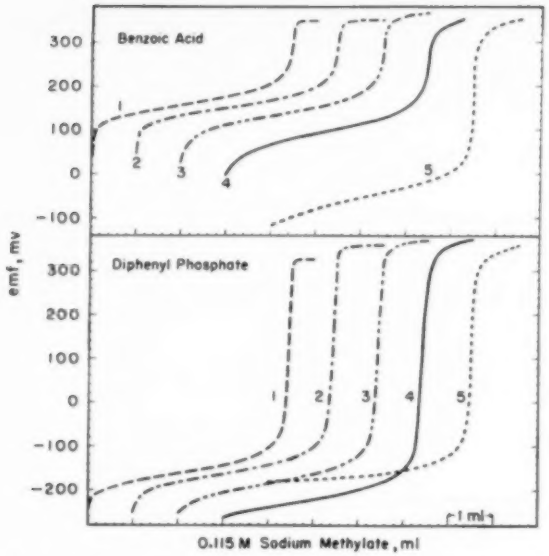

FIGURE 3. *Effect of composition of the solvent in the potentiometric titration of benzoic acid and of diphenyl phosphate with sodium methylate.*

Electrodes: glass, saturated calomel. Initial solution: 50 ml of 0.01-*M* acid. Composition of solvent: (1) benzene-methanol, 17:3 (by volume); (2) benzene-methanol, 4:1; (3) benzene-methanol, 1:1; (4) methanol containing 0.5 weight-percent of water; (5) water-methanol, 9:1. Curves 2 to 5 have each been shifted 1 ml to the right of the preceding curve.

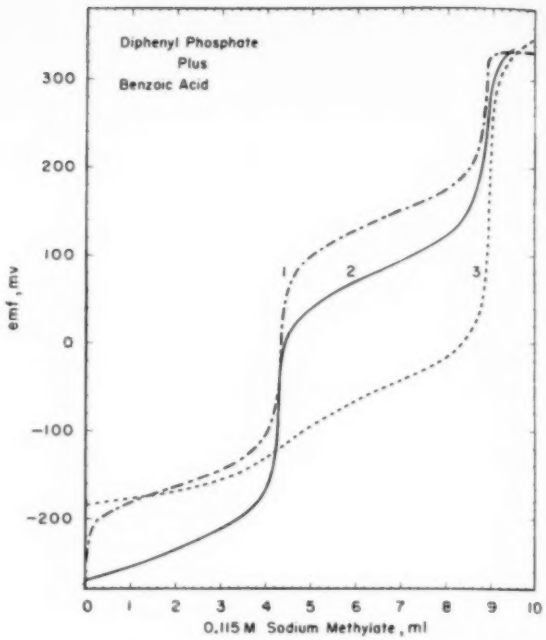

FIGURE 4. *Effect of composition of the solvent in the potentiometric titration of a mixture of diphenyl phosphate and benzoic acid with sodium methylate.*

Electrodes: glass, saturated calomel. Initial volume: 50 ml. Initial concentration of each acid: 0.01-*M*. Composition of solvent: (1) benzene-methanol, 4:1 (by volume); (2) methanol containing 0.5 weight-percent of water; (3) water-methanol, 9:1.

Figure 4 shows the results of titrating a mixture of equivalent quantities of diphenyl phosphate and benzoic acid in three different solvents.[17] The buffering effect of benzoic acid on the end-point for the titration of diphenyl phosphate in water (curve 3) was absent in the titrations in methanol or benzene-methanol, thus making possible a sharp determination of the end-point for each acid. The results support Hantzsch's assertion that water "levels" the strengths of acids, making strong acids weaker and weak acids stronger [33]. An "unleveling" of the strengths of two such acids as benzoic acid and diphenyl phosphate can be brought about by changing to a nonaqueous solvent like methanol or benzene-methanol. While benzoic acid is thereby reduced in apparent strength, the reduction is not sufficient to impair seriously the accuracy of the titration. A few examples of a related character have been reported previously by others [34, 35].

b. Titrations in 4:1 Benzene-Methanol Using Indicators

Benzene-methanol, 4:1 by volume, is currently popular as a solvent for nonaqueous titrations of carboxylic acids [36], particularly if the acid is one of high molecular weight. As was shown in figure 4 (curve 1), when an equimolar mixture of benzoic acid and diphenyl phosphate in this solvent was titrated potentiometrically with sodium methylate, the separate end-points could be located satisfactorily. In practice, it would often be more convenient to locate both such end-points by the use of indicators. As a preliminary step in finding a suitable pair of indicators, 5-ml samples of 0.1-*M* diphenyl phosphate were repeatedly titrated potentiometrically with sodium methylate, each time with the addition of a different indicator dye, and the approximate emfs at which the color changes of the various indicators occurred were noted. For the purposes of the experiment, it was satisfactory to regard the indicator end-point as the emf midway between the emf values obtained immediately before and after addition of the drop of alkali that produced the most striking color change.[18] The results thus obtained with 17 different indicator dyes are shown in figure 5. It will be noted that three of the symbols are enclosed in parentheses (α–NR, *p*–EC, MR); the parentheses are used here to signify that these basic azo dyes did not undergo a sharp color change at the end-point. For all of the other indicators, the color change at the end-point was very sharp. In the cases of the sulfonephthaleins (BPB, BCG, BCP, PR, BTB, CR, CP, TB) and phenolphthalein, there was a roughly linear relationship between the emf values in 4:1 benzene-methanol at our arbitrarily set end-points and the mid-points of the *p*H ranges as commonly given for aqueous solutions of these indicators. Nile blue A and Nile blue 2B did not fit into this linear relationship—their color change in benzene-methanol occurred in too negative an emf region.

[17] Note that distances along the vertical scale are twice as great as in figure 3.

[18] It should be made clear that the end-points thus arbitrarily established are only approximate. For the most part, only one titration of a kind was performed. Indicators were dissolved in methanol, benzene, or benzene-methanol; the concentrations of the indicator solutions ranged from 0.1 percent to 1.0 percent. The amounts added (1 to 5 drops) were such that one drop of sodium methylate produced a vivid color change at the end-point.

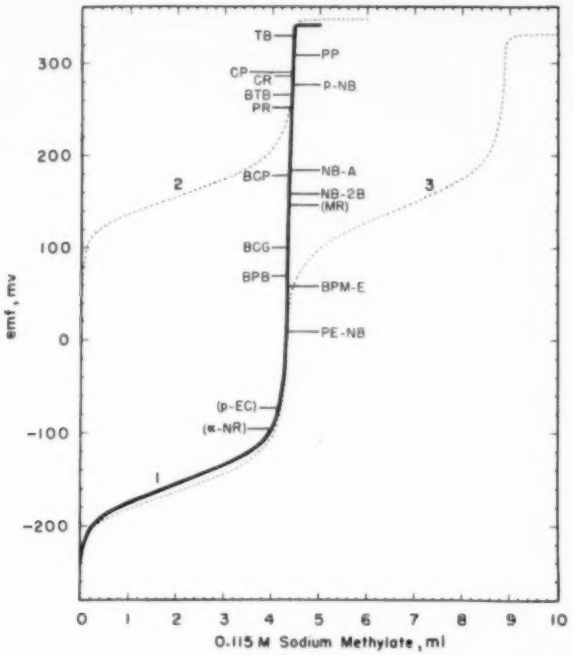

FIGURE 5. *Titration of (1) diphenyl phosphate, (2) benzoic acid, and (3) a mixture of diphenyl phosphate and benzoic acid with sodium methylate in 4:1 benzene-methanol.*

Initial volume, 50 ml; initial concentration of each acid, 0.01 *M*. Electrodes: glass, saturated calomel. Indicators: α-NR, α-naphthyl red; *p*-EC, *p*-ethoxy chrysoidin; PE-NB, phenyl diethyl Nile blue; BPM-E, bromophthalein magenta E; BPB, bromophenol blue; BCG, bromocresol green; MR, methyl red; NB-2B, Nile blue 2B; BCP, bromocresol purple; NB-A, Nile blue A; PR, phenol red; BTB, bromothymol blue; *p*-NB, *p*-naphtholbenzein; CR, *o*-cresol red; CP, *m*-cresol purple; PP, phenolphthalein; TB, thymol blue.

It is clear from figure 5 that all of the indicators tried, except α-naphthyl red, *p*-ethoxychrysoidin, and methyl red, should be usable for titrating diphenyl phosphate under the conditions chosen. Bromophthalein magenta E is one of the best. *p*-Naphtholbenzein and the three Nile blues are also excellent. The relative vertical position of the Nile blues is that which would be predicted from the differences in structure (see section 2.4.c). Some of the sulfonephthaleins (PR, CR, CP, TB) showed a dual color change, as in water; however, the color change in the acid region was very gradual. Other sulfonephthaleins (BPB, BCG, BCP, BTB) were practically colorless at first, then gradually became a bright yellow as sodium methylate was added, eventually undergoing the characteristic vivid color change at the end-point.[19]

Two additional curves (lightly dashed) are shown in figure 5—the titration curve for benzoic acid alone and the titration curve for an equimolar mixture of diphenyl phosphate and benzoic acid. For the mixture of the two acids, as well as for benzoic acid alone, the choice of indicators is greatly narrowed. Phenyl diethyl Nile blue is the only possible indicator in the group studied which can be used for the first end-point. Bromophthalein magenta E changes color just a little too late (and therefore too gradually). The 5 topmost indicators should be usable for the second end-point. The one that we liked best was *p*-naphtholbenzein, the indicator that was adopted for an important ASTM procedure for determining acidity in petroleum products dissolved in benzene-isopropanol [38]. The combination of phenyl diethyl Nile blue and *p*-naphtholbenzein was very satisfactory for titrating the mixture of diphenyl phosphate and benzoic acid; the first color change was greenish blue to violet pink and the second color change, salmon pink to violet. It is preferable to add *p*-naphtholbenzein after reaching the first end-point; both indicators can be added at the start, but the first end-point is then a little less striking. The same combination of indicators should, of course, be usable for other pairs of acids comparable in strength to diphenyl phosphate and benzoic acid, and the method used for selecting suitable indicators is of still wider application.

4.4 Comparative Titrations of Diphenylguanidine, Triethylamine, and Tris(hydroxymethyl)aminomethane With Diphenyl Phosphate in Solvents of Various Compositions

1,3-Diphenylguanidine, triethylamine, and tris(hydroxymethyl)aminomethane were titrated with diphenyl phosphate in the same series of solvents as those listed under figure 3 and also in 1:1 water-methanol. The titration curves are shown in figure 6. The conditions were closely similar to the ones used in the titrations of diphenyl phosphate and benzoic acid.[20] The values obtained in titrating triethylamine were a little low and not closely reproducible, probably indicating some volatilization of the amine; the loss seemed to be least in the solutions containing the highest proportion of methanol.

These bases were selected as representing a large group of organic bases having aqueous dissociation constants, expressed as pK_b, in the approximate range 3 to 6.[21] The tendency for triethylamine to volatilize permits only a tentative comparison of its behavior with that of the other two bases. However, the curves suggest that triethylamine is more affected in strength than the other two bases when the water content of the solvent is progressively reduced and the benzene content is increased. There are also indications that diphenylguanidine is stronger than triethylamine in methanol and benzene, although weaker in water. Such a conclusion would be in harmony with results obtained in spectrophotometric studies of the comparative reactivities of triethylamine and diphenylguanidine with bromophthalein magenta E in benzene [1, 39].

[19] Analogous changes in color of these dyes in benzene were reported earlier, and the probable structural changes involved were discussed [37].

[20] In the titration of diphenylguanidine a solution 0.01-*M* in 9:1 water-methanol could not be prepared. The sample was dissolved in 100 ml of solvent (instead of the usual 50 ml), with the aid of about 4 ml of the standard diphenyl phosphate solution, and the titration was then continued from that point (curve 6).

[21] Values of pK_b for triethylamine, diphenylguanidine, and tris(hydroxymethyl)aminomethane are 3.3, 4.0, and 5.9, respectively [1, 4].

UNIVERSITY OF MICHIGAN LIBRARIES

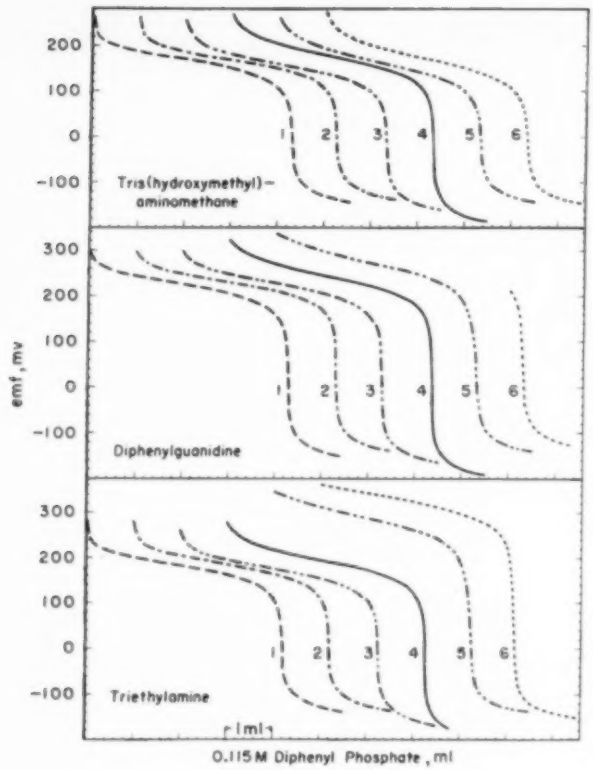

FIGURE 6. *Effect of composition of the solvent in the potentiometric titration of tris(hydroxymethyl)aminomethane, 1,3-diphenylguanidine, and triethylamine with diphenyl phosphate*

Electrodes: glass, saturated calomel. Initial solution: 50 ml of 0.01-*M* base (for exceptions, see text). Composition of solvent: (1) benzene-methanol, 17:3 (by volume); (2) benzene-methanol, 4:1; (3) benzene-methanol, 1:1; (4) methanol containing 0.5 weight-percent of water; (5) water-methanol, 1:1; (6) water-methanol, 9:1. Curves 2 to 6 have each been shifted 1 ml to the right of the preceding curve.

4.5. Titrations of Diphenylguanidine and Di-*o*-tolylguanidine With Diphenyl Phosphate in Benzene, Using Indicators

a. General Discussion

Acid-base titrations using only benzene as the solvent differ from the titrations discussed in preceding sections in that ions play a very minor role. The reaction in benzene or other aprotic solvents consists essentially of the combination of the base with the acid to form a salt. An illustration is the combination of an amine with a monobasic, nonassociated acid, as follows:

$$\underset{\text{(amine)}}{R_3N} + \underset{\text{(acid)}}{HA} \rightleftarrows \underset{\text{(salt)}}{R_3NH^+ \ldots A^-}. \qquad (1)$$

As indicated in the equation, the major part of the salt is not separated into ions when the solvent is benzene or a like solvent; instead, the salt behaves more like a highly polar molecule.[22] The end-point can easily be located by adding a minute amount of an indicator dye, which likewise forms a salt according to eq (1). The dye can, of course, be either an amine or an acid, but it must undergo a striking change in color when converted to a salt.

Vorländer [42] was the first to perform titrations involving the chemical reaction shown as eq (1); he referred to this type of titration as "aminometry" or "alkalimetry without hydroxyl ions."[23] In Europe and Australia aminometry has been applied successfully to a large variety of organic bases, and the method would probably find more widespread application if acids of suitable strength and purity were readily obtainable.[24]

b. Titrations of Diphenylguanidine and Di-*o*-tolylguanidine With Diphenyl Phosphate in Benzene

Few solid organic bases of strengths comparable with those of the aliphatic amines ($pK_b \simeq 3$ to 5) are readily available. Important among the few are 1,3-diphenylguanidine, $\underset{1}{C_6H_5NH}\underset{2}{(C{=}NH)}\underset{3}{NHC_6H_5}$, and the closely related compound, 1,3-di-*o*-tolylguanidine. Previously benzene solutions of these bases have been titrated satisfactorily with *d*-camphorsulfonic acid, picric acid, and trichloroacetic acid in this laboratory [1]. As shown in tables 4 and 5, the two bases can also be titrated successfully with diphenyl phosphate in benzene.

Table 4 presents two titrations of 0.05-*M* diphenylguanidine with 0.05-*M* diphenyl phosphate with bromophthalein magenta E as the indicator. In an acid solution the indicator is yellow; the color in a basic medium is magenta to blue, depending on the concentration and on the solvent [1, 39]. Experiments 1 and 2 were performed under slightly different conditions, as indicated in the footnotes. In experiment 1 the solution gradually increased in its content of diphenylguanidinium diphenyl phosphate, becoming about 0.01-*M* at the end of the titration; the concentration of bromophthalein magenta E was about 60 percent as great at the end of the titration as at the beginning. Experiment 2 was performed in such a way as to maintain the content of diphenylguanidinium diphenyl phosphate approximately constant (0.01-*M*) at each end-point; the concentration of bromophthalein magenta E was also the same at each end-point.

The change from yellow to magenta was always sharp. After this end-point had been reached, sufficient acid was added to restore the yellow color. This second end-point ought to be a little more accurate than the magenta end-point because to obtain the magenta color sufficient diphenylguanidine must be added to combine with both diphenyl phosphate and bromophthalein magenta E. The data do not indicate any advantage in performing

[22] It should be noted, however, that in spite of the minute concentration of free ions in such a solution, LaMer and Downes successfully performed certain acid-base titrations potentiometrically and conductimetrically in benzene [40], and Maryott performed some additional acid-base titrations conductimetrically in benzene [41].

[23] A review of the literature and additional examples from work in this laboratory were given in [1].

[24] For successful titration the reaction (eq 1) must, of course, proceed to completion. Benzoic and acetic acids, for example, are much too weak to be used for such titrations. Vorländer used hydrogen chloride, dissolved in benzene, ligroin, or chloroform, and had to restandardize it daily. *p*-Toluenesulfonic acid is quite strong but the commercial monohydrate must be dehydrated by individual workers and is not of high purity. Picric acid has found some use, but is not as strong as would be desirable; other objectionable features are the yellow color of its salts and the hazards in handling the acid and its salts.

TABLE 4. *Titrations of 0.05-M diphenylguanidine with 0.05-M diphenyl phosphate in benzene, using bromophthalein magenta E*

Acid		Base	Molarity of salt	Strength of base in terms of acid	
Yellow	Magenta			Yellow	Magenta
		Experiment 1[a]			
ml	*ml*	*ml*			
1.11	1.09	1.08	0.0016	1.02_5	1.00_5
2.03	2.01	2.02	.0029	1.00_5	$.99_5$
3.03	3.00	3.01	.0042	1.00_7	$.99_7$
4.04	4.01	4.02	.0053	1.00_5	$.99_8$
5.06	5.04	5.04	.0063	1.00_4	1.00_0
6.03	6.01	6.02	.0071	1.00_2	$.99_8$
7.07	7.05	7.06	.008	1.00_1	$.99_8$
8.03	8.00	8.03	.0087	1.00_0	$.99_6$
9.02	9.00	9.02	.0094	1.00_0	$.99_8$
9.99	9.96	9.97	.01	1.00_2	$.99_9$
Average				1.00_3	$.99_8$
		Experiment 2[b]			
1.03	1.01	1.03	0.01	1.00_5	0.98_1
2.02	2.00	2.02	.01	1.00_3	$.99_0$
3.04	3.02	3.05	.01	$.99_7$	$.99_0$
4.04	4.02	4.06	.01	$.99_5$	$.99_0$
5.07	5.05	5.08	.01	$.99_8$	$.99_4$
6.03	6.01	6.03	.01	1.00_0	$.99_7$
7.02	7.00	7.01	.01	1.00_1	$.99_9$
8.03	8.00	8.03	.01	1.00_0	$.99_5$
9.02	9.00	9.02	.01	1.00_0	$.99_8$
10.00	9.98	9.99	.01	1.00_1	$.99_9$
Average				$.99_8$	$.99_3$

[a] Thirty ml of benzene and 2 drops of 0.1-percent bromophthalein magenta E in benzene were added to the titration flask at the beginning of the titration. Acid and base were added to the solvent in approximately 1-ml increments and end-points were determined for the successive increments. The approximate calculated molarity of diphenylguanidinium diphenyl phosphate at the end-point is given in the fourth column.

[b] Thirty ml of benzene and 2 drops of 0.1-percent bromophthalein magenta E in benzene were mixed, and 3 ml of this solution was added from a buret at the beginning of the experiment and before each succeeding end-point was determined. The concentration of diphenylguanidinium diphenyl phosphate was therefore 0.01-*M* at each end-point

the titration by the more cumbersome procedure used in experiment 2. Analogous results were obtained in titrating 0.02-*M* di-*o*-tolylguanidine with 0.02-*M* diphenyl phosphate by the same two procedures.

Table 5 presents examples of titrations of 0.02-*M* di-*o*-tolylguanidine with 0.02-*M* diphenyl phosphate in benzene using three different indicator dyes—an acidic indicator, bromophthalein magenta E, and two basic indicators, tamarack green (base) and Victoria blue B (base). The titration using bromophthalein magenta E was analogous to experiment 1 of table 4 and needs no further discussion. In the use of tamarack green (base) the initially yellow color becomes green when sufficient diphenyl phosphate has been added to combine with both ditolylguanidine and the indicator; the yellow color was restored by adding a little ditolylguanidine. In titrations with Victoria blue B (base) as the indicator, three distinct colors—orange, blue, and an intermediate gray—were observed. There is scarcely any difference in the results obtained with the three indicators, although on the whole we liked bromophthalein magenta E the best.

TABLE 5. *Titrations of 0.02–M ditolylguanidine with 0.02–M diphenyl phosphate in benzene, using different indicators*

Acid		Base	Strength of base in terms of acid	
Yellow	Magenta		Yellow	Magenta
		Experiment 1. Using bromophthalein magenta E[a]		
ml	*ml*	*ml*		
1.02	1.00	1.01	1.01_0	0.99_5
2.03	2.01	2.02	1.00_5	$.99_5$
3.02	3.01	3.02	1.00_5	$.99_7$
4.03	4.01	4.02	1.00_2	$.99_8$
5.03	5.01	5.01	1.00_4	1.00_0
6.03	6.00	6.01	1.00_3	$.99_8$
7.02	7.00	7.01	1.00_1	$.99_8$
8.06	8.03	8.05	1.00_1	$.99_8$
9.04	9.02	9.02	1.00_2	1.00_0
9.99	9.97	9.98	1.00_1	$.99_9$
Average			1.00_3	$.99_7$

Acid	Base		Strength of base in terms of acid	
	Yellow	Green	Yellow	Green
	Experiment 2. Using tamarack green (base)[b]			
ml	*ml*	*ml*		
1.01	1.00	0.99	1.01_0	1.02_0
2.05	2.07	2.06	$.99_0$	$.99_5$
3.05	3.07	3.06	$.99_3$	$.99_7$
4.01	4.02	4.01	$.99_8$	1.00_0
5.04	5.05	5.03	$.99_8$	1.00_2
7.01	7.01	7.00	1.00_0	1.00_1
8.52	8.51	8.50	1.00_1	1.00_2
9.89	9.90	9.88	$.99_8$	1.00_1
Average			$.99_8$	1.00_2

Acid	Base			Strength of base in terms of acid		
	Orange	Gray	Blue	Orange	Gray	Blue
			Experiment 3. Using Victoria blue B (base)[c]			
ml	*ml*	*ml*	*ml*			
1.00	1.02	.....	1.00	0.98_0	.....	1.00_0
2.00	2.03	2.02	2.01	$.98_5$	0.99_0	$.99_5$
3.00	3.02	.....	3.01	$.99_3$	.....	$.99_7$
4.02	4.06	4.03	4.01	$.99_0$	$.99_8$	1.00_2
5.00	5.03	.....	5.00	$.99_4$	.....	1.00_0
6.01	6.04	.....	.....	$.99_5$	.....	.....
7.01	7.03	.....	7.01	$.99_7$	.....	1.00_0
8.03	8.06	8.04	8.02	$.99_6$	$.99_9$	1.00_1
9.05	9.08	9.06	9.04	$.99_7$	$.99_9$	1.00_1
9.97	10.00	9.99	9.97	$.99_7$	$.99_8$	1.00_0
Average	.....	.....	.....	$.99_2$	$.99_7$	1.00_0

[a] Thirty ml of benzene and 2 drops of 0.1-percent bromophthalein magenta in benzene were added at the beginning of the titration.

[b] One drop of 0.1-percent tamarack green in benzene was added at the start.

[c] Thirty ml of benzene and 2 drops of 0.1-percent Victoria blue B in benzene were added at the beginning.

In addition to these titrations 0.02–*M* diphenylguanidine and 0.01–*M* di-*o*-tolylguanidine were titrated in benzene with diphenyl phosphate of equivalent concentration. The precision and accuracy were excellent, especially in view of the small volumes and low concentrations used. Diphenyl phosphate should be satisfactory for titrating other moderately strong bases in benzene and other aprotic solvents. It is probably a weaker acid than *p*-toluenesulfonic acid and other sulfonic acids, but is superior to the sulfonic acids in being more soluble in aprotic solvents and more easily obtained in a pure anhydrous state.

4.6. Concluding Remarks

In the preceding sections it has been shown that accurate titrations with diphenyl phosphate can be performed in solvents as different as benzene and water, as well as in solvents of intermediate character. In view of its high acidic strength, its relatively high equivalent weight (250.19), the ease with which it can be obtained and maintained as anhydrous crystals, and its apparent resistance to hydrolysis and alcoholysis at ordinary temperatures, it promises to be a useful material for acid-base titrations in both aqueous and nonaqueous solutions. More rigorous tests must be applied before it can be recommended as an acidimetric standard for work of the highest accuracy.

The properties of diphenyl phosphate suggest its use as an acid catalyst. Furthermore, it offers a means for extending knowledge of the behavior of acids. The great majority of the studies of acidic behavior made so far have been performed with aliphatic or aromatic carboxylic acids. However, studies of the sort illustrated in figures 3 and 4 show that generalizations reached through observations of the behavior of carboxylic acids in various solvents cannot safely be applied to all types of acids. The investigations with diphenyl phosphate are suggestive of interesting work still to be done with acids which as yet are not widely known, such as bisarylphosphonic acids.

The authors are indebted to James Stewart for measuring the benzene content of cyclohexane (table 1), and to the following companies for donating materials: American Cyanamid Company, for 5-phenyl-9-diethyl Nile blue; Dow Chemical Company, for diphenyl phosphate; Heyden Chemical Corporation, for *o*-chlorobenzotrichloride.

5. References

[1] (a) M. M. Davis and P. J. Schuhmann, J. Research NBS **39,** 221 (1947) RP1825.
(b) NBS Tech. News Bull. **36,** 168 (1952).
[2] Dow Special Products, p. 88 (The Dow Chemical Company, Midland, Michigan, 1st edition, March 1939). See also the 1950 edition of this catalog.
[3] C. J. Penther and F. B. Rolfson, Ind. Eng. Chem., Anal. Ed. **15,** 337 (1943).
[4] R. G. Bates and G. D. Pinching, J. Research NBS **43,** 519 (1949) RP2043.
[5] A. Baeyer and V. Villiger, Ber. deut. chem. Ges. **37,** 2848 (1904).
[6] K. Venkataraman, The chemistry of synthetic dyes, ch. XXIII (Academic Press, Inc., New York, N. Y., 1952).
[7] R. Meldola, J. Chem. Soc. (London) **41,** 187 (1882).
[8] T. L. Hill, G. E. K. Branch, and M. Patapoff, J. Am. Chem. Soc. **67,** 454 (1945).
[9] M. Nathansohn and P. Müller, Ber. deut. chem. Ges. **22,** 1875 (1889).
[10] E. Noelting and J. Saas, Ber. deut. chem. Ges. **46,** 952 (1913).
[11] I. M. Kolthoff, Acid-base indicators (The Macmillan Company, New York, N. Y., 1937; 4th German Edition, 1932, translated by C. Rosenblum).
[12] M. L. Crossley, R. J. Turner, C. M. Hofmann, P. F. Dreisbach, and R. P. Parker, J. Am. Chem. Soc. **74,** 578 (1952).
[13] (a) H. Hlasiwetz and A. Grabowski, Liebigs Ann. **139,** 95 (1866); Zeitschrift für Chemie **9,** 390 (1866).
(b) O. Rembold, Zeitschrift für Chemie **9,** 651 (1866).
[14] L. Glutz, Liebigs Ann. **143,** 181 (1867).
[15] G. Jacobsen, Ber. deut. chem. Ges. **8,** 1519 (1875).
[16] M. Rapp, Liebigs Ann. **224,** 156 (1884).
[17] W. Autenrieth, Ber. deut. chem. Ges. **30,** 2369 (1897).
[18] J. M. A. Hoeflake, Rec. trav. chim. **36,** 24 (1916).
[19] A. Bernton, Ber. deut. chem. Ges. **55B,** 3361 (1922).
[20] F. Zetzsche and M. Nachmann, Helv. Chim. Acta **9,** 705 (1926).
[21] S. Forssman, Biochem. Z. **263,** 135 (1933), through Chem. Abstracts **27,** 4726 (1933) and Brit. Chem. Abstracts **1933A,** 897.
[22] C. Morton, Quart. J. Pharm. Pharmacol. **3,** 438 (1930).
[23] W. D. Kumler and J. J. Eiler, J. Am. Chem. Soc. **65,** 2355 (1943).
[24] R. H. A. Plimmer and W. J. N. Burch, J. Chem. Soc. (London) **1929,** 279.
[25] M. I. Smith and E. F. Stohlman, U. S. Public Health Repts. **48,** 734 (1933).
[26] F. L. Breusch and H. Keskin, Rev. fac. sci. univ. Istanbul **7A,** 182 (1942).
[27] E. Blumenthal and J. B. M. Herbert, Trans. Faraday Soc. **41,** 611 (1945).
[28] (a) H. A. Pagel and F. W. McLafferty, Anal. Chem. **20,** 272 (1948);
(b) H. A. Pagel, P. E. Toren, and F. W. McLafferty, Anal. Chem. **21,** 1150 (1949).
[29] C. S. Marvel, M. J. Copley, and E. Ginsberg, J. Am. Chem. Soc. **62,** 3109 (1940).
[30] (a) W. Gordy and S. C. Stanford, J. Chem. Phys. **8,** 170 (1940); **9,** 204 (1941).
(b) W. Gordy, J. Chem. Phys. **9,** 215 (1941).
(c) S. C. Stanford and W. Gordy, J. Am. Chem. Soc. **63,** 1094 (1941).
[31] L. F. Audrieth and R. Steinman, J. Am. Chem. Soc. **63,** 2115 (1941).
[32] (a) G. M. Kosolapoff and J. F. McCullough, J. Am. Chem. Soc. **73,** 5392 (1951), and other papers by Kosolapoff and coworkers.
(b) G. M. Kosolapoff, Organophosphorus compounds (John Wiley and Sons, Inc., New York, N. Y., 1950).
[33] A. Hantzsch, Z. Elektrochem. **29,** 221 (1923).
[34] (a) L. Lykken, P. Porter, H. D. Ruliffson, and F. D. Tuemmler, Ind. Eng. Chem., Anal. Ed. **16,** 219 (1944).
(b) L. Lykken, Lubrication Eng. **2,** 23, 64 (1946).
[35] S. Palit, Ind. Eng. Chem., Anal. Ed. **18,** 246 (1946).
[36] (a) J. S. Fritz and N. M. Lisicki, Anal. Chem. **23,** 589 (1951).
(b) J. S. Fritz, Acid-base titrations in nonaqueous solvents (G. Frederick Smith Chemical Company, Columbus, Ohio, 1952).
[37] M. M. Davis, P. J. Schuhmann, and M. E. Lovelace, J. Research NBS **41,** 27 (1948) RP1900.
[38] H. Ferguson, Anal. Chem. **22,** 289 (1950).
[39] M. M. Davis and H. B. Hetzer, J. Research NBS **46,** 496 (1951) RP2219; **48,** 381 (1952) RP2326.
[40] V. K. LaMer and H. C. Downes, J. Am. Chem. Soc. **53,** 888 (1931).
[41] A. A. Maryott, J. Research NBS **38,** 527 (1947) RP1794.
[42] (a) D. Vorländer, Ber. deut. chem. Ges. **36,** 1485 (1903).
(b) D. Vorländer, with J. Fischer and F. Wildner, Ber. deut. chem. Ges. **66,** 1789 (1933).
(c) D. Vorländer, Ber. deut. chem. Ges. **67,** 145 (1934).

WASHINGTON, January 20, 1955.

Journal of Research of the National Bureau of Standards Vol. 54, No. 6, June 1955 Research Paper 2594

An Improved Method of Measuring Efficiencies of Ultra-High-Frequency and Microwave Bolometer Mounts

R. W. Beatty and Frank Reggia

A method is presented for measuring efficiencies of bolometer mounts used for ultra-high-frequency and microwave power measurement. It is based upon the impedance method of Kerns, but avoids the direct measurement of impedance. Pertinent theory is developed, and the errors in measuring efficiency by this method are analyzed and discussed. Experimental results are given.

1. Introduction

The efficiency, η, of a bolometer mount may be defined as the ratio of the power dissipated in the bolometer element to the power input to the bolometer mount. If the power dissipated in the bolometer element, P_b, can be accurately determined, the power input, P_I, to the bolometer mount is

$$P_I = \frac{P_b}{\eta}. \tag{1}$$

P_b is usually measured by substitution techniques, in which it is customary to reduce the audio or d-c bolometer bias power (after the r-f power is applied) until the bolometer resistance returns to its original operating value. It is assumed that the change in bolometer resistance caused by the r-f power is identical to the change in resistance caused by an equal amount of a-f or d-c power P_d. The validity of this assumption has been analytically treated [1] for Wollaston wire bolometers cooled by convection. Based upon this analysis, Carlin and Sucher concluded that "Wollaston wire bolometers, when properly designed and mounted, afford a means of measuring cw power over a frequency range extending to the millimeter wavelength region, with an accuracy approaching that of low-frequency measurements." It should be noted, however, that under less favorable conditions the substitution error for convection-cooled Wollaston wire bolometers may be appreciable (let us say greater than 0.5 percent) at frequencies above the estimated limit of 3,000 Mc, depending upon the length and mounting of the bolometer element.

If the ratio of P_b to P_d is K_s,

$$P_I = \frac{K_s}{\eta} P_d. \tag{2}$$

It is possible to estimate the limits of K_s for a specific Wollaston wire bolometer from the calculated curves of Carlin and Sucher (see footnote 1).

An impedance method of determining bolometer mount efficiency has been described [2] by Kerns. Unfortunately, relatively small errors in the required impedance measurements can lead to a large error in the efficiency as determined by this method.

A modification of Kerns' method will be described, in which the direct measurement of impedance is avoided, permitting the efficiencies of tunable bolometer mounts to be obtained with increased accuracy. Efficiencies of untuned bolometer mounts can then be obtained with very little loss in accuracy from comparative power measurements.

2. Impedance Method

In the impedance method of determining efficiency the bolometer mount is thought of as replaced by an equivalent two-terminal-pair network terminated in the bolometer resistance. As shown in figure 1, the input impedance (of the equivalent network) corresponding to each of three different bolometer resistances is obtained.

The normal operating resistance of the bolometer is designated as R_2. The efficiency for this condition may be calculated from an expression (see footnote 2) involving the three terminating resistances and the three corresponding input impedances.

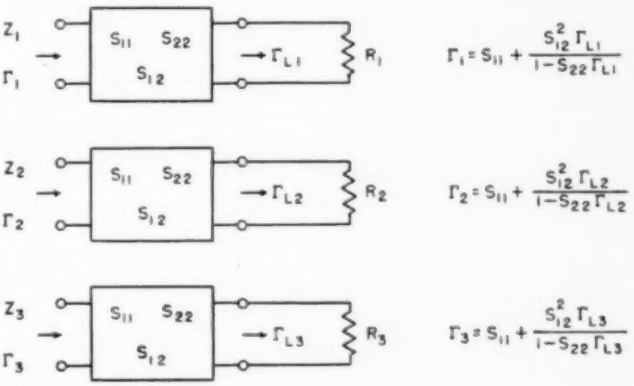

$$\eta_{R=R_2} = \frac{|S_{12}|^2 \left(1-|\Gamma_{L2}|^2\right)}{|1-S_{22}\Gamma_{L2}|^2 - |S_{11}(1-S_{22}\Gamma_{L2}) + S_{12}^2\Gamma_{L2}|^2}$$

FIGURE 1. *Efficiency of a two-terminal-pair network (terminated in a resistance R_2) determined from three measurements of input impedance or reflection coefficient.*

[1] H. J. Carlin and Max Sucher, Accuracy of bolometric power measurements, Proc. Inst. Radio Engrs. **40**, 1042 (Sept. 1952).

[2] D. M. Kerns, Determination of efficiency of microwave bolometer mounts from impedance data, J. Research NBS **42**, 579 (1949) RP1995.

An equivalent expression for the efficiency can be obtained[3] in terms of the voltage reflection coefficients corresponding to the above terminating resistances and input impedances.

$$\text{Efficiency } (\eta)_{R=R_2} = \left|\frac{(\Gamma_2-\Gamma_1)(\Gamma_3-\Gamma_2)(\Gamma_{L3}-\Gamma_{L1})}{(\Gamma_3-\Gamma_1)(\Gamma_{L2}-\Gamma_{L1})(\Gamma_{L3}-\Gamma_{L2})}\right| \frac{|1-|\Gamma_{L2}|^2}{|1-|\Gamma_2|^2}, \tag{3}$$

where Γ denotes an input, and Γ_L a terminating reflection coefficient.

If the bolometer forms one arm of a Wheatstone bridge, it is convenient to adjust the bolometer resistances R_1, R_2, and R_3 to predetermined values. If the factor containing the real parameters Γ_{L1}, Γ_{L2}, and Γ_{L3} is denoted by C, eq (3) becomes

$$\eta = \frac{C}{1-|\Gamma_2|^2}\left|\frac{(\Gamma_2-\Gamma_1)(\Gamma_3-\Gamma_2)}{\Gamma_3-\Gamma_1}\right|, \tag{4}$$

where

$$C = \{1-|\Gamma_{L2}|^2\}\left|\frac{\Gamma_{L3}-\Gamma_{L1}}{(\Gamma_{L2}-\Gamma_{L1})(\Gamma_{L3}-\Gamma_{L2})}\right| = \frac{2R_2(R_3-R_1)}{(R_2-R_1)(R_3-R_2)},$$

and

$$\Gamma_L = \frac{R_L-Z_0}{R_L+Z_0},$$

Where Z_0 is an arbitrary real impedance.

It is generally true that the factor C can be more accurately determined than the other factors in eq (4), because C is a function of resistances determined by dc measurement.

The reflection coefficients Γ_1, Γ_2, and Γ_3 occur in difference terms of eq (4), with the unfortunate result that a given error in measuring individual reflection coefficients may produce a much larger error in the calculated efficiency.

For example, if $C=19.92$, $\Gamma_1=0.0676$, $\Gamma_2=0$, and $\Gamma_3=0.174\ e^{j61\pi/60}$, the efficiency is approximately 97 percent. An error of only ± 1 percent in measuring the voltage standing-wave ratios

$$\left(\text{VSWR}=\frac{1+|\Gamma|}{1-|\Gamma|}\right) \text{ corresponding to } |\Gamma_1| \text{ and } |\Gamma_3|$$

can produce an error of approximately ± 6 percent in the calculated efficiency.

In order to reduce this error in efficiency to the more useful value of ± 1 percent, it would be necessary in the example to make VSWR measurements to an accuracy better than approximately ± 0.2 percent. It is apparent that the determination of efficiency by this method places rather severe requirements on the accuracy of UHF or microwave impedance measurements.

[3] Equation (3) can be obtained by simultaneous solution of the equations appearing in figure 1, which are based upon the scattering equations of a two-terminal-pair network. See R. W. Beatty and A. C. MacPherson, Mismatch errors in microwave power measurements, Proc. Inst. Radio Engrs. **41**, 1112 (Sept. 1953).

3. Improved Method

It is possible to avoid the direct measurement of impedance of tunable bolometer mounts having a high efficiency (above approximately 90%) and thereby increase the accuracy of the efficiency determination.

Assuming that the bolometer mount can be made reflection-free ($\Gamma_2=0$) by an appropriate tuning adjustment when the bolometer is operating at its normal rated resistance, R_2, eq (4) becomes

$$\eta = C\left|\frac{\Gamma_1\Gamma_3}{\Gamma_1-\Gamma_3}\right|. \tag{5}$$

If, in addition, the bolometer mount has a high efficiency, it can be assumed with small error (as discussed later) that the vectors representing Γ_1 and Γ_3 terminate on a straight line [4] passing through the origin. The efficiency is

$$\eta = C\left|\frac{\Gamma_1\Gamma_3}{|\Gamma_1|\pm|\Gamma_3|}\right|. \tag{6}$$

The plus sign is used if the vectors representing Γ_1 and Γ_3 terminate on opposite sides of the origin, and the negative sign is used if they terminate on the same side.

Bolometer resistances R_1 and R_3 should be chosen above and below R_2 in order to obtain the greatest possible spread. In this case the vectors representing Γ_1 and Γ_3 terminate on opposite sides of the origin, and

$$\eta = C\frac{|\Gamma_1\Gamma_3|}{|\Gamma_3|+|\Gamma_1|} = \frac{C}{2}\frac{(\sigma_1-1)(\sigma_3-1)}{\sigma_1\sigma_3-1}, \tag{7}$$

where σ represents the VSWR corresponding to $|\Gamma|$.

Instead of measuring σ_1 and σ_3, more accurate results may be obtained by measuring the relative voltage output of a loosely coupled, properly positioned fixed probe.

A simplified representation of a slotted section and probe is shown in figure 2. It is seen that the voltage, E_P, (in wave guide of rectangular cross section operating in the dominant mode, E_P corresponds to the strength of the transverse electric field) is a function of the reflection coefficients of the generator, probe, and load referred to the probe position. From inspection of the equivalent circuit

$$E_P = E_G\frac{(1-\Gamma_G)(1+\Gamma_P)(1+\Gamma_L)}{(1+\Gamma_G)(1-\Gamma_P)(1+\Gamma_L)+2(1+\Gamma_P)(1-\Gamma_G\Gamma_L)}, \tag{8}$$

in which the subscripts G, P, and L, refer to the generator, probe, and load, respectively.

By means of a matching transformer following the generator, it is possible to make Γ_G vanish. In this case,

$$E_P = E_G\frac{1}{y_P+\dfrac{2}{1+\Gamma_L}}, \tag{9}$$

[4] See appendix, section 6.

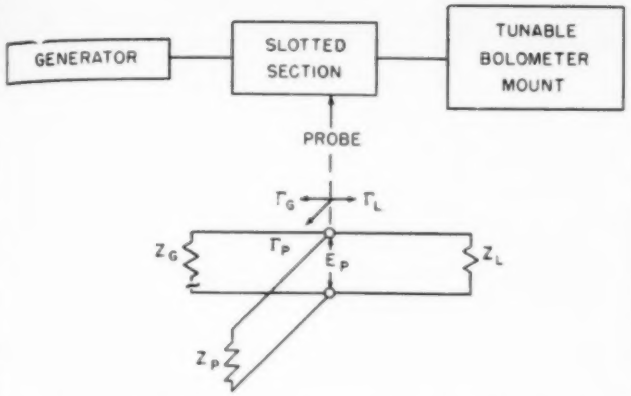

FIGURE 2. *Simplified block diagram of measuring apparatus and an equivalent circuit representation.*

where $y_P=(1-\Gamma_P)/(1+\Gamma_P)$.

If in addition, the probe is loosely coupled ($y_P \approx 0$),

$$E_P \approx \frac{E_G}{2}(1+\Gamma_L). \tag{10}$$

If the probe is located at a position where its response is maximum when the bolometer resistance is R_1, E_{P1} is proportional to $(1+|\Gamma_1|)$. With the probe fixed in that position, the bolometer resistance is changed to R_2 and then R_3, observing the probe response,

$$\begin{aligned} E_{P1} &= k(1+|\Gamma_1|) \\ E_{P2} &= k \\ E_{P3} &\approx k(1-|\Gamma_3|). \end{aligned} \tag{11}$$

Defining the ratios K_1 and K_3 as follows,

$$\begin{aligned} K_1 &= \frac{E_{P1}}{E_{P2}} = 1+|\Gamma_1| \\ K_3 &= \frac{E_{P3}}{E_{P2}} \approx 1-|\Gamma_3|, \end{aligned} \tag{12}$$

the efficiency may be written

$$\eta = C\frac{(E_{P1}-E_{P2})(E_{P2}-E_{P3})}{E_{P2}(E_{P1}-E_{P3})} = C\frac{(K_1-1)(1-K_3)}{K_1-K_3}. \tag{13}$$

A correction to eq (13), to compensate for failure of the assumption that the vectors representing Γ_1 and Γ_2 are colinear, can be made if the other sources of error are neglected for the moment. Let the ratio of η given by eq (5) to that given by eq (13) be

$$\zeta_1 = \left|\frac{\Gamma_1\Gamma_3}{\Gamma_1-\Gamma_3}\right| \frac{(K_1-K_3)}{(K_1-1)(1-K_3)}. \tag{14}$$

If the angular difference between Γ_1 and Γ_3, as shown in figure 3, is $\pi+\delta$, where $\delta \lessgtr 0.1$, it can be

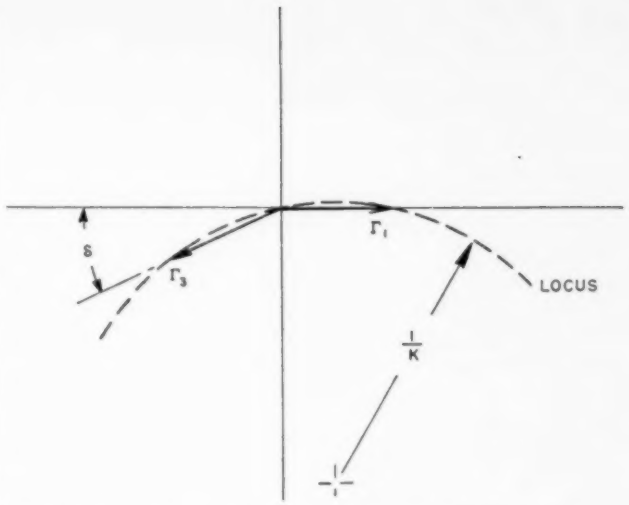

FIGURE 3. *Typical curvature of input reflection coefficient locus for resistive termination of bolometer mount.*

shown that

$$|\Gamma_3| \approx (1-K_3)(1+\delta^2/2K_3),$$

$$|\Gamma_3-\Gamma_1| \approx (K_1-K_3)\left[1+\delta^2\frac{K_1(1-K_3)^2}{2K_3(K_1-K_3)^2}\right],$$

and

$$\zeta_1 \approx 1+\delta^2\frac{(K_1-1)(K_1-K_3^2)}{2K_3(K_1-K_3)^2}. \tag{15}$$

The angular difference, δ, is simply related to the curvature, K, of the locus of the reflection coefficient. This locus may be determined by measuring the input reflection coefficient (referred to the fixed position of the probe) as the bolometer resistance is varied. The expression relating K and δ is

$$\delta \approx \frac{K}{2}(K_1-K_3) \qquad (\delta \lessgtr 0.1). \tag{16}$$

Equation (15) may be written in terms of K:

$$\zeta_1 \approx 1+K^2\frac{(K_1-1)(K_1-K_3^2)}{8K_3}. \tag{17}$$

A graph representing the percentage correction according to eq (17) is shown in figure 4.

Another correction to eq (13) is based upon the fact that there may be appreciable losses between the fixed probe position and the bolometer mount input. The efficiency of a length of line or waveguide having a known attenuation is shown in figure 5. If the line or guide section is not uniform, the efficiency must be determined by other means, such as measuring the bolometer mount efficiency with another identical slotted section inserted between the bolometer mount and the measuring slotted section.

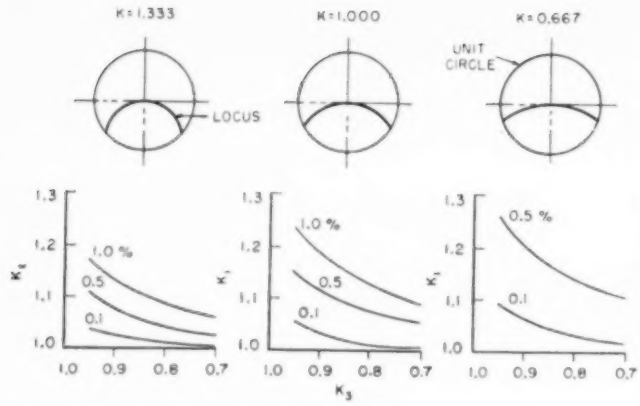

FIGURE 4. *Percentage correction to efficiency corresponding to curvature of reflection coefficient locus for three values of curvature.*

If the efficiency of that portion of the circuit between the fixed probe position and the bolometer mount input is η_{P-B}, the efficiency of the bolometer mount, applying the above corrections is

$$\eta = \frac{C}{\eta_{P\text{-}B}} \left| \frac{(K_1-1)(1-K_3)}{K_1-K_3} \right| \left\{ 1+K^2 \frac{(K_1-1)(K_1-K_3^2)}{8K_3} \right\}. \tag{18}$$

It is seen that both corrections increase the efficiency over the value obtained in eq (11).

The method just described is applicable to tunable bolometer mounts, in which the bolometer element can be represented by a resistance terminating the bolometer mount. (Barretters are generally suitable, but there is evidence that thermistors do not fulfill this condition.)

The efficiency of tunable bolometer-mount assemblies, including matching transformers, can also be measured by this method. After the efficiency of a tunable bolometer-mount assembly has been determined, at a specified operating frequency, the efficiency of another tunable or untuned bolometer mount or assembly can be obtained by comparing the power readings of the two mounts when alternately connected to a stable, well-padded generator. Assuming that the power dissipated in the element can be accurately measured by d-c substitution techniques,[5] and letting the subscripts A and B refer to the two mounts,

$$\begin{aligned} \eta_A P_A &= P_{Ad} \\ \eta_B P_B &= P_{Bd}, \end{aligned} \tag{19}$$

where η is the efficiency, P is the input power, and P_d is the power dissipated in the bolometer element.

If Γ_B is the input reflection coefficient of the bolometer mount whose efficiency is to be determined, the ratio of powers absorbed by the two

[5] See a text on microwave measurements, for example, C. G. Montgomery, Technique of microwave measurements (McGraw Hill Book Co., Inc., New York, N. Y., 1948).

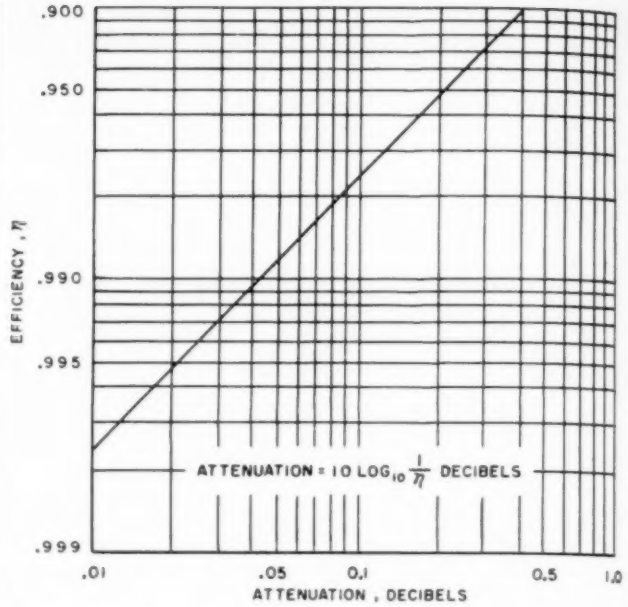

FIGURE 5. *Efficiency of a symmetrical, matched attenuator (or a length of uniform line) terminated in a reflection-free load.*

bolometer mounts or assemblies, (assuming a matched generator) is (see footnote 3)

$$\frac{P_A}{P_B} = \frac{1}{1-|\Gamma_B|^2} = \frac{(\sigma_B+1)^2}{4\sigma_B}. \tag{20}$$

The efficiency of the second bolometer mount is

$$\eta_B = \frac{P_A}{P_B} \frac{P_{Bd}}{P_{Ad}} \eta_A = \frac{(\sigma_B+1)^2}{4\sigma_B} \frac{P_{Bd}}{P_{Ad}} \eta_A, \tag{21}$$

where σ_B is the VSWR corresponding to $|\Gamma_B|$.

An error in measuring σ_B will cause an error in determining η_B, but fortunately the error is small in most practical cases. For example, if σ_B is determined to be 1.20 with an accuracy of ± 2 percent, the corresponding error in η_B is approximately ± 0.2 percent.

4. Discussion of Errors

An accurate knowledge of the efficiency of bolometer mounts used for microwave power measurement is essential to accurate power measurement. For this reason, it is felt that a detailed discussion of the error in measuring efficiency is desirable.

Certain sources of error seem to be common to most measurements at high frequency. Among these are instability of oscillators and amplifiers, unwanted frequency modulation (FM), spurious amplitude modulation (AM) and harmonics in the generator output, pulling of the oscillator by changes in loading, erratic or unknown detector characteristics, errors in measuring the detector output, impedance mismatches at junctions, and mechanical

instability of the components. Error from these sources is minimized by careful instrumentation and the use of recognized good practice in measurement techniques. For example, the stability of electronic equipment is improved by using voltage-stabilized power supplies and by avoiding ambient temperature variations. Oscillator pulling is minimized by the use of nonreciprocal transmission-line elements or attenuator pads with at least 20-db attenuation. Unwanted FM is reduced by careful modulation practices or by the use of high-Q transmission cavities to attenuate undesired side bands. Parasitic oscillations, causing spurious AM, can be eliminated by usual procedures, e. g., damping, shielding; and minimizing feedback. Low-pass filters are used to reduce the harmonic output of generators. Detectors can be calibrated before use or the need for known detector characteristics may be avoided by use of calibrated attenuators. Matching transformers can be used to reduce impedance mismatches, and careful attention to reducing movement of the components will reduce mechanical instability.

After the above precautions are taken, observations should be made to verify the desired conditions. For example, the generator output can be observed with a spectrum analyzer to verify the reduction in unwanted FM and spurious AM. The oscillator-output amplitude and frequency can be monitored during load changes to observe pulling, and the detector output can be monitored with a continuous recorder to observe system stability.

Additional sources of error, which can be minimized by careful instrumentation and experimental procedure, are instability of the bolometer bias supply, inaccuracy of resistance measurement, mechanical irregularities in the slotted section and traveling probe, excessive coupling, and incorrect position of the probe. The use of heavy-duty, low-discharge storage batteries will generally provide a stable bias supply.

Resistance R_1, R_2, and R_3 are measured at direct current and assumed to be the same at UHF or microwaves. It was pointed out by Kerns (see footnote 2), and can be seen from eq (4), that even if the d-c resistances are multiplied by a constant real factor, there will be no error in efficiency. The effect of random errors in resistance measurement upon the efficiency is the same as the random errors in VSWR measurements, discussed in section 2. It was seen that an error in VSWR between the limits ± 0.2 percent will produce an error in efficiency between the limits of approximately ± 1 percent.

Resistance measurements between 100 and 300 ohms can be made with an accuracy of approximately ± 0.05 percent with a good Wheatstone bridge. The corresponding error in efficiency would be approximately ± 0.25 percent.

The choice of a slotted section and traveling probe is important in adjusting Γ_G and Γ_2 for minimum value, and in approximating the assumed uniform, lossless line or waveguide.

The error caused by excessive probe coupling is difficult to evaluate analytically (see eq (8) and (9)). However, it is possible to determine experimentally when the probe is sufficiently decoupled by making a series of efficiency measurements, each with a diminshing value of probe coupling. When there is no further appreciable change in the measured efficiency, the probe has been sufficiently withdrawn. Another method of checking the effect of probe coupling consists in making two efficiency measurements, one with the probe set to the position for maximum response corresponding to a bolometer resistance R_1, and the other with the probe set to the position for maximum response when the bolometer resistance is R_3. If nothing else is changed, the two probe positions are separated by approximately $\lambda/4$, so that the phase of the reflection from the load as seen at the probe position differs by approximately 180 degrees in the two cases. An example of this method is given in table 1, where it is assumed that the average of the two efficiency measurements closely approximates the correct efficiency with the probe sufficiently decoupled. This assumption was found to be valid for small variations in efficiency.

It is possible to evaluate the effect of certain sources of error analytically. The error in measurement of the relative voltage output of the probe, the incorrect positioning of the probe, the generator and load mismatch, and the curvature of the input reflection coefficient locus can be taken into account if the resulting error in efficiency is small.

If ϵ_1, ϵ_2, and ϵ_3 are the errors made in measuring the probe relative voltages E_{P1}, E_{P2}, and E_{P3}, respectively, the error in efficiency from this source alone is approximately

$$\epsilon \approx \frac{-1}{K_1 - K_3}\left[\frac{K_1(1-K_3)}{(K_1-1)}(\epsilon_1-\epsilon_2)+\frac{K_3(K_1-1)}{(1-K_3)}(\epsilon_2-\epsilon_3)\right]. \tag{22}$$

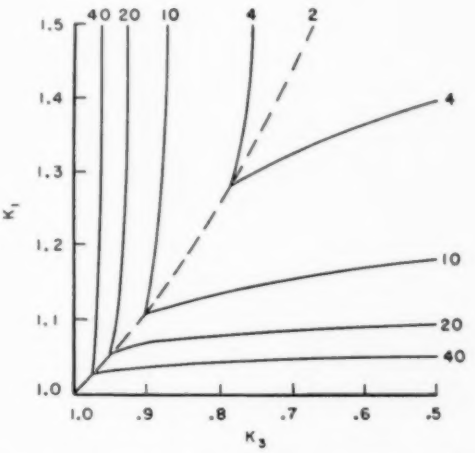

FIGURE 6. *Factor by which the random error in measuring the relative output voltage of the probe is multiplied in order to obtain the corresponding error in efficiency.*

If the individual errors lie within the range indicated by $|\epsilon_1|=|\epsilon_2|=|\epsilon_3|\leq\epsilon'$, the maximum error in efficiency would be less than

$$\epsilon=\pm\frac{2K_1(1-K_3)}{(K_1-1)(K_1-K_3)}\epsilon' \text{ or } \epsilon=\pm\frac{2K_3(K_1-1)}{(1-K_3)(K_1-K_3)}\epsilon', \tag{23}$$

whichever is largest. A graph of this relationship is shown in figure 6. Using a 200-ohm barretter, the limiting values of K_1 and K_3 were determined to be approximately 1.33 and 0.75. Referring to figure 6, with ϵ' assumed equal to ± 0.1 percent, the error in efficiency would be less than ± 0.4 percent. As this is a random error, improved accuracy can be obtained by averaging the results of a number of measurements.

An analysis of the error in efficiency caused by generator and load mismatch, curvature of the reflection coefficient locus, and incorrect probe position yields, after some manipulation, a correction factor to apply to eq (13). It is

$$\zeta_2\approx\left\{1+\left[\left(\frac{1-K_3}{K_1-K_3}\right)\frac{\alpha^2}{2K_1}+\left(\frac{K_1-1}{K_1-K_3}\right)\frac{(\delta+\alpha)^2}{2K_3}+\frac{\delta^2}{2}\frac{(K_1-1)(1-K_3)}{(K_1-K_3)^2}+\frac{(1-K_1K_3)}{(K_1-1)(1-K_3)}|\Gamma_2|\cos\psi_2\right.\right.$$
$$\left.\left.-\frac{1}{(K_1-1)}|\Gamma_2|\cos(\psi_2-\alpha)+\frac{1}{(1-K_3)}|\Gamma_2|\cos(\psi_2-\delta-\alpha)-\frac{K_1(1-K_3)}{(K_1-K_3)}|\Gamma_G|\cos(\psi_G+\alpha)\right.\right.$$
$$\left.\left.-\frac{K_3(K_1-1)}{(K_1-K_3)}|\Gamma_G|\cos(\psi_G+\delta+\alpha)\right]\right\} \tag{24}$$

where ψ and ψ_2 are the angular arguments of Γ_G and Γ_2, respectively, and α represents twice the angular error ($2\beta\Delta l$) in setting the probe to its correct position. (Δl is the distance the probe position is in error.)

In the derivation of eq (24) approximations were made (very small higher-order terms were neglected), assuming that $|\Gamma_G|<0.005$, $|\Gamma_2|<0.005$, $\delta<0.1$, and $\alpha<0.1$. The magnitude of the error represented by eq (24) can be illustrated by considering some of the sources of error separately. For example, if $\delta=\alpha=0$,

$$\zeta_2\approx 1-|\Gamma_G|\cos\psi_G+|\Gamma_2|\cos\psi_2. \tag{25}$$

If $|\Gamma_G|=|\Gamma_2|=0.005$, the total mismatch error lies between the limits ± 1 percent.

If $\Gamma_G=\Gamma_2=0$,

$$\zeta_2\approx 1+\frac{1}{2(K_1-K_3)}\left[\left(\frac{1-K_3}{K_1}\right)\alpha^2+\left(\frac{K_1-1}{K_3}\right)(\delta+\alpha)^2+\frac{(K_1-1)(1-K_3)}{(K_1-K_3)}\delta^2\right]. \tag{26}$$

A graph of the effect of changing the probe position upon the calculated efficiency is shown in figure 7

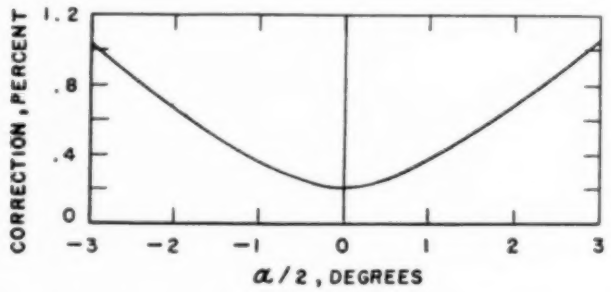

FIGURE 7. *Effect of varying probe position upon the efficiency correction according to equation (26).*

for $K_1=1.0676$, $K_2=0.826$, and $\delta=5°$.

If $\Gamma_G=\Gamma_2=\alpha=0$, eq (24) reduces to eq (15), as represented by figure 4.

5. Experimental Results

The efficiencies of two commercially available bolometer mounts were measured at 600, 1,000, 2,000, and 3,000 Mc. The efficiency of a commercially available tunable bolometer mount (A) was measured first, and then the efficiency of a commercially available bolometer mount (B) was determined from comparative power measurements. The data obtained in a typical measurement of the efficiency of a bolometer mount is shown in table 1. It was found that the efficiency of the tunable bolometer mount remained at approximately 96 percent over the above frequency range, while the efficiency of mount B decreased with rising frequency, as shown in figure 8. Because only one of each of the two types of mounts was investigated, the measured efficiencies are not necessarily representative of these types of bolometer mounts.

TABLE 1.—*Typical efficiency measurement at 1,000 Mc.*

K	$R_1=150$ ohms		$R_1=250$ ohms	
	R_n	E_{pn}	R_n	E_{pn}
1	150.0	1.270	250.0	1.277
2	200.0	1.119	200.0	1.155
3	250.0	1.000	150.0	1.000

In each case, the probe was in position for maximum response when $R=R_1$.
$C=16.00$ (calculated from eq (4))
$\eta=0.951$ (measured when $R_1=150$ ohm)
$\eta=0.946$ (measured when $R_1=250$ ohm)
$\eta=0.948$ (average of above two values)
$\eta_{F\text{-}B}=0.988$ (measured)
$C_1=1.002$ (correction for locus curvature)
$\eta_A=0.962$ ((mount A) calculated from eq (18))
$P_{Ad}=0.807$ mw,
$P_{Bd}=0.823$ mw,
$\sigma_B=1.020$ (measured)
$\eta_B=0.981$ ((mount B) calculated from eq (21)).

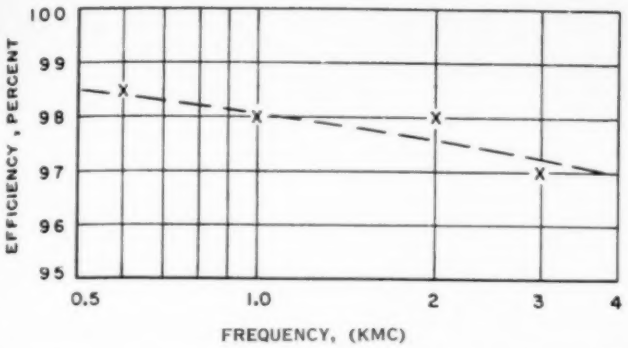

FIGURE 8. *Measured efficiency of a coaxial bolometer mount B.*

TABLE 2.—*Estimate of limits of error in single efficiency measurement*

Principal sources of error	Approximate limits of error in efficiency
	%
Measurement of $\eta_{P\text{-}B}$	±0.5
Measurement of probe voltage	±.4
Measurement of resistances	±.2
Generator mismatch	±.1
Load mismatch	±.1
Estimated limits of error in single efficiency measurement of tunable bolometer mount	±1.3
Measurements of power	±0.2
Measurement of VSWR	±.1
Estimated limits of error in single efficiency measurement of untuned bolometer mount	±1.6

An approximate evaluation of the error in measuring efficiency is given in table 2. It represents an estimate of the limits of error in a single measurement of efficiency. The actual error can be considerably less than this, if the effect of random errors is reduced by averaging the results of a number of measurements. A further reduction of error could be obtained by use of better equipment and improved measuring techniques.

6. Appendix

It will be shown that the locus of the input voltage reflection coefficient of a lossless, tuned, linear, passive, two-terminal-pair network terminated in loads having real reflection coefficients is a straight line passing through the origin.

The lossless condition requires that [6]

$$S^*S=1, \tag{27}$$

where S represents the scattering matrix of the network, S^* is its complex conjugate, and their product equals the unit matrix. Solution of this equation for a two-terminal-pair network yields the relationships

$$\begin{aligned} &|S_{12}|^2=1-|S_{11}|^2=1-|S_{22}|^2\equiv 1-S^2 \\ &2\psi_{12}=\psi_{11}+\psi_{22}\pm\pi, \end{aligned} \tag{28}$$

where ψ represents the angular argument of a scattering coefficient and $S=|S_{11}|=|S_{22}|$.

The input reflection coefficient of a two-terminal-pair network terminated in a load having a real reflection coefficient $|\Gamma_L|$, is

$$\Gamma=S_{11}+\frac{S_{12}^2|\Gamma_L|}{1-S_{22}|\Gamma_L|}. \tag{29}$$

Because the network is matched ($\Gamma=0$) when terminated in a load having a reflection coefficient Γ_{L2},

$$S_{11}=-\frac{S_{12}^2|\Gamma_{L2}|}{1-S_{22}|\Gamma_{L2}|}. \tag{30}$$

Combining eq (28) and eq (30),

$$Se^{j\psi_{11}}=S^2|\Gamma_{L2}|e^{j(\psi_{11}+\psi_{22})}-(1-S^2)|\Gamma_{L2}|e^{j2\psi_{12}} \tag{31}$$

or

$$Se^{j\psi_{11}}=|\Gamma_{L2}|e^{j(\psi_{11}+\psi_{22})}.$$

It is evident that $S=|\Gamma_{L2}|$ and $\psi_{22}=0$ for the above lossless, tuned, two-terminal-pair network. Substituting the results of eq (28) and eq (31) into eq (29), the input reflection coefficient is

$$\Gamma=\frac{|\Gamma_{L2}|-|\Gamma_L|}{1-|\Gamma_{L2}\Gamma_L|}\,e^{j\psi_{11}} \tag{32}$$

As $|\Gamma_L|$ varies, the locus of Γ is a straight line passing through the origin.

It should be noted that the above conditions imposed upon the network (lossless, matched input when terminated in a load having the real reflection coefficient Γ_{L2}) are sufficient to produce a linear input reflection coefficient locus passing through the origin, but are not necessary. The amount of locus curvature is not necessarily an indication of the amount of loss, because it is possible to obtain a straight line locus with a lossy network having $\psi_{22}=0$.

BOULDER, COLO., September 16, 1954.

[6] C. G. Montgomery, R. H. Dicke, and E. M. Purcell, Principles of microwave circuits, p. 149 (McGraw-Hill Book Co., Inc., New York, N. Y., 1948).

Journal of Research of the National Bureau of Standards Vol. 54, No. 6, June 1955 Research Paper 2595

A Study of Some Strontium Aluminates and Calcium-Strontium Aluminate Solid Solutions

Elmer T. Carlson

Tristrontium aluminate hexahydrate, $3SrO \cdot Al_2O_3 \cdot 6H_2O$, was prepared hydrothermally as well as by various methods employing ordinary temperatures and atmospheric pressure. It crystallizes in the isometric system, with a unit cell edge of 13.04 A, and has a refractive index of 1.588. It is isomorphous with $3CaO \cdot Al_2O_3 \cdot 6H_2O$, and a complete series of solid solutions exists between the two. No evidence was found of hexagonal hydrated strontium aluminates analogous to those of calcium. Tristrontium aluminate hexahydrate is stable up to about 454° C at 420 atmospheres water vapor pressure. One of the products of hydrothermal decomposition appears to have the composition $5SrO \cdot 4Al_2O_3$. This compound breaks down on being heated, forming $SrO \cdot Al_2O_3$ and $3SrO \cdot Al_2O_3$. Attempts to prepare a strontia-alumina-silica hydrogarnet were unsuccessful.

1. Introduction

As a result of numerous investigations [1,2,3][1] of chemical reactions related to the hardening of hydraulic cements, it is known that lime and alumina in solution may combine to form an isometric tricalcium aluminate hexahydrate, $3CaO \cdot Al_2O_3 \cdot 6H_2O$. Flint, McMurdie, and Wells [2] showed that this compound is isomorphous with grossularite garnet, $3CaO \cdot Al_2O_3 \cdot 3SiO_2$, and that there is a solid solution series between them.

Although strontia is a relatively minor constituent of cement, the compounds it may be expected to form with silica, alumina, and water, at both ordinary and elevated temperatures, are of some interest. The strontium silicates have been discussed in a previous paper [4]. The existence of tristrontium aluminate hexahydrate has been reported by Brandenberger [5] and by Maekawa [6]. The latter gave data relative to its structure and thermal decomposition.

2. Materials and Procedure

Reagent grade chemicals were used without further purification except in the case of strontium hydroxide, which was recrystallized to remove carbonate. The alumina used was a commercial preparation of gibbsite ($Al_2O_3 \cdot 3H_2O$) containing about 0.30 percent of Na_2O; other impurities were negligible in amount.

Pressure bombs of the Morey type were employed for the hydrothermal work. These were of stainless steel, with a capacity of about 18 ml. The reaction mixture was placed in a platinum thimble, to minimize contamination, and in most cases was made up to a paste with water. Pressure was dependent on the temperature and the quantity of water in the bomb. For temperatures below the critical point, excess liquid water was present, except as otherwise noted. The pressures indicated in the tables were calculated from steam tables for the lower temperatures, and from the pressure-volume-temperature data of Kennedy [7] for the higher temperatures used. The pressure values given are only approximate, as they are not corrected for such calculable factors as thermal expansion of the bomb, nor for the unknown effects of dissolved solids in the liquid and vapor phases and the hydration of the solids. Temperatures were maintained constant within ±2 deg., and the temperatures reported herein are probably accurate within ±5 deg.

In general, the reaction products were filtered, washed with alcohol and ether, and examined with a petrographic microscope. No special precautions were taken to avoid carbonation, either during the hydrothermal treatment or during the filtration. Carbonate, when present, was readily distinguishable under the microscope, but the amounts present were considered negligible. X-ray powder diffraction patterns were made, as needed, using a recording X-ray diffractometer with copper $K\alpha$ radiation. Chemical analyses, when required, were made by conventional methods, water being calculated from the ignition loss, and strontium determined as the sulfate.

3. Experimental Results

3.1. Tristrontium Aluminate Hexahydrate

Tristrontium aluminate hexahydrate ($3SrO \cdot Al_2O_3 \cdot 6H_2O$) was prepared by the following methods: (1) Addition of aluminum chloride solution, slowly, to a boiling solution of strontium hydroxide. The product was well crystallized in the form of cubes and octahedra, many of the latter having rounded knobs at the corners. (2) Action of strontium hydroxide solution on freshly precipitated alumina gel. The reaction was rapid at the boiling temperature, and the product was predominantly cubic in habit, as shown in figure 1. At room temperature the reaction was much slower. (3) Treatment of gibbsite with boiling strontium hydroxide. The product crystallized as dodecahedra, but the reaction was incomplete even after boiling overnight. (4) Hydrothermal treatment of a gibbsite-strontium hydroxide mixture. The reaction was essentially complete after 7 days at 155° C (see table 1). (5) Hydrothermal treatment of anhydrous tristrontium alumi-

[1] Figures in brackets indicate the literature references at the end of this paper.

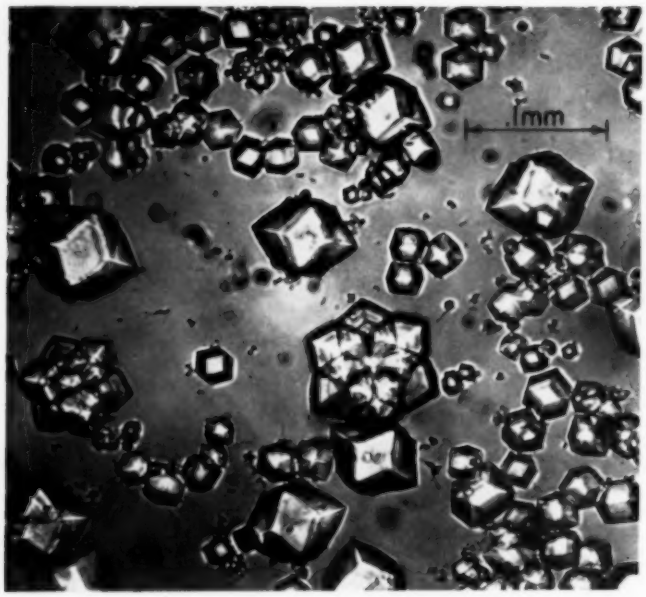

FIGURE 1. *Crystals of* $3SrO{\cdot}Al_2O_3{\cdot}6H_2O$ *prepared by the action of boiling strontium hydroxide solution on alumina gel.*

nate at 164 to 440° C. The crystals were generally cubic in shape, but with rounded edges.

In none of these experiments was there any evidence obtained of a hexagonal aluminate such as is formed by calcium. Apparently strontium forms only the isometric hydrated aluminate.

Tristrontium aluminate hexahydrate is isomorphous with the corresponding calcium compound. This is shown by the X-ray diffraction patterns which indicate the same reflecting planes with such changes in relative intensities as might be expected from isomorphous substitution. There is also a shift in the lines corresponding to a somewhat larger unit cell for the strontium compound. The lattice constant for the latter is calculated to be 13.04 A, as compared with 12.57, the generally accepted figure for the calcium analog. Maekawa [6] reported a unit cell edge of 13.10 A for the strontium compound. The index of refraction determined in this study was 1.588, in agreement with the figure reported by Maekawa.

The hydrothermal decomposition of $3CaO{\cdot}Al_2O_3{\cdot}6H_2O$ to $4CaO{\cdot}3Al_2O_3{\cdot}3H_2O$ was reported by Thorvaldson [8], and confirmed by Peppler and Wells [9], who placed the decomposition temperature at about 215° C in the presence of saturated steam. The strontium compound, $3SrO{\cdot}Al_2O_3{\cdot}6H_2O$, proved to have a higher range of stability, but the nature of the breakdown and the conditions affecting it are not at all clear. Experiments intended to be duplicates sometimes gave rise to quite dissimilar products. Apparently the decomposition may occur in at least three different ways.

The first consists of a breakdown to $Sr(OH)_2$ and an unidentified crystalline compound. This occurred incompletely in experiment 9, and completely in experiments 13 and 14, table 1. In experiment 9, the temperature was 305° C, and there was no water in the reaction vessel except the small amount resulting from the decomposition. The reaction was still incomplete after 4 days. In experiments 13 and 14, the reaction appeared to be complete after 7 days at about 450° C. In this pair of experiments the amount of water in the vessel, and hence the pressure, was greater in experiment 14 than in No. 13, but the results were the same. The oven-dried charge was weighed before and after the hydrothermal treatment to determine the loss of water from the solid. Consideration of hypothetical reactions that would result in a water loss approximating that observed (3.4 moles) leads to the conclusion that the unknown phase is either an anhydrous form of alumina or a strontium aluminate, possibly a low hydrate, relatively low in strontium. Its X-ray diffraction pattern does not fit any of the published patterns for anhydrous forms of alumina or the known strontium aluminates. It dissolves readily in N/20 HCl, hence, it cannot be separated from the strontium hydroxide by this means. This decomposition mechanism appears to be favored by low pressure.

A second process involves the formation of an anhydrous strontium aluminate believed to have the

TABLE 1. *Hydrothermal synthesis and decomposition of tristrontium aluminate hexahydrate*

Experiment	Reactants (solid)	Temperature	Pressure	Time	Products
		°C	*atm*	*Days*	
1	$3(Sr(OH)_2{\cdot}8H_2O)+Al_2O_3{\cdot}3H_2O$	155	5	7	$3SrO{\cdot}Al_2O_3{\cdot}6H_2O$.
2	do	452	410	7	$3SrO{\cdot}Al_2O_3{\cdot}6H_2O$ (reaction incomplete).
3	$3SrO{\cdot}Al_2O_3$	164	5	3	$3SrO{\cdot}Al_2O_3{\cdot}6H_2O$.
4	do	303	90	4	Do.
5	do	440	380	1	Do.
6	do	454	420	3	$5SrO{\cdot}4Al_2O_3+Sr(OH)_2$.
7	do	518	560	3	Do.
8	$3SrO{\cdot}Al_2O_3{\cdot}6H_2O$	258	2	4	$3SrO{\cdot}Al_2O_3{\cdot}6H_2O$ (no apparent change).
9	do	305	2	4	$3SrO{\cdot}Al_2O_3{\cdot}6H_2O+Sr(OH)_2$+an unidentified phase.
10	do	397	40	7	$3SrO{\cdot}Al_2O_3{\cdot}6H_2O+Sr(OH)_2$+"$3SrO{\cdot}Al_2O_3{\cdot}1.5\ H_2O$"+an unidentified phase; lost 2.9 moles H_2O.
11	do	402	130	7	$3SrO{\cdot}Al_2O_3{\cdot}6H_2O$; probably some $Sr(OH)_2$.
12	do	402	280	4	$3SrO{\cdot}Al_2O_3{\cdot}6H_2O$ (no apparent change).
13	do	453	40	7	$Sr(OH)_2$+unidentified phase; lost 3.4 moles H_2O.
14	do	449	150	7	$Sr(OH)_2$+unidentified phase; lost 3.4 moles H_2O.
15	do	508	540	8	$5SrO{\cdot}4Al_2O_3+Sr(OH)_2$.
16	do	513	550	8	"$3SrO{\cdot}Al_2O_3{\cdot}1.5\ H_2O$"; small amounts of $Sr(OH)_2$ and an unidentified phase; lost 4.2 moles H_2O.

composition $5SrO{\cdot}4Al_2O_3$. Because of its coarse crystalline habit it can be separated readily from the matrix of strontium hydroxide. It will be described more completely in the following section. As indicated in table 1, this compound was obtained at temperatures ranging from 454° to 518° C (experiments 6, 7, 15).

The third process of decomposition is exemplified by experiment 16 in table 1. The conditions here were intermediate between those of experiments 7 and 15, both of which yielded the 5:4 compound described above, but in No. 16 the result was quite different. The major part of the product, perhaps 90 percent, consisted of isotropic crystals, similar in size to those of the original material, but having a refractive index of 1.603. A very sharp X-ray diffraction pattern was obtained, the spacings indicating a body-centered cubic lattice with unit cell edge of 9.47 A. The pattern also contained a few very weak lines of $Sr(OH)_2$ and one weak unidentified line. From microscopic and X-ray evidence, it was estimated that the preparation was about 90 percent one phase. The water remaining in combination amounted to about 1.8 moles. An arbitrary allowance for the water in the $Sr(OH)_2$ reduces this to about 1.5 moles, from which the composition of the new crystalline phase is concluded to be $3SrO{\cdot}Al_2O_3{\cdot}1.5H_2O$. Numerous unsuccessful attempts were made to duplicate preparation 16. The X-ray patterns for No. 10, and for at least one other preparation not recorded in table 1, showed the presence of the same compound, but mixed with other phases. Neither of these was sufficiently pure to permit a determination of the composition; hence, the formula is not established with certainty.

The fact that the hypothetical compound $3SrO{\cdot}Al_2O_3{\cdot}1.5H_2O$ is not readily obtained may indicate that it is not very stable. As a reasonable explanation for the conflicting data on the decomposition of $3SrO{\cdot}Al_2O_3{\cdot}6H_2O$ under hydrothermal conditions it is suggested that the third process described, involving merely a loss of water, may actually occur first, followed more or less quickly by a breakdown to strontium hydroxide and some form of alumina or anhydrous strontium aluminate, and finally by a recombination to the anhydrous $5SrO{\cdot}4Al_2O_3$.

The decomposition of the hexahydrate in air has not been thoroughly studied, but differential thermal analysis indicates that the water is driven off between 280° and 700° C. Determination of free strontia by the glycerol-alcohol method [10] showed evidence of some liberation of strontia after an hour's heating at 400° C, but none after an hour at 700° C. X-ray diffraction analysis proved that the sample held at 700° had been converted to anhydrous tristrontium aluminate.

3.2. $5SrO{\cdot}4Al_2O_3$

Among the products of the hydrothermal decomposition of $3SrO{\cdot}Al_2O_3{\cdot}6H_2O$ at 454 to 518° C, the one most readily distinguished appeared in the form

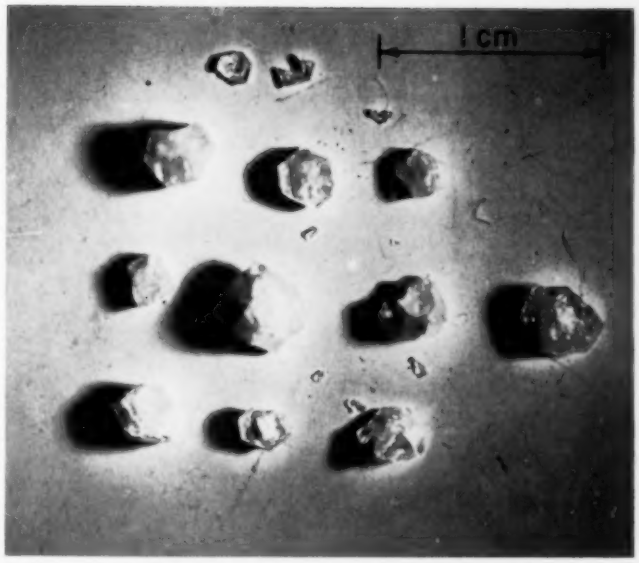

FIGURE 2. *Crystals of* $5SrO{\cdot}4Al_2O$.

of short hexagonal prisms up to 2 mm in size (see fig. 2). Because of the large size of the crystals, they could readily be separated by hand from the rest of the material (consisting of strontium hydroxide and sometimes undecomposed $3SrO{\cdot}Al_2O_3{\cdot}6H_2O$) and cleaned by washing with dilute HCl. Analysis showed that the compound is anhydrous, but there is some doubt as to the correct formula. From the analyses of three preparations, the calculated ratio of SrO to Al_2O_3 ranged from 1.22 to 1.28. A ratio of 1.25 would correspond to the formula $5SrO{\cdot}4Al_2O_3$, which therefore is considered to be the most probable. This does not correspond to any previously reported compound. An attempt to prepare a compound of this ratio by heating the mixed oxides in air resulted in a mixture of $SrO{\cdot}Al_2O_3$ and $3SrO{\cdot}Al_2O_3$.

Differential thermal analysis of a sample of the 5:4 aluminate revealed very small endothermic effects at 120, 280, and 480° C. The first of these may indicate the expulsion of water from a trace of strontium hydroxide occluded in the crystals. The other two may be associated with a breakdown of the structure. X-ray analysis of the sample after it had been heated up to 1,450° C showed only $SrO{\cdot}Al_2O_3$ and $3SrO{\cdot}Al_2O_3$. The heat effects were not observed on reheating, but a new endothermic break appeared at 675°. The effect at 675° appears to be due to an inversion characteristic of monostrontium aluminate, $SrO{\cdot}Al_2O_3$, as it was duplicated in the heating curve of a sample of the latter compound.

The following optical properties of the 5:4 strontium aluminate were determined: Refractive indices, $\omega = 1.644$ and $\epsilon = 1.638$; character uniaxial negative. The X-ray diffraction pattern is given in table 2, together with a pattern for a sample of $SrO{\cdot}Al_2O_3$. The latter was prepared by sintering a mixture of strontium carbonate and gibbsite, followed by fusion in an oxygen blast. It may be noted that the two patterns are quite dissimilar, indicating that the 5:4

compound is not merely a solid solution of SrO in $SrO \cdot Al_2O_3$, as might have been inferred.

TABLE 2. *Interplanar spacings and relative intensities of X-ray diffraction lines for certain strontium aluminates*

$3SrO \cdot Al_2O_3 \cdot 6H_2O$			$5SrO \cdot 4Al_2O_3$		$SrO \cdot Al_2O_3$	
hkl *	*d*	*I*	*d*	*I*	*d*	*I*
	A		*A*		*A*	
211	5.32	93	4.53	31	6.09	5
321	3.48	86	4.47	41	5.14	3
400	3.26	18	3.68	30	4.44	58
420	2.92	100	3.59	2	4.41	30
332	2.78	2	3.48	29	4.02	13
422	2.66	21	3.25	83	3.91	14
510	2.56	10	3.18	100	3.85	11
521	2.381	60	3.05	24	3.54	9
440	2.305	8	2.98	88	3.35	4
611	2.115	64	2.84	24	3.14	100
631	1.924	5	2.75	62	3.05	82
444	1.882	12	2.71	32	2.98	73
710	1.845	2	2.63	22	2.57	45
640	1.808	35	2.52	6	2.55	71
721	1.774	13	2.48	3	2.47	15
642	1.743	26	2.41	10	2.42	17
732	1.656	13	2.34	7	2.41	14
800	1.630	5	2.30	7	2.37	6
653	1.559	4	2.26	7	2.33	5
840	1.458	7	2.20	66	2.32	6
842	1.422	17	2.16	81	2.224	22
921	1.406	9	2.11	14	2.213	10
664	1.390	6	2.10	5	2.205	16
932	1.345	7	2.055	33	2.197	15
941	1.317	2	2.051	46	2.188	13
10-1-1	1.291	3	2.007	3	2.155	16
10-2-0	1.278	2	1.971	21	2.141	8
10-3-1	1.243	7	1.966	12	2.106	20
10-4-0	1.210	12	1.946	40	2.027	6
10-3-3	1.200	3	1.909	3	2.010	14
10-4-2	1.190	15	1.881	43	1.953	18
11-2-1	1.162	10	1.868	8	1.926	25
8-8-0	1.152	4	1.862	5	1.911	8
11-3-2	1.126	4	1.841	5	1.901	11
9-6-5	1.094	3	1.778	1	1.867	13
			1.758	13		
			1.742	9		
			1.719	15		
			1.710	5		
			1.651	3		
			1.631	21		
			1.617	2		
			1.606	19		
			1.597	7		
			1.583	12		
			1.567	10		
			1.555	2		
			1.512	4		
			1.510	6		
			1.504	8		
			1.493	3		
			1.479	9		
			1.425	1		
			1.407	1		
			1.390	15		
			1.379	13		
			1.374	3		
			1.366	3		
			1.349	4		
			1.332	8		
			1.326	8		
			1.298	3		

* Where more than one set of indices is possible, only one is given.

3.3. $3CaO \cdot Al_2O_3$-$3SrO \cdot Al_2O_3$ Solid Solutions

The existence of a strontium compound isomorphous with tricalcium aluminate hexahydrate having been established, it was of interest to try to prepare members of a solid solution series intermediate between the two. For this purpose anhydrous sinters were prepared of $3CaO \cdot Al_2O_3$, $3SrO \cdot Al_2O_3$, and three intermediate compositions having CaO:SrO ratios of 3:1, 1:1, and 1:3, respectively. These were prepared by mixing the alkaline earth carbonates with gibbsite in the desired proportions and heating at 1,450° C. The products were ground and reburned at 1,470 to 1,500°, but were still not completely homogenous. X-ray powder diffraction patterns were all similar, exhibiting a regular shift in passing from the calcium to the strontium compound. The end members of the series have been shown to belong to the cubic system [11]. On this basis, the unit cell dimension was calculated from the spacings. The relation between composition and unit cell size is shown in figure 3. The ratio of unit cell edge of the strontium compound to that of the calcium compound is 1.038.

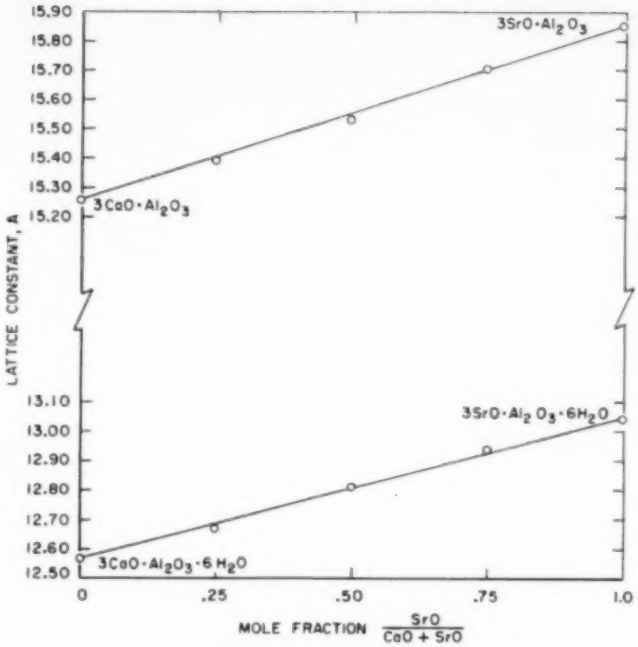

FIGURE 3. *Dimensions of unit cells for members of the* $3CaO \cdot Al_2O_3$—$3SrO \cdot Al_2O_3$ *solid-solution series and the* $3CaO \cdot Al_2O_3 \cdot 6H_2O$—$3SrO \cdot Al_2O_3 \cdot 6H_2O$ *solid-solution series.*

3.4. $3CaO \cdot Al_2O_3 \cdot 6H_2O$-$3SrO \cdot Al_2O_3 \cdot 6H_2O$ Solid Solutions

The anhydrous sinters described above were treated hydrothermally at about 160° C. The product in each case was isotropic, and the X-ray diffraction patterns formed a regular series, as in the case of the anhydrous sinters. The relation between composition and unit cell edge is shown in figure 3. The relationship is linear, as was the case with the anhydrous solid solution series, and the ratio of the lattice constants for the end members is 1.037.

An attempt was made to prepare an intermediate $3(Ca,Sr)O \cdot Al_2O_3 \cdot 6H_2O$ composition by direct hydrothermal treatment of the mixed oxides. This was unsuccessful. The X-ray pattern of the product indicated two separate solid solution members, one close to the calcium and the other to the strontium end. It is reasonable to assume that the strontia reacted first, by reason of its higher solubility, leaving a solution richer in lime to react later.

It has been noted that under hydrothermal conditions the calcium aluminate hydrate breaks down at about 215° C to form $4CaO{\cdot}3Al_2O_3{\cdot}3H_2O$ and $Ca(OH)_2$, also that the strontium compound may decompose at somewhat higher temperatures, forming a variety of products. It remains to be seen how the intermediate members behave in this respect. Table 3 (Nos. 17 to 24 and 5, 6) gives the data for pairs of hydrothermal experiments bracketing the decomposition temperatures for the 5 compositions described above. The data for experiments 5 and 6, table 1, are repeated here for comparison. The range of stability increases with the strontium content. The mechanism of the decomposition of the third and fourth members of the series is still somewhat obscure, but for the second member, with strontia constituting one-fourth of the alkaline earth present, the course of the reactions is fairly clear. The data for experiments 25 to 28 in table 3 serve to illustrate the nature of the process. In this series the temperature was kept approximately constant, while the duration of treatment was varied. The temperature used was well above the decomposition temperature (approximately 228° C, as indicated by experiment 20). The data for No. 25 show that the anhydrous sinter was essentially all converted to the hexahydrate during the 4-hour period in which the temperature was raised from room temperature to 265° C. No. 26 was held for 90 min at 278° following the warmup period. This preparation gave an X-ray pattern indicating two distinct isometric phases of the same structure but different lattice constants. The predominant phase had a unit cell edge of 12·66 A, substantially in agreement with the size of the cell in preparations 19 and 20. The other phase had a unit cell edge of 12·83 A, indicative of a much higher strontium content (see fig. 3). Lines of calcium hydroxide and $4CaO{\cdot}3Al_2O_3{\cdot}3H_2O$ were also present in the X-ray pattern. The data for No. 27 indicate increased conversion to the strontium-rich phase with longer hydrothermal treatment. Finally, after 7 days (No. 28) the original isometric phase had disappeared. It should be noted that the change from the calcium-rich to the strontium-rich isometric phase is abrupt; that is, there is not a gradual shift in the position of the X-ray lines. It may reasonably be concluded that the initial calcium-rich phase (probably formed during the warmup period) goes into solution, from which $Ca(OH)_2$, $4CaO{\cdot}3Al_2O_3{\cdot}3H_2O$, and the strontium-rich isometric phase are then precipitated. The slight variation in the reported unit cell size for the initially-formed isometric phase, 12·65 to 12·69 A, is believed not to be significant. On the other hand, the range from 12·83 to 12·92 A for the other phase is rather too large to be attributed to experimental error. It probably reflects an actual difference in composition, but whether systematic or accidental cannot be determined without further data.

The mechanism of decomposition is believed to be essentially the same for the other two calcium-strontium compositions, in the initial stage. Calcium hydroxide was identified in the products of experiments 22 and 24, table 3, and there were some crystals having the general appearance and the refractive index of $4CaO{\cdot}3Al_2O_3{\cdot}3H_2O$. The latter compound was insufficient in quantity to affect the X-ray pattern. At higher temperatures the X-ray patterns showed evidence of the presence of other phases which were not identified. The reactions giving rise to these were not investigated further.

TABLE 3 *Results of hydrothermal treatment of calcium-strontium aluminate sinters* ($3RO{\cdot}Al_2O_3$)

Experiment	Molar ratio SrO:(SrO+CaO)	Temperature	Pressure	Time	Products
		°C	atm		
17	0	216	20	7 days	$3CaO{\cdot}Al_2O_3{\cdot}6H_2O$.
18	0	225	25	7 days	Mostly $3CaO{\cdot}Al_2O_3{\cdot}6H_2O$; some $4CaO{\cdot}3Al_2O_3{\cdot}3H_2O$ and $Ca(OH)_2$.
19	¼	219	20	7 days	$3RO{\cdot}Al_2O_3{\cdot}6H_2O$.
20	¼	228	25	7 days	$3RO{\cdot}Al_2O_3{\cdot}6H_2O$; trace of $4CaO{\cdot}3Al_2O_3{\cdot}3H_2O$.
21	½	244	35	4 days	$3RO{\cdot}Al_2O_3{\cdot}6H_2O$.
22	½	260	45	7 days	$3RO{\cdot}Al_2O_3{\cdot}6H_2O+Ca(OH)+4CaO{\cdot}3Al_2O_3{\cdot}3H_2O$.
23	¾	315	100	7 days	$3RO{\cdot}Al_2O_3{\cdot}6H_2O$.
24	¾	325	120	7 days	$3RO{\cdot}Al_2O_3{\cdot}6H_2O+Ca(OH)_2+4CaO{\cdot}3Al_2O_3{\cdot}3H_2O$.
5	1	440	380	1 day	$3SrO{\cdot}Al_2O_3{\cdot}6H_2O$.
6	1	454	420	3 days	$5SrO{\cdot}4Al_2O_3+Sr(OH)_2$.
25	¼	265	50	(*)	$3RO{\cdot}Al_2O_3{\cdot}6H_2O$ (single phase a=12.69).
26	¼	278	60	90 min	$3RO{\cdot}Al_2O_3{\cdot}6H_2O$ (2 phases, a=12.66 predominant, and a=12.83); Ca(OH); $4CaO{\cdot}3Al_2O_3{\cdot}3H_2O$.
27	¼	276	60	1 day	$3RO{\cdot}Al_2O_3{\cdot}6H_2O$ (2 phases, a=12.65 and a=12.90, predominant); $Ca(OH)_2$; $4CaO{\cdot}3Al_2O_3{\cdot}3H_2O$.
28	¼	278	60	7 days	$3RO{\cdot}Al_2O_3{\cdot}6H_2O$ (single phase a=12.92); $Ca(OH)_2$; $4CaO{\cdot}3Al_2O_3{\cdot}3H_2O$.

* Cooled immediately after temperature reached 265°; duration of warmup period, 4 hr.

3.5. Attempts to Prepare a Strontia-Alumina-Silica Hydrogarnet

One of the primary aims of the present study was to ascertain whether strontium hydrogarnets analogous to the $3CaO{\cdot}Al_2O_3{\cdot}6H_2O$-$3CaO{\cdot}Al_2O_3{\cdot}3SiO_2$ series could be prepared. Numerous experiments were carried out in an attempt to replace part of the water of $3SrO{\cdot}Al_2O_3{\cdot}6H_2O$ by silica. The methods used were those which have been successfully employed in preparing the calcium hydrogarnets.

Table 4 gives a few representative data indicating the range of experimental conditions and the type of products obtained. Tristrontium aluminate hexahydrate was identified in the products of Nos. 29 to 32 and 37. In every case the unit cell edge, calculated from the X-ray diffraction pattern, was the same as that for the pure compound, within the limits of experimental error. On the basis of analogy with the lime-alumina-silica hydrogarnets [2] it may be estimated that substitution of as little as one-tenth mole of SiO_2 in the structure would result in a measurable change in the lattice constant. It is therefore concluded that little or no silica was taken up into the strontium aluminate hexahydrate structure. Experiment No. 37, unlike the others, was performed

TABLE 4. *Results of experiments with reaction mixtures containing strontia, alumina, silica, and water.*

Experiment	Reactants (solid)	Molar ratio $SrO:Al_2O_3:SiO_2$	Temperature	Pressure	Time	Products
			°C	atm	Days	
29	Glass	3:1:½	151	5	6	$3SrO{\cdot}Al_2O_3{\cdot}6H_2O$ and small amount of unidentified material.
30	do	3:1:½	244	35	6	$3SrO{\cdot}Al_2O_3{\cdot}6H_2O$ and unidentified material, slightly more than in No. 29.
31	do	3:1:1	152	5	7	$3SrO{\cdot}Al_2O_3{\cdot}6H_2O$ and unidentified material; similar to No. 30.
32	$3SrO{\cdot}Al_2O_3{\cdot}6H_2O+SiO_2$ gel	3:1:1	203	16	42	3 $SrO{\cdot}Al_2O_3{\cdot}6H_2O$ and unidentified material.
33	$3SrO{\cdot}2SiO_2{\cdot}4H_2O+Al_2O_3{\cdot}3H_2O$	3:1:2	190	12	7	Unidentified; at least 2 phases present.
34	$Sr(OH)_2{\cdot}8H_2O$+activated kaolin	3:1:2	376	220	7	$SrO{\cdot}SiO_2$ and unidentified material.
35	Glass	3:1:3	249	39	7	Unidentified; at least 2 phases present.
36	$Sr(OH)_2{\cdot}8H_2O+Al_2O_3{\cdot}3H_2O+SiO_2$ gel	3:1:3	300	85	7	$SrO{\cdot}SiO_2$ and unidentified material.
37	$NaAlO_2+Na_2SiO_3+Sr(OH)_2$ (all in solution).		100	1		$3SrO{\cdot}Al_2O_3{\cdot}6H_2O+3SrO{\cdot}2SiO_2{\cdot}3H_2O$.

by boiling a mixed solution of the reactants in a flask at atmospheric pressure. The reaction was complete in a few minutes, and the product consisted of $3SrO{\cdot}Al_2O_3{\cdot}6H_2O$ and $3SrO{\cdot}2SiO_2{\cdot}3H_2O$, both well crystallized. In the experiments at higher temperatures and pressures, the siliceous phases were not identified, except that in certain cases $SrO{\cdot}SiO_2$ was detected both microscopically and by X-ray diffraction analysis. The rest of the lines on the X-ray patterns failed to fit any known patterns for compounds that might conceivably have been present. It is assumed, therefore, that compounds were formed containing all three oxides, SrO, Al_2O_3, and SiO_2, and possibly H_2O. The variation in the optical properties and X-ray patterns indicated that at least 2 and probably 3 such compounds were present in the various preparations. Identification probably would involve a thorough study of the system SrO-Al_2O_3-SiO_2-H_2O, which is beyond the scope of the present investigation.

The essential conclusion to be drawn from this set of experiments is that $3SrO{\cdot}Al_2O_3{\cdot}6H_2O$ will not take up any appreciable amount of silica, but instead will react with silica present in the system to form a strontium silicate or perhaps one or more SrO-Al_2O_3-SiO_2 compounds.

4. Summary

In this investigation of compounds formed in the system strontia-alumina-water, the only hydrated strontium aluminate definitely identified was $3SrO{\cdot}Al_2O_3{\cdot}6H_2O$. This compound was readily prepared by various methods at temperatures ranging from room temperature to 440° C. It crystallizes in the isometric system, with a unit cell of 13.04 A, and has a refractive index of 1.588. It is isomorphous with $3CaO{\cdot}Al_2O_3{\cdot}6H_2O$ and a complete series of solid solutions exists between the two.

The strontium aluminate hydrate decomposes under hydrothermal conditions at temperatures as low as 305° C at 2 atm pressure, and 454° at 420 atm. The products of decomposition appear to depend on both temperature and pressure, but a given set of conditions did not always produce the same results. In a few instances a product was formed which is believed to be a lower hydrate, probably with 1.5 molecules of water. In most cases decomposition occurred with liberation of strontium hydroxide. One of the products in several experiments was a coarsely crystalline anhydrous strontium aluminate having the approximate composition $5SrO{\cdot}4Al_2O_3$. This compound, not previously reported, crystallizes in the form of hexagonal prisms, with refractive indices $\omega=1.644$, $\epsilon=1.638$. It decomposes on heating, with formation of $SrO{\cdot}Al_2O_3$ and $3SrO{\cdot}Al_2O_3$.

The stability range of tristontium aluminate hexahydrate is higher than that of the corresponding calcium compound, which decomposes at about 215° C. Intermediate members of the solid solution series break down at intermediate temperatures, apparently with precipitation of most of the calcium as hydroxide and $4CaO{\cdot}3Al_2O_3{\cdot}3H_2O$, accompanied by formation of a solid solution richer in strontium.

Attempts were made to prepare a strontia-alumina-silica hydrogarnet, but without success. The product obtained had the properties of $3SrO{\cdot}Al_2O_3{\cdot}6H_2O$, indicating that no appreciable amount of silica had been taken into solid solution.

The X-ray diffraction patterns for this study were made by G. M. Ugrinic, the photomicrographs by F. A. Heckman, and the differential thermal analyses by E. S. Newman. The author acknowledges their assistance with thanks.

5. References

[1] T. Thorvaldson, N. S. Grace, and V. A. Vigfusson, Can. J. Res. **1,** 201 (1929).
[2] E. P. Flint, H. F. McMurdie, and L. S. Wells, J. Research NBS **26,** 13 (1941) RP1355.
[3] L. S. Wells, W. F. Clarke, and H. F. McMurdie, J. Research NBS **30,** 367 (1943) RP1539.
[4] E. T. Carlson and L. S. Wells, J. Research NBS **51,** 73 (1953) RP 2433.
[5] E. Brandenberger, Schweiz. mineralog. petrog. Mitt. **13,** 569 (1933).
[6] G. Maekawa, J. Soc. Chem. Ind. Japan **45,** 751 (1943); Chem. Abstr. **43,** 1278 (1949).
[7] G. C. Kennedy, Am. J. Sci. **248,** 540 (1950).
[8] H. Johnson and T. Thorvaldson, Can. J. Res. **21,** 236 (1943).
[9] R. B. Peppler and L. S. Wells, J. Research NBS **52,** 75 (1954) RP2476.
[10] E. G. Swenson and T. Thorvaldson, Can. J. Chem. **30,** 257 (1952).
[11] K. Lagerqvist, S. Wallmark, and A. Westgren, Z. anorg. u. allgem. Chem. **234,** 1 (1937).

WASHINGTON, December 15, 1954.

Journal of Research of the National Bureau of Standards Vol. 54, No. 6, June 1955 Research Paper 2596

A Measurement of the Velocity of Propagation of Very-High-Frequency Radio Waves at the Surface of the Earth

Edwin F. Florman

The velocity of propagation of electromagnetic waves was measured at the surface of the earth, using a radio-wave interferometer operating at a frequency of 172.8 Mc. The measured phase velocity, converted to velocity in vacuum, or the "free-space" value, was found to be 299795.1 ±3.1 km/sec. The uncertainty of ±3.1 km/sec includes a 95-percent confidence interval for the mean, plus an estimated limit to the systematic error of ±0.7 km/sec. Based on a 50-percent confidence interval (probable error of the mean), the uncertainty, including the estimated limit to the systematic error of ±0.7 km/sec, becomes ±1.4 km/sec.

The accuracy with which the free-space phase velocity of radio waves could be measured was limited primarily by the accuracy to which the refractive index of air could be obtained from measured values of pressure, temperature, and relative humidity.

1. Introduction

Measurements of the velocity of propagation of electromagnetic waves have been carried out by a large number of investigators over a long period of time and by various methods [1 to 10].[1] The primary object of their work has been to obtain an accurate value of the "free-space" velocity of electromagnetic waves for use both in theoretical and practical applications of this fundamental constant.

From a study of various methods that could be used to measure the velocity of propagation of radio waves, it was concluded that the radio-wave interferometer principle could be applied to yield field-test results having a high order of accuracy. A VHF radio wave (172.8 Mc) was used in carrying out the phase-velocity measurements covered by this report in order to avoid sky-wave interference, minimize ground effects, and reduce the physical size of the measuring system to dimensions that were convenient for standard distance-survey techniques.

2. Theory and Operational Technique

Determination of the phase velocity of radio waves described in this report was dependent upon the measurement of:

(a) the linear distance, S, between two (radio-signal) receiving points,

(b) the frequency, f, of the radio transmission,

(c) the net change in phase, Φ, of the signals at the two receiving points when the radio transmitter was moved over a prescribed course, and

(d) the average wave index of refraction of the air, n.

The free-space phase velocity, V, of the radio waves in terms of the phase velocity between the two receiving points at the surface of the earth is given by

$$V=f\lambda n=f\frac{S}{\Phi}n, \tag{1}$$

where λ is the wavelength of the radio waves at the earth's surface.

If the source of the radio-wave transmission is more than several hundred wavelengths distant from the receiving points, the effect of the earth's surface on the velocity of propagation of radio waves is small and can be calculated [16]; furthermore, "induction field" effects [21] are negligible under these conditions.

The basic elements of the system used to carry out the phase-velocity measurements are shown in figure 1. R_1 and R_2 are two receiving points, S is the accurately surveyed distance from R_1 to R_2, and T_1 and T_2 are radio transmitters located on the extensions of the straight line through the receivers.

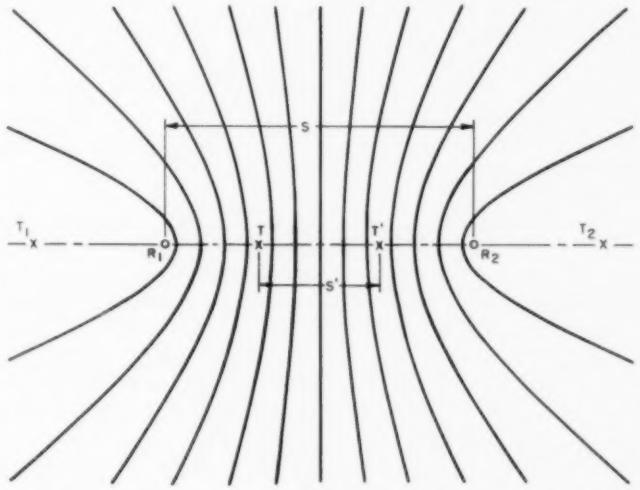

FIGURE 1. *Phase field in the vicinity of two radio receivers.*

[1] Figures in brackets indicate the literature references at the end of this paper.

The family of hyperbolic curves are equiphase contours in the horizontal plane through R_1 and R_2, with these receiving points as foci. In other words, if a radio transmitter is moved along any one of these hyperbolas, the change in phase difference between signals at the receiving points is zero. In the regions of the receiver-line extensions, the hypervolic contours degenerate to the straight lines R_1-T_1 and R_2-T_2.

Referring to figure 1, if a radio transmitter is moved from T to T', on the receiver line, the phase of the signal will be retarded at R_1 and advanced at R_2. Designating the change in phase difference as $2\Phi'$, it is evident that the value of λ in eq (1) is

$$\lambda=\frac{S'}{\Phi'}. \tag{1a}$$

Practical considerations show that the accuracy of the measurement of λ can be improved by increasing the length of the path S'. The limiting case occurs when S' equals S, but it is not feasible to move the radio transmitter from R_1 to R_2 because of radio-receiver overloading and near-zone effects [10, 11, 12, 13, 21] that occur when the radio transmitter is in the vicinity of the receiving points. A study of the equiphase contours in figure 1 shows that moving the radio transmitter from T_1 to T_2, along a path that avoids points R_1 and R_2 by several hundred wavelengths, is equivalent to moving the transmitter from R_1 to R_2, except that in the former case, receiver overloading and near-zone effects are avoided. The net change in phase, 2Φ, which occurs at R_1 and R_2 as the radio transmitter is moved from T_1 to T_2, together with the measured distance S, give a value of λ when substituted in eq (1a).

It should be noted that the path traversed by the radio transmitter must begin on one extension of the receiver line and must end on the other extension of this line.

In order to avoid transporting the radio transmitter around the system, we can use two radio transmitters (of the same frequency) located at the ends of the above path and obtain a measure of Φ by noting the change in phase at the two receiving points when transmission is switched from one radio transmitter to the other. The ambiguity of this measurement can be resolved by making one (preliminary) trip with a radio transmitter halfway around the system and noting the number of whole wavelength changes in phase that occur between the signals at the receiving points.

Furthermore, it is convenient to make the actual phase measurement at an audiofrequency rather than at a radio frequency. This audiofrequency signal can be obtained by heterodyning the radio-frequency signal with another radio-frequency signal differing in frequency by an audiofrequency rate. The phase changes between the resulting audiosignals at the receiving points is the same as the phase changes between the original radio-frequency signals, as explained below.

The phase relationships of the various signals at the receiving points R_1 and R_2 can be determined from the following considerations. With radio transmissions from T_0 and T_1, assuming that the frequency of T_0 is lower than the frequency of T_1, the vector relationship of the signals at R_1 and R_2 will be as shown in figure 2. In this figure the heterodyne-frequency phase is shown as the angle Φ_1, and is equal to the number of degrees by which the phase of the heterodyne-frequency signal at R_1 leads the heterodyne-frequency signal at R_2. Likewise, in figure 3, when T_0 and T_2 are transmitting with the

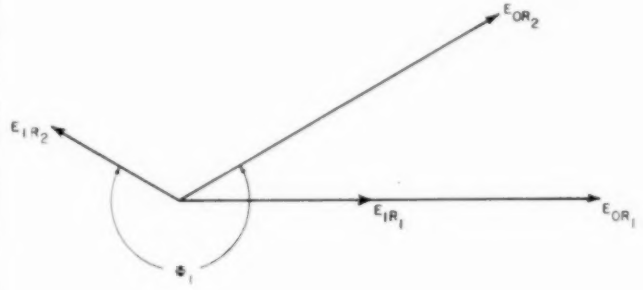

E_{OR_1} = VOLTAGE AT R_1 DUE TO TRANSMISSION FROM T_0
E_{OR_2} = VOLTAGE AT R_2 DUE TO TRANSMISSION FROM T_0
E_{1R_1} = VOLTAGE AT R_1 DUE TO TRANSMISSION FROM T_1
E_{1R_2} = VOLTAGE AT R_2 DUE TO TRANSMISSION FROM T_1

FIGURE 2. *Vector relationship of voltages at receiving points R_1 and R_2 with transmissions from T_0 and T_1.*

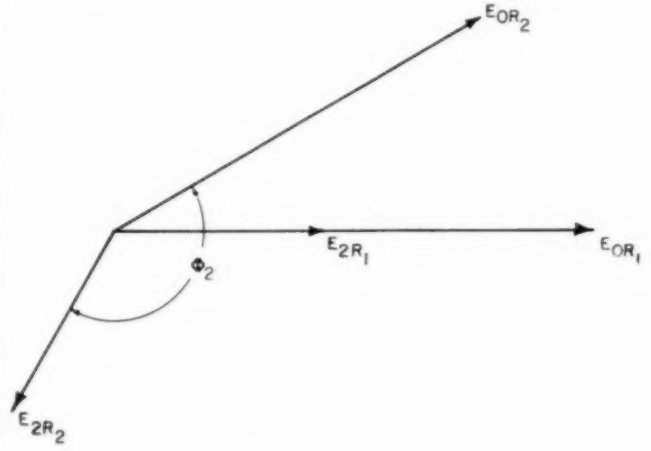

E_{OR_1} = VOLTAGE AT R_1 DUE TO TRANSMISSION FROM T_0
E_{OR_2} = VOLTAGE AT R_2 DUE TO TRANSMISSION FROM T_0
E_{2R_1} = VOLTAGE AT R_1 DUE TO TRANSMISSION FROM T_2
E_{2R_2} = VOLTAGE AT R_2 DUE TO TRANSMISSION FROM T_2

FIGURE 3. *Vector relationship of voltages at receiving points R_1 and R_2 with transmissions from T_0 and T_2.*

frequency of T_0 lower than the frequency of T_2, Φ_2 is the angle by which the heterodyne-frequency signal at R_1 leads the heterodyne-frequency signal at R_2. The change in heterodyne-frequency phase noted between figures 2 and 3 is

$$2\Phi = \Phi_1 - \Phi_2 + 2\pi M, \qquad (2)$$

where M is an integer.

The above considerations apply whether the transmitting frequency of T_0 is higher or lower than the transmitting frequencies of T_1 and T_2.

The phase change given by eq (2) is equal to the change in phase between the radio-frequency signals at R_1 and R_2 when T_1 is moved halfway around the system to the position occupied by T_2; this is seen to be true from the following considerations. If T_1 is moved over a path such that at all times it is at a fixed distance from R_1, then all vectors shown in figures 2 and 3 will remain fixed except E_{1R_2} (which advances and finally becomes colinear with E_{2R_2} in fig. 3), and the angle swept out by E_{2R_2} is equal to the radio-frequency phase change in the signal from T_1 (at R_2) as the transmitter moves halfway around the system; this angle is identical to the angle 2Φ. The ambiguity of the value of Φ must, of course, be resolved by adding the correct number of whole wavelength changes in phase (M), obtained when T_1 is moved halfway around the system. It should be noted that the above considerations involve only relative phase and change in relative phase. It should also be noted that the phases of the transmissions from T_0 to R_1 and R_2 do not affect the value of Φ, provided that these factors remain constant during the time required to measure Φ_1 and Φ_2.

The complete system used to make the phase-velocity measurements is shown in block form in figure 4. As in figure 1, R_1 and R_2 are the two receiving points (antennas) between which the radio-wave phase velocity was measured; the transmission from radio transmitter T_0 combines with the signal from T_1 (or T_2) to produce heterodyne-frequency signals at R_1 and R_2. Radio transmitters T_1 and T_2 were located on the extensions of the straight line through R_1 and R_2 and provided signals on which the phase-velocity measurements were made. Two types of receiving antennas were used: (1) vertically polarized, unbalanced quarter-wave antennas with base at ground level, and (2) balanced horizontally polarized, half-wave antennas approximately $\lambda/4$ above the ground.

The following procedure was used when making a phase-velocity measurement: Radio transmitters T_0 and T_1 were turned on, and the frequency of T_0 was adjusted to 172.801 Mc. The frequency of T_1 was then adjusted to 172.800 Mc in terms of the 1-kc heterodyne-frequency signals appearing in the outputs of the radio receivers at R_1 and R_2. These 1-kc heterodyne-frequency signals were transmitted via the two UHF radio links to the frequency-monitoring scope and the phase-measuring system. The value of Φ_1 (eq 2) was then obtained from the dial of the "manual phase shifter", with this instrument adjusted to give a closed pattern on the "phase monitor oscilloscope." Radio transmitter T_1 was then turned off and the above procedure was repeated, using T_2 as the signal source, to give a value for Φ_2 in terms of a new setting of the dial on the manual phase shifter (and a closed pattern on the phase monitor scope). From the above values of Φ_1 and Φ_2 and eq (2), a value for Φ was obtained, which in turn was used in eq (1) to yield a value for the radio-wave phase velocity between R_1 and R_2 for a frequency of 172.800 Mc.

Figure 4 shows two (parallel) sets of instruments for measuring relative phases and change in phase. The manual phase-shifter–phase-monitor oscilloscope arrangement was used to obtain accurate, routine measurements of Φ_1 and Φ_2; the RC (resistance-capacitance) phase-shifter–phase-meter assembly was used to obtain a recording of the total change in phase when radio transmitter T_1 was moved over a path halfway around the system. This total change in phase was used to resolve the ambiguity in the value of Φ obtained from eq (2).

Figure 5 is a block diagram of the frequency-monitoring system used to adjust and monitor both the frequency of T_0 and the 1-kc heterodyne-signal frequency used in making phase measurements of Φ_1 and Φ_2.

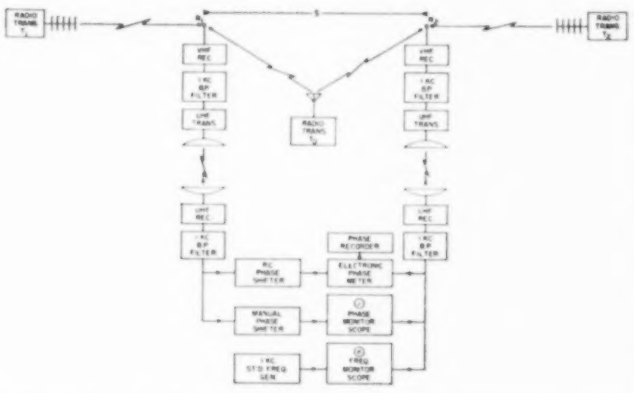

FIGURE 4. *Block diagram of phase-velocity measuring system.*

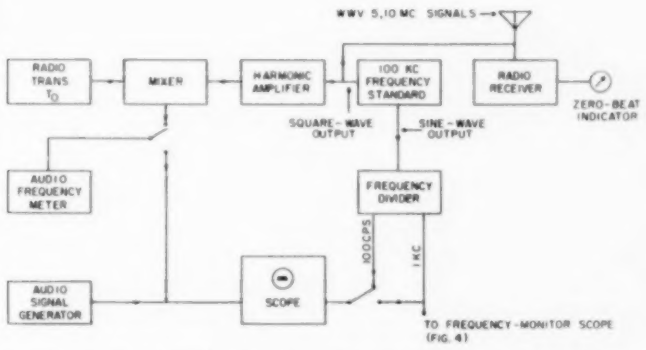

FIGURE 5. *Block diagram of frequency-monitoring system.*

The frequency standard used in this system was a 100-kc crystal oscillator. The frequency of the oscillator was periodically checked and adjusted to ± 1 part in 10^7 by comparing either its fiftieth or its one-hundredth harmonic with the 5- or 10-Mc WWV signal, respectively, by means of a radio receiver. Allowing for the ionospheric doppler effect, it is estimated that the frequency of the WWV signal as received was accurate to 1 part in 10^7. The frequency of radio transmitter T_0 was adjusted to be within 1 part in 10^7 of the 100-kc frequency standard by mixing the output of the T_0 oscillator (7.2000417 Mc) with the seventy-second harmonic of the 100-kc frequency standard to give a mixer output of 41.7 cps. The accuracy of the frequency meter was checked to within 0.5 cps against the 100-cps output from the frequency divider, which in turn was controlled by the 100-kc output from the frequency standard.

As a precautionary measure, the audiosignal generator was used to check the frequency-divider output in order to make sure that the frequency-divider ratios were exactly 100 to 1 and 1,000 to 1.

3. Consideration of Factors Governing Accuracy

The over-all accuracy of the phase-velocity measurements depends upon the accuracy with which the factors in eq (1) can be determined.

The frequency, f, was adjusted in terms of station WWV frequency to within 1 part in 10^7. Allowing for frequency drift in the 100-kc (local oscillator) frequency standard and also for drift of T_0, T_1, T_2 during the short time (approximately 2 min) required to make a phase-velocity measurement, it is estimated that the accuracy of the frequency term in eq (1) was 5 parts in 10^7, or better.

The distance, S, between the receiving points (R_1 and R_2) was measured by means of three standard invar 50-m tapes. These tapes were standardized at the National Bureau of Standards, and the actual survey and calculation of this distance was carried out by using the U. S. Coast and Geodetic survey techniques described in "Manual of Geodetic Triangulation," special publication 247. The standard deviation of the measurements of distance S was 2 parts in 10^6. The calculated straight-line distance between points R_1 and R_2 differs from the great-circle distance over the surface of the earth by less than 1 part in 10^8, a negligible amount when S equals 1,500 m.

The factors involved in the measurement of the phase change Φ are numerous and are listed as follows:

(a) The actual paths traversed by the radio waves at the surface of the earth are curved because of the variation of the index of refraction of the air with altitude [20]. Normal atmospheric conditions are such that the radius of curvature of the radio-wave paths is greater than the radius of the earth, and if we pessimistically estimate that the radius of curvature of the radio rays is equal to one-fifth of the earth's radius, we find that the calculated error in Φ, for a path length of 1,500 m, is of the order of 1 part in 10^7 and, therefore, can be ignored.

(b) Spurious signals from T_1 (and T_2) to receiving points R_1 and R_2 can alter the value of Φ and can cause errors in the measurement of the phase velocity. These spurious signals usually are due to multipath reflections from nearby objects, such as power lines, large metallic objects, mountains, etc. For the conditions under which the phase-velocity measurements listed in this paper were made (using 5-element Yagi transmitting antennas at T_1 and T_2), it was determined experimentally that this multipath effect on Φ was approximately 1 electrical degree, which in turn corresponds to an error in phase-velocity measurement of 1.7 parts in 10^6, for a distance of 1,500 m between R_1 and R_2. The test for multipath phase error consisted of moving each of the radio transmitters T_1 and T_2 along the extensions of the receiving-point line; an oscillating variation of the phase difference between the signals at R_1 and R_2 indicates the presence of and the amount of multipath phase error.

Tests showed negligible multipath phase errors due to the presence of the trucks that housed the equipment and the metal enclosures that housed the radio receivers, but there was definite evidence that sufficient radiation was reflected from nearby mountains (5 to 20 miles distant) to cause the multipath phase error of 1 degree noted above. This phase error was increased to approximately 8 degrees when omnidirectional antennas were used to transmit from T_1 and T_2.

(c) The true value of Φ is the maximum value obtained by moving a radio transmitter from a position on one extension of the line through the receiving points, halfway around the system to the other extension of the receiving-point line. The start and stop points of the path of the moving transmitter on the extensions of the receiving-point line correspond to the fixed positions of radio transmitters T_1 and T_2, respectively. It was found experimentally that the positions of T_1 and T_2, which gave a maximum value for Φ, were on the optical line through receiving points R_1 and R_2. The positioning of T_1 and T_2 was sufficiently accurate to insure that the error in the measurement of Φ was less than 2.5 parts in 10^7. It should be noted that an error in the positioning of T_1 or T_2 has the effect of giving a measured value of Φ that is always smaller than its true value.

(d) The phase velocity of a radio wave varies considerably in the "near-region" [10, 11, 12, 13, 21] of the transmitting antenna. Tests were made to determine the limits of the near-region, and the results indicated that the phase velocity approached a constant value, within 5 parts in 10^7, at a distance of 500 wavelengths or more from the transmitting antenna. Phase-velocity measurements considered in this work were made at a distance of 500 wavelengths, or more, from the transmitting antenna, and hence are sufficiently free of near-region effects.

(e) One source of error in the measurement of Φ was found to be due to spurious pickup by the cables

connected to the receiving antennas at R_1 and R_2. Unfortunately, the existence of this condition was not definitely established until the equipment had been moved from the special field site at which the phase-velocity measurements were carried out. This error was found to vary considerably, depending upon the arrangement of the receiving-antenna cables, and it was not possible to duplicate exactly the original conditions of the phase-velocity measurements; a pessimistic estimate of this error is 5 parts in 10^6. This cable-pickup error applies only to the unbalanced quarter-wave receiving antennas and not to the balanced half-wave antennas.

(f) Tests made on the two VHF radio receivers (connected to receiving points R_1 and R_2) showed that the relative phase of the heterodyne-frequency output was dependent upon the signal level of the radio-frequency input to the receivers and also upon the equivalent percentage modulation of the input signal; hence a phase error was introduced by the radio receivers when transmissions were switched from T_1 to T_2 because of the resultant change in signal levels at R_1 and R_2. Corrections were made for the radio-receiver phase errors in the calculated values of the free-space phase velocities listed in this report. The estimated error in the phase-velocity measurements due to the phase characteristic of the VHF radio receivers was 1 part in 10^6, after proper corrections had been made for these receiver phase characteristics.

(g) A series of comprehensive tests on the system indicated that there was no measurable error due to any form of cross-modulation between any sections of the system. Furthermore, the phase stability and the relative-phase accuracy of the system were found to be sufficiently good to insure a phase-change measurement of Φ, which was accurate to within 1 electrical degree. This accuracy in the measured value for Φ corresponds to a phase-velocity measurement accuracy of 1.7 parts in 10^6, for a receiver-point spacing (R_1 to R_2) of 1,500 m.

(h) The effect of the diameter and the length of the receiving antennas on the value of Φ was determined experimentally. The diameters of the receiving antennas were varied from 0.010 to 0.25 in. and the lengths were varied from $\lambda/20$ to $\lambda/4$. The results indicated no measurable effect on the value of Φ due to these variations.

As the velocity of propagation of radio waves through the air depends upon the refractive index of the air, it is necessary to measure the atmospheric pressure, temperature, and vapor pressure in order to obtain a calculated value for the index of refraction of the air. It should be noted that the velocity measurements were made by using a monochromatic source, and hence the wave index of refraction applies in this case.

The estimated accuracies of measurement of air pressure, temperature, and relative humidity are: pressure, 1 millibar; temperature, 1° C; relative humidity, 3 percent. Using the relationship [14],

$$(n-1)10^6=N=\left\{\frac{77.6}{T}\left(p+4810\frac{e}{T}\right)\right\}, \qquad (3)$$

where

n = index of refraction of air,
p = total atmospheric pressure, in millibars,
e = partial pressure of water vapor in air, in millibars,
T = absolute temperature, deg K = °C + 273°.

The estimated accuracy of the calculated value for the index of refraction of the air is 4 parts in 10^6.

The atmospheric pressure, temperature, and relative-humidity measurements were made in the vicinity of the radio-wave path between receiving points R_1 and R_2, at a distance of 1 m above the ground; hence these measurements represent a localized check and not an average or integrated value of the air constants along the actual path of the radio waves between R_1 and R_2.

It is of interest to note at this point that at times when the wind was extremely gusty (and crosswise of the path from R_1 to R_2) the measured value of Φ quite often fluctuated suddenly in synchronism with the gusts of wind. The maximum fluctuations in Φ corresponded to an apparent change in the index of refraction of air of approximately 10 parts in 10^6.

Table 1 is a summary of the various factors that influenced the accuracy of the phase-velocity measurements, together with the estimated limits of errors of measurement in these factors. Two types of errors are listed in this table: one type is a fixed (or systematic) error, and the other type of error is random and varies in amount from one measurement of phase velocity to another.

TABLE 1. *Factors which influenced accuracy of phase-velocity measurements*

Factor	Estimated limit to resulting error of measurement
Measurement of the radiofrequency, f	*0.5×10⁻⁶
Surveyed distance, S	2
Curvature of radio beam	0.01
Multipath effect	*1.7
Positions of T_1 and T_2	0.25
Receiving-antenna cable-pickup error	*5
Phase characteristics of VHF radio receivers	*1
Phase-measuring system	*1.7
Measurement of the refractive index of air	*4.0
Total estimated maximum systematic (bias) error	2.25×10⁻⁶=0.7 km/sec

* These errors are likely to vary from one set of phase-velocity measurements to another, and therefore, are components of the over-all random error.

4. Experimental Results

Three sites were used to carry out the phase-velocity measurements. The first site was at the obsolete Blue Ridge Airport near Willard, Va., and was used to make preliminary tests on the system for sources of systematic errors, reliability of operation, and phase stability of the equipment. The equipment was set up in the center of a level area clear of objects in all directions to a distance of at least 250 m. The distance between the receiving points R_1 and R_2 was 200 m. Tests at this site indicated the possibility of large phase errors due to reflections from nearby objects, such as power lines, metal buildings, woods, etc. [15]. For some positions of the radio transmitters

T_1 and T_2, along the extensions of the receiving-point line, the phase error in the measured value for Φ was found to be as much as 50 electrical degrees; this error in phase measurement corresponded to an error in the measurement of the radio-wave phase velocity of 1 part in 16,000.

The second site used to make phase-velocity measurements was a dry lake bed 8 miles south of Willcox, Ariz., at an altitude of 4,100 ft above sea level. The system was set up on the south end of the lake bed, approximately 4 miles east of Cochise, Ariz., in an area where the ground was level to within ± 2 in. and was completely devoid of vegetation. The minimum distance to nearby reflexing objects (excluding trucks) was at least 4 miles. Line of sight conditions existed between the receiving and the transmitting antennas. The geometry of the system was as shown in figure 1, with the receiving-point line extending north and south. The distance S was varied, depending upon the type of test being made; for the reported phase-velocity measurements, two values of S were used: 850.0013 and 1500.0018 m. The distances from T_0 to R_1 and T_0 to R_2 (see fig. 4) were each approximately 1,400 m, and T_0 was located on the west side of the receiving-point line. The distances from T_1 to R_1 and from T_2 to R_2 were varied during the tests but for all precise measurements of the phase increment Φ these distances were greater than 500 wavelengths; that is, greater than 850 m.

After a series of preliminary tests on the system, a series of phase-velocity measurements were made at this second site over a period of 3 weeks during the months of April and May 1953. The phase-velocity measurements were supplemented by recorded values of the atmospheric temperature, pressure, and relative humidity. The radio-frequency signal levels at R_1 and R_2 were also noted and recorded in terms of the VHF radio-receiver first-limiter grid current. The results of these tests are shown in table 2. The value for Φ (as measured) was obtained from eq (2). The whole-number wavelengths between R_1 and R_2 were measured by recording the total change in phase differential as radio transmitter T_1 was moved halfway around the system.

For a receiving-point spacing (S) of 1500.0018 m, the whole-number wavelength distance was 864 wavelengths, and for $S=850.0013$ m, the whole-number wavelength distance was 490 wavelengths; corresponding values for M (eq 2) were 1,729 wavelengths and 980 wavelengths, respectively.

From the above considerations the free-space phase velocity in kilometers per second, as calculated from eq (1) (with Φ in degrees), is

$$V=\frac{360\times 172.8\times 10^6\times 1500.0018\times n}{10^3\times\Phi}$$

$$=\frac{93{,}312{,}114\times 10^3\times n}{\Phi}$$

for $S=1500.0018$ m and,

$$V=\frac{360\times 172.8\times 10^6\times 850.0013\times n}{10^3\times\Phi}$$

$$=\frac{52{,}876{,}881\times 10^3\times n}{\Phi}$$

for $S=850.0013$ m.

The data in table 2 were obtained with the distance from T_1 to R_1 (and T_2 to R_2) equal to 1,000 m and with the transmitter antennas 3 m above ground level. The receiving antennas (R_1 and R_2) were only 0.2 m above ground, and as the received signals were the resultants of the three modes of transmission, the direct, ground-reflected, and surface waves [16], it was necessary to apply a correction to the measured phase velocity. This calculated correction was found to be -0.6 km/sec.

During July, August, and September 1953 the equipment was set up at the third test site, at Sterling, Va., and a comprehensive set of system tests were made. These tests showed that cross-modulation phase errors in the system were less than a measurable value, that is, less than 0.1 electrical degree. These tests also indicated that there was a phase error due to spurious pickup of the receiving-antenna cables when using an unbalanced quarter-

TABLE 2. *Summary of results of radio-wave phase-velocity measurements*

1953	Number of measurements	Distance between receiving points R_1 and R_2	Polarization	Daily average value of N $N=(n-1)10^6$	Range of calculated values of free-space phase velocity of radiowaves	Daily average value of free-space phase velocity of radiowaves
		m			*km/sec*	*km/sec*
Apr. 27	3	1500.0018	Vertical	243.4	299791.5 to 299791.8	299791.7
28	1	1500.0018	do	271.2	299791.4 to 299791.4	299791.4
29	25	1500.0018	do	248.3	299792.2 to 299797.5	299794.0
30	3	1500.0018	do	252.3	299792.3 to 299797.7	299795.5
May 1	11	1500.0018	do	257.6	299789.3 to 299800.0	299794.9
2	7	1500.0018	do	243.0	299797.1 to 299801.0	299800.0
3	8	1500.0018	do	247.5	299799.9 to 299802.0	299801.1
4	39	1500.0018	do	257.1	299798.6 to 299800.1	299799.4
5	4	850.0013	do	251.6	299792.8 to 299794.5	299793.8
13	4	850.0013	Horizontal	245.3	299789.4 to 299796.3	299794.8
13	5	1500.0018	do			

Weighted mean value (see text) of free-space phase velocity, based on 110 measurements, 299795.7 k n/sec.
Geometrical correction (transmitting antenna 3 m high, receiving antenna 0.2 m high), plus multimode transmission correction, -0.6 km/sec.
Resultant mean value of free-space phase velocity of radiowaves, 299795.1 km/sec.

wave vertical antenna and negligible phase error for a balanced half-wave horizontal antenna. This receiving-antenna cable pickup error was estimated to be 5 parts in 10^6 for the phase-velocity measurements made at the Willcox, Ariz. site and is listed in table 1.

Further tests at the Sterling site disclosed that the relative phase of the VHF radio-receivers (R_1 and R_2) heterodyne-frequency output varied with the radio-frequency signal-level input to the receivers. A set of phase-correction curves were drawn, based on the results of these tests, and proper phase corrections were made for these phase errors in the radio receivers. These corrections were based on the known (and recorded) radio-frequency signal-input levels and the equivalent amplitude modulation.

5. Discussion

The phase velocity of propagation of radio waves in free space, as determined experimentally in the work covered by this report, is 299795.1 ±3.1 km/sec. This is a weighted average, or mean value, based on 110 independent measurements made during 10 days and is calculated by weighting each of the 10 daily means equally. However, this weighted mean for the phase-velocity measurement is subject to two types of errors. One type is a systematic error (or bias), which appears in approximately the same amount in every measurement and reflects the inherent limitations of the measuring system to measure the true value of the phase velocity of radio waves. The other type of error is random, and appears in different amounts randomly in each measurement of the phase velocity.

Assigning equal weights to each daily mean is justified on the following considerations. In terms of the random variations, the data indicate that measurements taken within a day tend to show better agreement than measurements taken on different days. Thus these measurements contain two sources of variability [17]. One source, called the "within days variation" or the "internal precision", reflects the degree of agreement between repeated measurements made on the same day. The other source of variability, termed the "between days variation" or the "external precision", reflects how well measurements made on different days agree with each other. The internal and external variability can be expressed quantitatively by σ_1 and σ_2, respectively. Both of these quantities are inversely proportional to their associated precisions and are defined as follows: If an infinite number of measurements were made on one day, then the standard deviation (σ_1) of the measurements referred to the daily average will reflect how well these measurements agree with each other. Now, if this process is continued for an infinite number of days, the standard deviation (σ_2) of the daily averages referred to the grand average will reflect how well measurements made on different days agree with each other. However, as only a finite amount of data is available, it is necessary to estimate the quantities σ_1 and σ_2. Table 3 shows the numerical computations for estimating σ_1 and σ_2 [18].

The standard deviation for a daily average based on n measurements is given by $\sqrt{(\sigma_1^2/n)+\sigma_2^2}$. For proper weighting, each daily average should be weighted in proportion to $1/\{(\sigma_1^2/n)+\sigma_2^2\}$. However, if σ_2^2 is large compared to σ_1^2/n, then the daily averages can be weighted equally to give a grand mean that will not differ appreciably from the mean that would be obtained by (exact) proper weighting.

Table 1 lists the possible sources of errors, with an estimated limiting value for the effect of each source on the reported figure for the phase velocity of radio waves. From table 1 the total estimated systematic error is 2.25 parts in $10^6 = \pm 0.7$ km/sec. This (systematic) error can be either positive or negative, and unless there is good evidence of its polarity, the safe procedure is to assume that it introduces an error spread equal to twice its above value, centered about the mean value.

TABLE 3. *Analysis of variance*

Source	Degrees of freedom	Sums of squares of deviations	Mean-square deviation	Expected value [19] of mean square
Between days	9	927.41	103.0456	$\sigma_1^2+9.701\sigma_2^2$
Within days	100	318.37	3.1837	σ_1^2

Estimated value of $\sigma_2^2 = \frac{103.0456-3.1837}{9.701} = 10.29$

From table 2 the standard deviation of the weighted mean (of the 110 measurements) is 1.05 km/sec, which is a measure of the random error or of the precision of the weighted mean, calculated from the relationship.

$$\text{Std. dev.} = \frac{1}{m}\sqrt{\sigma_1^2\left(\frac{1}{n_1}+\frac{1}{n_2}+\ \ldots\ .+\frac{1}{n_m}\right)+m\sigma_2^2},$$

where m is the number of days; n_1, n_2, etc. are the number of measurements taken on the respective days; σ_1 is the standard deviation for any one measurement—calculated by referring each measurement to its own daily average; and σ_2 is the standard deviation of a daily average referred to the mean of all the daily averages.

A 95-percent confidence interval for the mean of an infinite family of such determinations is 299795.1 ±2.4 km/sec; that is, if the same experiment were repeated 100 times and the resulting means and associated confidence intervals calculated, then, on the average, 95 of these intervals will cover the "true value," where the true value is the average value obtained from an infinite number of measurements.

Hence to find a conservative estimate of the accuracy for the above measurements of the free-space phase velocity of radio waves, the maximum estimated systematic error of 0.7 km/sec has been added to one-half the length of the confidence interval of ±2.4 km/sec to give the limits of accuracy as ±3.1 km/sec, which applies to the above-reported mean

value of the measurement of the free-space phase velocity of radio waves.

It should be noted that a 50-percent confidence interval for the mean value of the measurements would be 299795.1 ± 0.7 km/sec, and a corresponding estimate of the accuracy for the above measurement of the free-space phase velocity of radio waves would be 299795.1 ± 1.4 km/sec.

6. Conclusions

From the results of the measurements made in this work, shown in table 2, and from the estimated value for the total maximum systematic error, shown in table 1, it is concluded that the free-space phase velocity of VHF radio waves is 299795.1 ± 3.1 km/sec.

A study of the factors in table 1 indicates that the over-all accuracy of the measurement of the free-space phase velocity could be improved by equipment modifications and by improved techniques; the accuracy of this phase-velocity measurement seems to be limited by the accuracy with which the "true" (or "effective") value of the refractive index of air can be measured over the path traversed by the radio waves.

Table 4 lists the values obtained for the velocity of propagation of electromagnetic waves by various workers during the past half century.

TABLE 4. *Some published values of the velocity of electromagnetic waves*

Date	Observer	Velocity, km/sec, in free space	Method
1906 *	Rosa and Dorsey [2]	299781 ±30	Ratio of esu to emu.
1926	Michelson [7]	299796 ±4	Rotating mirror.
1935	Michelson, Pease, and Pearson [1].	299774 ±11	Rotating mirror in vacuum.
1941	Anderson [3]	299776 ±14	Modulated light beam.
1949	Aslakson [22]	299792.4±2.4	Shoran (radar).
1950	Essen [6]	299792.5±3	Resonant cavity.
1950	Bol [5]	299789.3±0.4	Do.
1951	Bergstrand [23]	299793.1±.2	Modulated light beam.
1951	Aslakson [24]	299794.2±1.9	Shoran (radar).
1952	Froome [9]	299792.6±0.7	Microwave radio interferometer.

* In an unpublished NBS memorandum from F. B. Silsbee to I. C. Gardner (April 22, 1954) Dr. Silsbee shows that if corrections are based on recently measured effects of humidity on the index of refraction for air, and if the 1948 value for the adopted International ohm is used, then the Rosa and Dorsey value becomes $V = 299800 \pm 31$ km/sec.

The measured value of the free-space phase velocity of radio waves obtained in this work checks the results obtained by resonant-cavity methods [5,6] and by SHF interferometer methods [9] but does not check very well with some of the work done on the measurement of the velocity of light [1,3,8].

The author expresses his appreciation to the following members of the National Bureau of Standards who have assisted in carrying out this work: John C. Onda, Louis R. Russell, A. C. Tavenner, William O. Hutchison, N. Rahal, and J. Donhaiser. We are also grateful to Myron H. Allen of Safford, Ariz., who contributed a good deal of time and effort in locating a site suitable for the tests. H. W. Hemple, A. J. Hoskinson, and other members of the U. S. Coast and Geodetic Survey, Washington, D. C. have been extremely cooperative in giving advice and lending equipment for use on this project. W. J. Youden and Marvin Zelen of the Statistical Engineering Laboratory, National Bureau of Standards, deserve credit for guidance of the statistical analysis of the results of this work.

7. References

[1] A. A. Michelson, F. G. Pease, and F. Pearson, Velocity of light in a partial vacuum, Astrpohys. J. **82,** 26 (1935).
[2] E. B. Rosa and N. E. Dorsey, Bul. BS **3,** 433 (1907) S65
[3] W. C. Anderson, Final measurements of the velocity of light, J. Opt. Soc. Am. **31,** 187 (1941).
[4] R. A. Smith, E. Franklin, and F. B. Whiting, Accurate measurement of the group velocity of radio waves in the atmosphere, using radar techniques, J. Inst. Elec. Engrs. (London) **94,** pt. III, 391 (1947).
[5] Kees Bol, A determination of the speed of light by the resonant cavity method, Phys. Rev. **80,** 298 (October 15, 1950).
[6] L. Essen, The velocity of propagation of electromagnetic waves derived from the resonant frequencies of a cylindrical cavity resonator, Proc. Roy. Soc. (London) [A] **204,** 260 (1950).
[7] N. Ernest Dorsey, The velocity of light, Trans. Am. Phil. Soc. [V] **34,** 109 (1944).
[8] D. H. Rank, R. P. Ruth, K. L. Vander Sluis, Precision determination of the velocity of light derived from a band spectrum method, J. Opt. Soc. Am. **42,** 693 (1952).
[9] K. D. Froome, Determination of the velocity of short electromagnetic waves by interferometry, Proc. Roy. Soc. (London) [A] **213,** 123 (1952).
[10] J. L. Alpert, V. A. Migulin, and P. A. Ryasin, Investigation of the phase structure of the electromagnetic field and the velocity of radio waves, J. Phys. (U. S. S. R.) **4,** 13 (1941).
[11] J. L. Alpert and B. Gorozhankin, Experimental investigation of the structure of an electromagnetic field over the inhomogeneous earth's surface, J. Phys. (U. S. S. R.) **9,** 115 (1945).
[12] K. A. Norton, A new source of systematic error in radio navigation systems requiring the measurement of the relative phases of the propagated waves, Proc. Inst. Radio Engrs. **35,** 284 (March 1947).
[13] A. B. Schneider, Phase variations with range of the ground wave signal from c. w. transmitters in the 70–130 kc/s band, J. British Inst. Radio Engrs. **12,** 181 (March 1952).
[14] Ernest K. Smith and Stanley Weintraub, The constants in the equation for atmospheric refractive index at radio frequencies, Proc. Inst. Radio Engrs. **41,** 1035 (August 1953).
[15] R. Bateman, E. F. Florman, and A. Tait, A source of error in radio phase measuring systems, Proc. Inst. Radio Engrs. **38,** 612 (June 1950).
[16] K. A. Norton, The calculation of ground-wave field intensity over a finitely conducting spherical earth, Proc. Inst. Radio Engrs. **29,** 623 (December 1941).
[17] Raymond T. Virge, The calculation of errors by the method of least squares, Phys. Rev. **40,** 207 (1932).
[18] Anderson and Bancroft, Statistical theory in research, ch. 22 (McGraw-Hill Book Co., Inc., New York, N. Y., 1952).
[19] Statistical Research Group, Columbia Unviersity, Selected techniques of statistical analysis, ch. 8, sec. 5.2 (McGraw-Hill Book Co., Inc., New York, N. Y., 1947).

[20] P. A. Sheppard, The structure and refractive index of the lower atmosphere, p. 37 in Meteorological Factors in Radio Wave Propagation, Report of a conference held on April 8, 1946, at the Royal Institution, London, by the Physical Society and the Royal Meteorological Society.
[21] H. H. Skilling, Fundamentals of electric waves, 2d ed., pp. 164–171 (1948).
[22] Carl I. Aslakson, Can the velocity of radio waves be measured by Shoran? Trans. Am. Geo. Union **30,** No. 4 (August 1949).
[23] Erik Bergstrand, Arkiv Fysik (Stolkholm) Band 3, No. 26, 479 (1951).
[24] Carl I. Aslakson, New determination of the velocity of radio waves, Trans. Am. Geo. Union **32,** 813 (1951).

8. Appendix—Equipment

Figure 6 shows the type of quarter-wave vertical antennas used at receiving points R_1 and R_2. This assembly was provided with a plumb-bob attachment beneath the antenna base arranged so that the vertical axis of the plumb bob coincided with the vertical axis of the antenna. The lateral position of the antenna was adjusted to bring the point of the plumb bob over the benchmark inscribed on the copper plate on top of the wooden ground stake shown in the figure. The antenna proper was mounted normal to the adjustable portion of the base, which in turn was provided with adjustment leveling screws and a set of right-angle spirit levels.

Tests on the above antenna showed that this antenna could be set up in the field so that the top end of the antenna was within ± 0.50 mm of its true vertical position, and the lateral position of the antenna vertical axis (at the antenna base) could be set to within ± 0.20 mm of the benchmark.

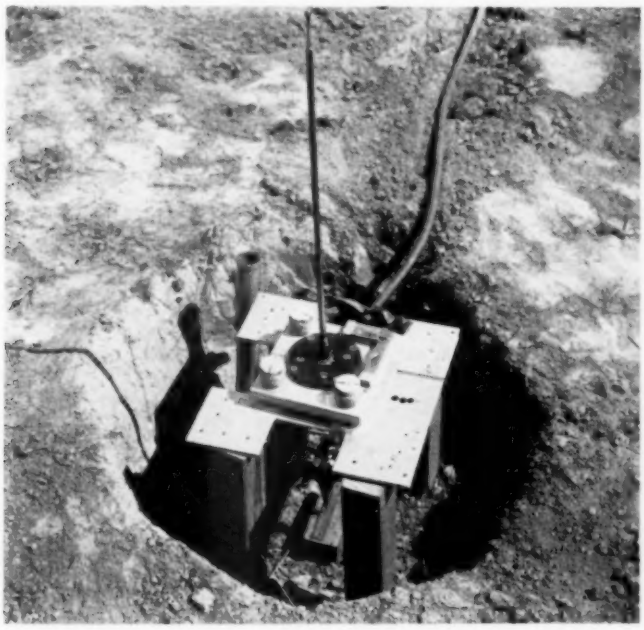

FIGURE 6. *Quarter-wave vertical receiving antenna.*

Double-shielded 50-ohm cable was used to connect the receiving antenna to the radio receiver. This cable, shown in figure 6, was 150 ft long and was placed on the ground at right angles to the line through the receiving antennas and led to the radio receiver in the shelter shown in figure 8.

The horizontal half-wave balanced receiving antenna and balanced-to-unbalanced transformer is shown in figure 7. This antenna was positioned laterally over the benchmarks by means of a plumb bob suspended from the center of the antenna. The horizontal position of the antenna was checked by means of a carpenter's level, and the azimuth of the antenna, relative to the line through the receiving-antenna centers, was checked by means of a square. The estimated accuracy of setting of this antenna was ± 1.0 mm.

Figure 8 shows one of the two metal enclosures that housed the VHF radio receivers, 1-kc band-pass filters, and the UHF radio transmitters (indicated in fig. 4). This enclosure was also used to house a set of storage cells for battery operation of the equipment. The VHF radio receiver was a commercial FM type, modified for amplitude-modulation reception and arranged so that the audio output and the first-limiter grid current could be monitored by a meter on the receiver panel. The UHF radio transmitter was a commercial type operating in the range 910 to 960 Mc. The UHF transmitter antenna and reflector are shown in figure 8, and the receiving antenna cable to R_1 (and R_2) can be seen on the ground to the right in the photograph.

The unit shown in figure 8 was manually operated and required an attendant at all times during which the phase-velocity measurements were made, hence the presence of the wind and sun shelter shown in the figure.

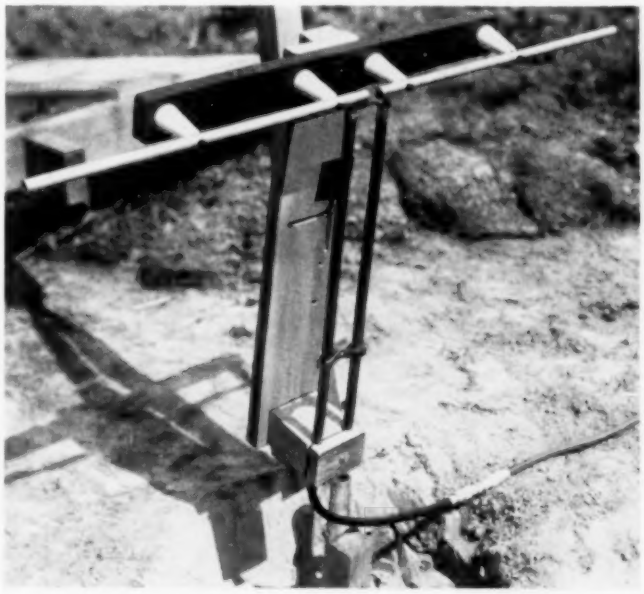

FIGURE 7. *Half-wave center-fed balanced receiving antenna.*

Figure 9 is a front view of radio transmitter T_1 (and T_2). These units, each of which was housed in an army-type truck, consisted of a 50-w radio transmitter and a 250-w power amplifier, covering the frequency range 148 to 174 Mc. The oscillator in the 50–w transmitter was modified with a vernier-frequency control so that the frequency of the transmitter output could be controlled by the knob shown in the right center, over a range of ± 5 kc and could easily be set to within ± 1 cps.

To provide mobility for the T_1 and T_2 units, a 5-kw gasoline-engine power unit was mounted on each of the trucks.

Figure 10 is a view of one of the five-element Yagi antennas used to radiate the signals from the T_1 and T_2 transmitters, mounted on the rear of the trucks that housed these transmitters. For some of the phase measurements, this same antenna was mounted on the end of an 8-ft boom in order to increase the spacing between the rear of the antenna and the truck.

Figure 11 is a view of the "control" truck that housed radio transmitter T_0, the two UHF radio receivers, phase-measuring equipment, and fre-

FIGURE 8. *Very-high-frequency radio receiver—ultra-high-frequency radio transmitter station.*

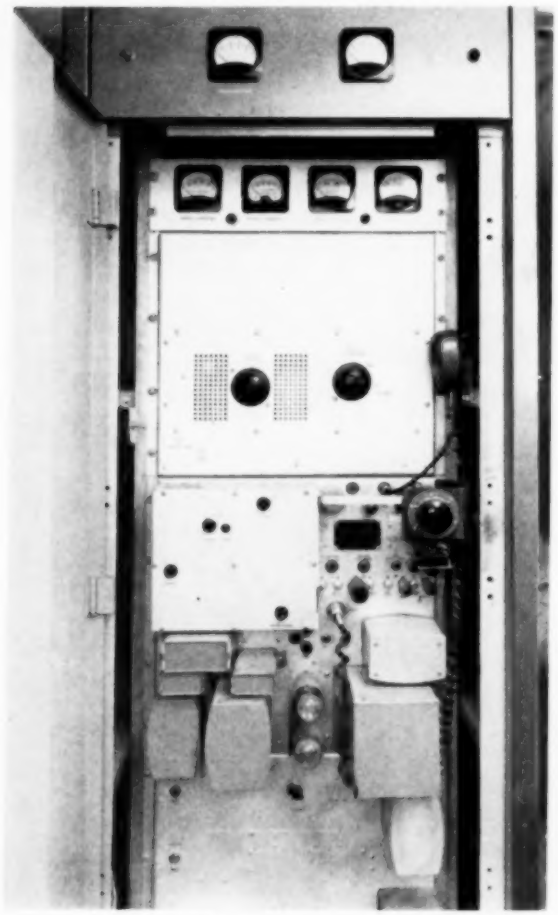

FIGURE 9. *Radio transmitter T_1 (T_2).*

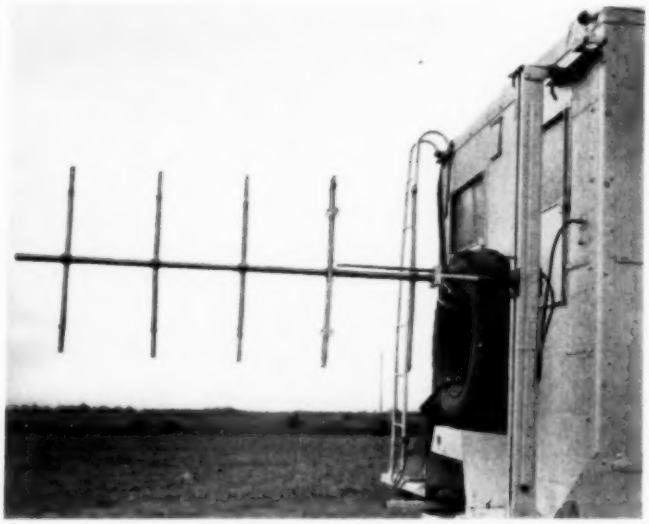

FIGURE 10. *Five element Yagi antenna used at T_1 and T_2 transmitters.*

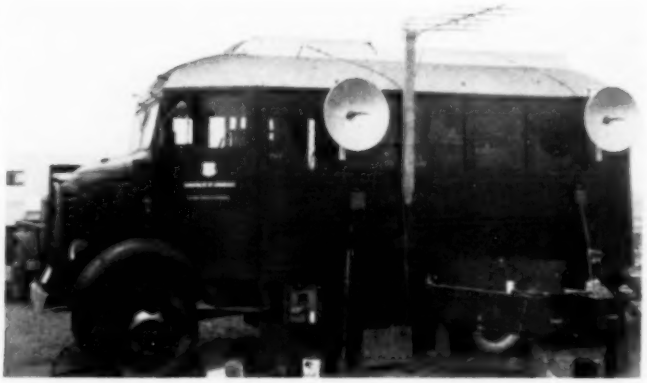

FIGURE 11. *Exterior view of control truck housing phase measuring, frequency-monitoring equipment, and radio transmitter T_0.*

quency-monitoring equipment shown in block form in figures 4 and 5. This view shows both types of antennas used with radio transmitter T_0: the quarter-wave vertical roof antenna and the five-element Yagi antenna, which could be used for either vertical or horizontal polarization. The UHF receiving antenna-reflector assemblies were positioned so as to point toward the transmitting antennas shown in figure 8.

Figure 12 shows a panel view of the equipment in the control truck. Taken in order from left to right and top to bottom, the main components of each rack are:

1. UHF radio receivers and heterodyne-frequency signal-level meters.
2. phase-monitor scope, RC phase shifter, and communication receivers.
3. electronic phase meter, manual phase shifter, and recorders.
4. frequency-monitor oscilloscope, audiofrequency signal generator, and radio transmitter T_0.
5. audiofrequency meter, radio receiver, 100-kc frequency standard, and frequency divider.

The meterological equipment consisted of a hygrothermograph, barograph, and an indicating barometer, all housed in a standard type of instrument shelter provided by the Weather Bureau. A sling psychrometer was used to calibrate the hygrothermograph twice each day.

To facilitate operation of the system, two-way communication was provided from the control truck to each of the other four manually operated stations.

BOULDER, COLO., June 7, 1954.

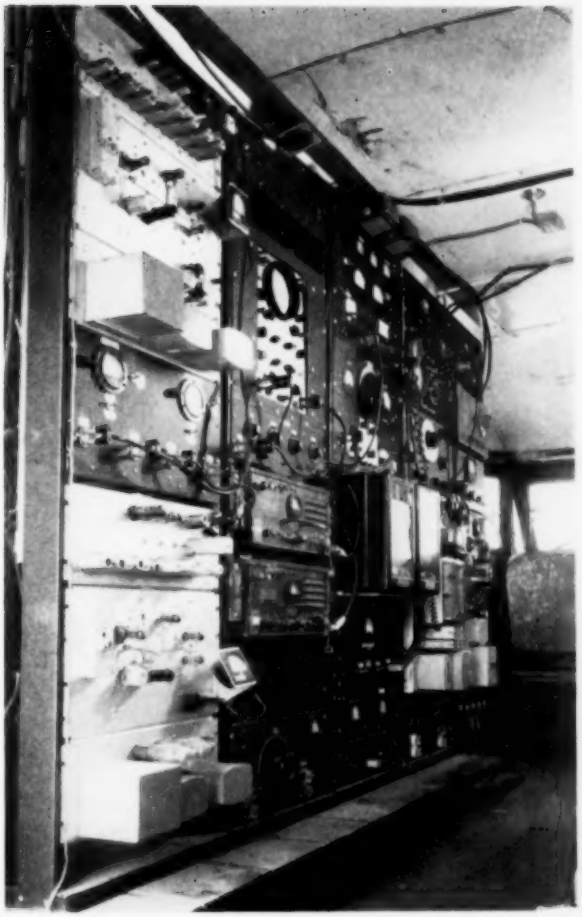

FIGURE 12. *Panel view of equipment in the control truck.*

Journal of Research of the National Bureau of Standards Vol. 54, No. 6, June 1955 Research Paper 2597

A Study of the System Magnesium Oxide–Magnesium Chloride–Water and the Heat of Formation of Magnesium Oxychloride

Edwin S. Newman

The precipitation of magnesium oxychlorides is discussed, and the results of solubility measurements are given. The heats of solution in HCl, 26·61H_2O (2.00 *N* HCl at 25° C) of four compounds in the system MgO-$MgCl_2$-H_2O were determined. From those data and other data taken from the literature, the heats of formation of the compounds at 25° C were calculated. The results are applied to the calculation of the heat of reaction of hardening of magnesium oxychloride cement.

1. Introduction

Magnesium oxychloride cement is widely used as a conductive flooring material in hospital operating rooms and other locations where an explosion hazard exists. It is also used widely as a general purpose floor in public buildings, stores, street cars, and elsewhere. Basic information concerning the stability of the components of magnesium oxychloride cement is needed to answer questions that arise from time to time in connection with its service life. The heats of formation of the compounds formed constitute part of the necessary fundamental information and are presented in this paper.

The compounds occurring in the system MgO-$MgCl_2$-H_2O have been the subject of many investigations since the discovery in 1867 of the cementitious properties of mixtures of magnesium oxide with magnesium chloride solutions. Robinson and Waggaman [1][1], Lukens [2], Chassevent [3], Bury and Davies [4], Feitknecht [5], Feitknecht and Held [6], and others have identified the three solid phases occurring at room temperature as $Mg(OH)_2$, $5Mg(OH)_2 \cdot MgCl_2 \cdot nH_2O$, and $3Mg(OH)_2 \cdot MgCl_2 \cdot nH_2O$. Most of the investigations have been concerned with the identification of the magnesium oxychloride compounds or with the study of the setting process of magnesium oxychloride cement. Only Andre [7] has given heat-of-solution data from which heats of formation have been calculated [8].

In the light of the more recent work cited above, Andre's data appears in doubt because of the absence of identification of his material with the presently recognized compounds. This paper gives the results of new measurements of the heats of solution of the two oxychlorides and the heats of formation calculated therefrom.

2. Materials, Apparatus, and Procedure

2.1. Preparation of Compounds

The compounds were prepared by precipitation at 25° C from metastable solutions of MgO in $MgCl_2$ solutions of various concentrations. Aqueous $MgCl_2$ solutions were prepared from $MgCl_2 \cdot 6H_2O$ of analytical reagent quality and distilled water. Magnesium chloride is deliquescent, and it is difficult to weigh out an amount containing an accurately known quantity of $MgCl_2$. Because of this difficulty, the solutions were prepared in a weighed 1-liter volumetric flask, adjusting the compositions by trial and error until the desired densities were obtained. Densities for solutions of the desired concentrations were taken from density-concentration data for $MgCl_2$ solutions in the International Critical Tables [9]. In order to reduce the CO_2 concentration, the solutions were transferred to an Erlenmeyer flask and a stream of CO_2-free air was introduced into each solution while boiling gently under a reflux condenser fitted with a CO_2 absorption tube. After cooling and filtering if necessary, the solutions were stored in 1/3 liter portions in tightly stoppered plastic bottles. It is estimated that water loss during boiling increased the concentration of $MgCl_2$ in the solution by not more than 0.05 percent. Solutions were prepared containing 5, 10, 15, 22, 27, 32, 37, 42, 47, 52, 57, 62, 67, and 72 percent by weight of $MgCl_2 \cdot 6H_2O$ respectively. Three series of mixtures in the system MgO-$MgCl_2$-H_2O were made using the separate portions of these $MgCl_2$ solutions.

The first series of mixtures consisted of metastable solutions of MgO prepared by shaking for 2 hr. a 1-g portion of freshly heated (18 hr at 400° C) MgO of analytical reagent quality with a ⅓-liter quantity of each of the 14 above mentioned magnesium chloride solutions. The mixtures were filtered several times if necessary to obtain clear solutions. Magnesium oxychloride began to precipitate after a few hours or days depending on the $MgCl_2$ contents of the solutions.

The second series of mixtures was made in an attempt to approach equilibrium from undersaturation. After from 1 to 3 weeks, about half of the magnesium oxychloride precipitated from each of the metastable solutions was removed by filtration and transferred to the second ⅓-liter portion of the solution of the same nominal $MgCl_2$ concentration as that in which the precipitate had formed. It was calculated that the change in $MgCl_2$ concentration

[1] Figures in brackets indicate the literature references at the end of this paper.

of the original solution caused by precipitation of the oxychloride compounds varied from +0.01 to −0.08 percent. This change was ignored in plotting the data shown hereafter and in discussing solutions of the same nominal concentration.

The third series of mixtures, also an attempt to approach equilibrium from undersaturation, was prepared by adding 0.33 g of $Mg(OH)_2$ to the remaining ⅓-liter portion of each of the $MgCl_2$ solutions. The $Mg(OH)_2$ was prepared by hydrating MgO for 72 hr in distilled water on the steam bath with subsequent drying at 110° C. A fourth series was prepared with new $MgCl_2$ solutions using 1 g of $Mg(OH)_2$ per ½-liter portion of solution, in order to obtain material for heat-of-solution determination. Subsequently additional mixtures of MgO in solutions containing 34 and 36 percent of $MgCl_2 \cdot 6H_2O$, respectively, were made for the same purpose.

The mixtures were stored in a constant-temperature room at 25° C and shaken daily during their early history. From time to time the alkalinity of the solutions was determined by titrating a 10-ml pipetted sample of the supernatant liquid with 0.02 *N* HCl, using phenolphthalein as an indicator. The HCl solution was standardized against a calcium hydroxide solution, the CaO content of which had been determined gravimetrically. The alkalinity was calculated to the equivalent MgO and is referred to as the MgO content of the solution throughout this paper. No implication is intended as to the state of the MgO in solution. X-ray diffraction patterns of the precipitates were obtained at the time the second series of mixtures was prepared and later for precipitates of special interest.

The precipitates were analyzed, sometimes after washing with alcohol and ether or acetone and drying for several hours at room temperature in a vacuum over $CaCl_2$, and sometimes after merely pressing out the solution on filter paper. Total magnesium was determined by heating the sample slowly to 450° to 500° C after the addition of a few drops of concentrated sulfuric acid and weighing as $MgSO_4$. Chloride was determined gravimetrically by precipitation as AgCl. From these data the equivalent $MgCl_2$ and MgO were calculated, and water was taken by difference.

To furnish material for the study of the variation of the heat of solution of $3Mg(OH)_2 \cdot MgCl_2 \cdot nH_2O$ with the change of water content, 4 liters of 58.5 percent $MgCl_2 \cdot 6H_2O$ solution was shaken with 15 g of freshly calcined MgO and filtered. At the end of 3 months, the oxychloride compound which had precipitated was recovered by filtration, washed with alcohol and acetone, and dried under vacuum. Analyses, heat-of-solution determinations, and dehydration studies were made using this material. Samples were exposed at room temperature to air of various humidities in desiccators containing water, saturated solutions of $Na_2Cr_2O_7$, $MgCl_2 \cdot 6H_2O$, KOH, or solid $Mg(ClO_4)_2$ respectively. Other samples were heated at 45°, 110°, and 180° C. The samples were weighed periodically to determine the loss or gain of water. Subsequently, their heats of solution in HCl, $26.61H_2O$ (2.00 *N* at 25° C) were determined.

2.2. Heat-of-Solution Measurements

The heats of solution of the oxychloride precipitates were determined in HCl $26.61H_2O$. The isothermal jacket calorimeter, described elsewhere [10], has been lined with platinum and is fitted with a four-blade platinum stirrer. The valve has been removed and the powdered samples are introduced by means of a funnel. Electrical calibration and calculations of the corrected temperature rise were performed by conventional methods [11].

3. Results and Discussion

3.1. Precipitation of Magnesium Oxychloride

The amount of MgO initially dissolved by $MgCl_2$ solutions varies with the time and temperature of heating of the MgO, with the concentration of the $MgCl_2$ solution, with the ratio of MgO to $MgCl_2$ solution, with the time of shaking, and, perhaps, with other factors. Using MgO from a single source, Lukens [2] has shown this variation in considerable detail for one particular concentration of $MgCl_2$ solution. In the present work, only sufficient MgO was used to give metastable solutions containing 3 g/liter or less of MgO, since solutions containing substantially more than this amount thickened to a gel upon precipitation of the oxychloride compounds. Under the conditions chosen, 3 g of solid MgO per liter of solution and 2 hr of shaking before filtration, solutions containing 27 percent or more of $MgCl_2 \cdot 6H_2O$ dissolved nearly all of the MgO. There were some variations in MgO content of the clear solutions, indicating perhaps that 2 hr was not the optimum shaking time, but all of these solutions after filtration contained from 20 to 40 times the concentration reached subsequently upon standing for 7 months. The solutions containing 22, 15, 10 percent of $MgCl_2 \cdot 6H_2O$ dissolved substantially less MgO, but even these after filtering contained 10 or more times the final concentration. The solution containing 5 percent of $MgCl_2 \cdot 6H_2O$ dissolved very little MgO.

The equivalent MgO content of magnesium chloride solutions shaken with $Mg(OH)_2$ depended on the relative amounts of $Mg(OH)_2$ and solution and upon the time of contact, as well as upon the concentration of $MgCl_2$. Many of the solutions of the series shaken with 1 g of $Mg(OH)_2$ per liter of solution dissolved it slowly, reaching maximum MgO concentration in about 2 weeks. These solutions were metastable, and subsequently with the precipitation of magnesium oxychloride the concentration of MgO fell, approaching the final value reached by the other solutions of the same $MgCl_2$ content. This behavior was characteristic of the solutions containing 37 percent or more of $MgCl_2 \cdot 6H_2O$. The solutions of less $MgCl_2$ content did not become greatly supersaturated, but slowly approached a final MgO concentration depending on the amount of $MgCl_2$ in solution. The magnesium chloride solutions shaken with 3 g of $Mg(OH)_2$ per liter behaved similarly,

except that the maximum MgO concentrations were generally higher and more quickly attained.

The changes of the MgO concentration of the solutions containing 47 percent $MgCl_2 \cdot 6H_2O$ are plotted in figure 1 as a function of time. The changes occurring in these solutions are typical of those found with the other solutions of such $MgCl_2$ concentration that oxychloride compounds were formed. The original supersaturated clear solution contained 3.02 g MgO per liter. In 13 days, precipitation of magnesium oxychloride reduced the concentration to 0.073 g MgO per liter, where it remained for more than 6 months. At 16 days about half of the precipitate formed was transferred to a fresh solution of the same $MgCl_2$ concentration. The MgO concentration of this solution, which, at 1 day, was 0.135 g/liter, was reduced in 5 days to 0.107 and in 9 days to 0.068 g/liter where it remained within experimental error. The possible significance of the 1-day value will be discussed later.

One-third gram of solid magnesium hydroxide suspended in ⅕ liter of 47-percent $MgCl_2 \cdot 6H_2O$ solution gave an MgO concentration of 0.132 g/liter in 1 day, and 1 g under the same conditions gave a concentration of 0.386 g MgO per liter. In the first solution, additional $Mg(OH)_2$ dissolved, raising the MgO concentration to 0.233 g/liter in 15 days. Thereafter precipitation of magnesium oxychloride reduced the concentration to 0.080 g/liter at 51 days and 0.063 g/liter at 219 days. In the second solution, the MgO concentration remained near the 1-day value for about a week, and then decreased to 0.109 g/liter at 21 days and to 0.078 g/liter at 43 days. It remained essentially constant thereafter until the precipitate was removed for analysis at 156 days.

In figure 2 are plotted the concentrations of MgO in the $MgCl_2$ solutions when the experiments were terminated at about 7 months. This figure represents the 25° C isotherm of the system MgO-$MgCl_2 \cdot 6H_2O$–H_2O with the MgO scale greatly expanded. A vertical line T—T is drawn through the concentration of $MgCl_2 \cdot 6H_2O$ (10.89% of $MgCl_2$) given by Bury and Davies [4a] as the triple point at which magnesium chloride solution, $Mg(OH)_2$, and 3 $Mg(OH)_2$-$MgCl_2 \cdot 8H_2O$ coexist. The data of Robinson and Waggaman [1] are represented by the open squares, and the solubility of $Mg(OH)_2$ in pure water at 30° C [15] is also shown. Chassevent's value of 0.030 g/liter for the solubility of magnesium oxide in magnesium chloride solution [3] is plotted in figure 2 as an open triangle.

A second vertical line X—X is drawn in figure 2 separating the diagram in two regions. To the right of this line the final precipitates were, with two exceptions, $3Mg(OH)_2 \cdot MgCl_2 \cdot 8H_2O$, and to the left, with three exceptions, they were $Mg(OH)_2$. The exceptions are indicated in the figure by the letters A, B, and M attached to the various points and indicating the presence of $3Mg(OH)_2 \cdot MgCl_2 \cdot 8H_2O$, $5\ Mg(OH)_2 \cdot MgCl_2 \cdot 8H_2O$, and $Mg(OH)_2$ respectively. The line X—X makes the same separation for the results of Robinson and Waggaman and thus indicates the approximate location of the triple point $Mg(OH)_2$-$3Mg(OH)_2 \cdot MgCl_2 \cdot 8H_2O$ solution for their work as well as for the author's.

In the present work it was planned to approach equilibrium from both directions. Because $Mg(OH)_2$, contrary to statements in the literature, formed supersaturated solutions, the approach from undersaturation was not accomplished with certainty when $Mg(OH)_2$ was added to $MgCl_2$ solutions. In every case the concentration of MgO in these solutions passed through a maximum within a few days after the $Mg(OH)_2$ had been added. With solutions containing 27 percent or less of $MgCl_2 \cdot 6H_2O$, the final concentrations of MgO were equal to or

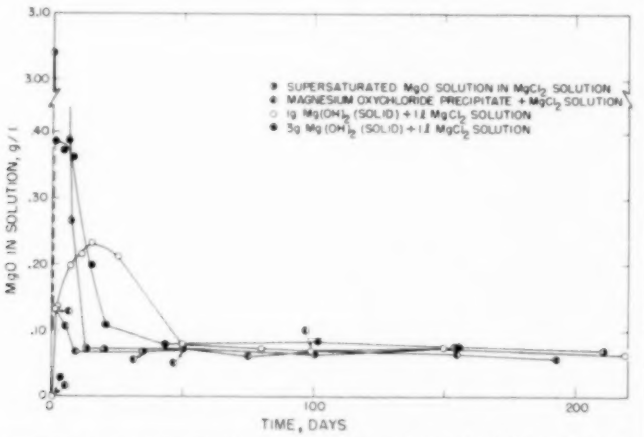
SUPERSATURATED MgO SOLUTION IN MgCl2 SOLUTION
MAGNESIUM OXYCHLORIDE PRECIPITATE + MgCl2 SOLUTION
1g Mg(OH)2 (SOLID) + 1L MgCl2 SOLUTION
3g Mg(OH)2 (SOLID) + 1L MgCl2 SOLUTION
MgO IN SOLUTION, g/l
TIME, DAYS

FIGURE 1. *Concentration-time relationship of* MgO *in* $MgCl_2$ *solution.*

Concentration of $MgCl_2$ solution, 47 percent of $MgCl_2 \cdot 6H_2O$. (22% of $MgCl_2$, equivalent to 23.6° B.)

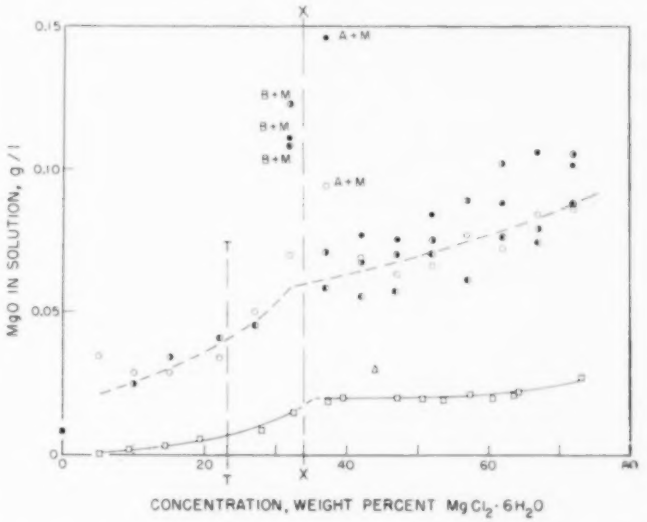

FIGURE 2. *Equivalent concentration of* MgO *in* $MgCl_2$ *solutions at 25° C.*

◑, Precipitated from metastable solution of MgO in $MgCl_2$ solution; ◐, precipitate from metastable solution added to fresh $MgCl_2$ solution; ○, 1 g/l of solid $Mg(OH)_2$ suspended in $MgCl_2$ solution; ●, 3 g/l of solid $Mg(OH)_2$ suspended in $MgCl_2$ solution; □, Robinson and Waggaman solubility data [1]; ■, solubility of $Mg(OH)_2$ in pure water [15]; △, Chassevent solubility data [3]; A, solid phase $3Mg(OH)_2 \cdot MgCl_2 \cdot 8H_2O$; B, solid phase $5Mg(OH)_2 \cdot MgCl_2 \cdot 8H_2O$; C, solid phase $Mg(OH)_2$.

greater than the early maxima. Thus, over the range 10 to 27 percent $MgCl_2 \cdot 6H_2O$ apparent equilibrium was approached from both directions. At higher concentrations, however, it was not approached from undersaturation even in solutions to which precipitated magnesium oxychloride had been added. For these solutions the same sort of early maximum was found in the curves of concentration versus time as for the solutions to which $Mg(OH)_2$ had been added. The final concentration was greater than the early maximum only for the solution containing 57 percent of $MgCl_2 \cdot 6H_2O$. In this solution the final concentration was approached both from under- and from supersaturation, the usual criterion for equilibrium. In spite of this approach, the final concentration was substantially higher than that reported by Robinson and Waggaman.

Both Bury and Davies and Robinson and Waggaman shook their mixtures continuously whereas in the present work the mixtures were shaken only occasionally. The former authors attribute the higher concentration found for the triple point by Robinson and Waggaman to the formation of metastable substances but state that this formation is less likely to occur in the absence of shaking. In a subsequent paper on the system MgO-CaO-$MgCl_2$-H_2O [4b] Bury and Davies state that continuous shaking is necessary to attain equilibrium in that system. The author can make no comment on the differing concentrations indicated for the triple point but considers that the scatter of the points and the generally higher solubilities obtained in the present work indicate that equilibrium was not attained in the absence of continuous shaking in spite of the duration and manner of approach.

The results of X-ray examination of the precipitates are given in table 1. Except in three instances, the final precipitates were $Mg(OH)_2$ or $3Mg(OH)_2 \cdot MgCl_2 \cdot 8H_2O$. The compound $5Mg(OH)_2 \cdot MgCl_2 \cdot 8H_2O$ was the first formed in a number of solutions and appeared as an intermediate phase in several instances when $Mg(OH)_2$ was placed in contact with $MgCl_2$ solution. The rate of conversion to $3Mg(OH)_2 \cdot MgCl_2 \cdot 8H_2O$ appears to increase with increase in the concentration of magnesium chloride in solution. The 5:1 oxychloride was not present (according to the X-ray patterns) at 1 day in the more concentrated $MgCl_2$ solutions and remained at 7 months in the most dilute in which it was formed. Lukens [2] found that in 71-percent $MgCl_2 \cdot 6H_2O$ solutions the 5:1 compound formed first, and Feitknecht and Held [6] found it was that precipitated first and subsequently converted to the 3:1 compound at all concentrations above about 27.8 percent of $MgCl_2 \cdot 6H_2O$. In the present work when the oxychloride precipitates were transferred to fresh solutions containing no MgO, these solutions became supersaturated (in terms of MgO) with respect to their final concentrations. This initial supersaturation may be an indication that $5Mg(OH)_2 \cdot MgCl_2 \cdot 8H_2O$ was still present at the time of transfer even in the precipitates from the three most concentrated magnesium chloride solutions where the X-ray patterns did not indicate its occurrence. There appears, however, to be no concentration range in which the 5:1 oxychloride is the stable compound in equilibrium with magnesium chloride solution.

TABLE 1. *X-ray identification of solid phases found in contact with magnesium chloride solutions*

$MgCl_2 \cdot 6H_2O$ concentration	Preparation[a]	Age in days and X-ray pattern[b]
%		
74.3	1	12–A
		14–A
72	1	1–A
		3–A
		6–A
		99–A
	2	0–M
		6–A+B
		203–A
		267–A
	3	0–A
		197–A
67	1	1–A
		2–A
		6–A
		203–A
	2	0–M
		6–A
		162–A
		203–A
	3	0–A
		197–A
64	1	1–A
62	1	2–A
		6–A
	2	0–M
		6–A+B
		162–A
		214–A
	3	0–A
58.5	1	134–A
		3–A+B
57	1	7–A
		160–A
	2	0–M
		225–A
	3	0–A
55	1	2–A
52.5	1	1–A
		15–A
		21–A
		2–B
		6–A+B
52	1	11–A
		17–A
		0–M
		6–A+B
	2	53–A
		100–A
		162–A
		198–A
	3	0–A+B
47	1	1–B
		2–B
		8–A
		16–A
		30–A
47	2	0–M
	3	6–M+A
42	1	53–A
		100–A
		166–A
		196–A
37	2	0–A
		13–B
		21–B
		100–A
		0–M
		21–M+A
		46–A
		65–A
	3	0–B
		78–A
36	1	14–B
		21–B
		92–A
		100–A
		150–A
32	1	0–M
		6–M
	2	46–M
		100–M
		155–M+A
		165–M+A
	3	0–B
		100–A+B
		212–A
30	1	7–B
		38–B
		21–B
		100–B
		225–B+M
27	2	0–M
		7–M
		46–M
		50–M
		155–M
		162–M
	3	0–B
		92–B+M
		15–M
	1	103–M
		(c)
	2	0–M
		(c)
	3	0–M
		50–M
		100–M
22	1	11–M
		(c)
	2	0–M
		(c)
	3	0–M
		(c)

[a] Preparation 1, made by shaking 1 g of freshly calcined MgO with ⅓ liter of $MgCl_2$ solution; 2, made by adding 0.3 g of $Mg(OH)_2$ to ⅓ liter of $MgCl_2$ solution and 3, made by transferring about half of the precipitate from companion preparation 1 to a MgO-free solution.

[b] The number preceding the dash indicates the age of the preparation at the time the X-ray sample was taken. The letter following the dash represents the compound indicated by the X-ray pattern. A=3 $Mg(OH)_2 \cdot MgCl_2 \cdot 8H_2O$, B=5 $Mg(OH)_2 \cdot MgCl_2 \cdot 8H_2O$, M=$Mg(OH)_2$.

[c] At the end of the experiments these precipitates were judged by inspection to contain only $Mg(OH)_2$ because of the difference between their appearance and that of the bulky slow-settling magnesium oxychlorides. X-ray patterns and heats of solution were not obtained.

3.2. Heats of Dilution of $MgCl_2$ Solutions

In order to obtain data for correcting the observed heats of solution of samples containing magnesium chloride solution, heat-of-dilution experiments were performed. Magnesium chloride solutions of various strengths were added in small quantities to 600 g of

HCl, 26.61H_2O to which had previously been added 1 g of MgO (equivalent to 0.02 moles MgO per mole HCl). The data are summarized in table 2. The precision of the data was not adequate to establish the variation of the heat of dilution with variation in the quantity of $MgCl_2$ solution used. Therefore, only the average values are given in the table.

TABLE 2. *Heat of dilution*

These data represent the heat effect of adding $MgCl_2$ solutions of various strengths to HCl, 26.61 H_2O to which 0.02 mol MgO per mol of HCl had previously been added.

Composition of $MgCl_2$ solution		Range of dilution ratio, R	Heat of dilution, $-\Delta H_{298}$°C
Percent $MgCl_2$	mol H_2O per mol $MgCl_2$	mol $MgCl_2$ per mol HCl	kcal/mol $MgCl_2$
35.1	9.77	0.012 to 0.060	2.33
24.1	16.64	.008 to .037	0.79
20.7	20.25	.006 to .032	.56
16.6	25.56	.005 to .024	.22

Measurements were made in duplicate at each of three dilution ratios for each solution. The standard deviation of a single determination was 0.07 kcal/mol $MgCl_2$, calculated by the formula

$$S=\sqrt{\frac{\Sigma(\Delta H_1-\Delta H_2)^2}{24}}$$

where ΔH_1 and ΔH_2 are the duplicate measurements. No significant values of $d(-\Delta H)/dR$ could be calculated from these data. Therefore, only the average value for each concentration is given.

3.3. Heats of Solution

a. $3Mg(OH)_2 \cdot MgCl_2 \cdot nH_2O$

Magnesium oxychloride having the ratio three $Mg(OH)_2$ to one $MgCl_2$ is the stable form in equilibrium with solutions in which an oxychloride is formed. This material could be filtered from the solution and washed with alcohol and ether without change in the X-ray pattern. Consequently most of the analyses and heat-of-solution measurements were performed on samples so treated. A few samples were prepared without washing, however, by removing as much $MgCl_2$ solution as possible by pressing. The results of the analyses and the heats of solution are given in table 3. The unwashed samples are indicated by the letter P and contain excess $MgCl_2$ solution as shown by the analyses.

Since the amount of material was limited, generally only one heat-of-solution determination was made on each sample. However, replicate determinations were made in a number of instances with a precision (standard deviation of a single test) of ± 1.15 cal/g (1 cal = 4.1840 abs j).

The heat of solution of magnesium oxychloride was calculated from the data in table 3. It was assumed that $Mg(OH)_2$ was present in excess in samples having a ratio $Mg(OH)_2/MgCl_2$ greater than three and that $MgCl_2 \cdot 6H_2O$ was present in samples having a smaller ratio. The first condition would be caused by the removal of $MgCl_2$ from the precipitated oxychloride by too vigorous washing.

TABLE 3. *Heats of solution of* $3Mg(OH)_2 \cdot MgCl_2 \cdot H_2O$ *preparations in* HCl, 26.61H_2O

Sample	Composition			Molar ratio		Heat of solution in HCl, 26.61H_2O
	MgO	$MgCl_2$	H_2O	$Mg(OH)_2/MgCl_2$	$H_2O/MgCl_2$ [a]	
	%	%	%			cal/g
74.3A [b]	28.85	23.31	47.84	2.923	7.926	165.8
74.3A						166.8
72 P	9.42	30.42	60.16	0.731	9.723	59.1
72 P	8.11	30.71	61.18	0.624	9.907	77.3
72 A	29.84	23.34	46.82	3.020	7.584	177.1
72 B	29.41	22.63	47.96	3.070	8.133	169.5
72 C	29.58	23.92	46.50	2.921	7.355	172.4
67 P	8.07	30.12	61.81	0.633	10.22	51.7
67 A	29.84	24.12	46.04	2.922	7.168	178.3
67 B	29.86	23.09	47.05	3.055	7.716	170.6
67 C	29.94	23.85	46.21	2.965	7.277	177.7
62 P	8.01	28.00	63.99	0.676	11.40	51.7
62 A	30.65	24.17	45.18	2.995	6.886	186.7
62 B	29.59	23.14	47.27	3.020	7.778	170.1
62 C	30.36	23.92	45.72	2.998	7.106	184.6
58.5 P	24.01 [c]	24.50 [c]	51.49 [c]	2.315	8.794	139.6
58.5 P						139.8
58.5 A	29.83	23.11	47.06	3.049	7.715	175.5
58.5 A	29.89	23.18	46.93	3.046	7.656	174.4
58.5 A	29.88	23.11	47.01	3.054	7.699	173.6
58.5 A	29.88	23.11	47.01	3.054	7.699	176.1
58.5 AD	33.80	26.19	40.01	3.048	5.027	219.6
58.5 AD	44.68	34.61	20.71	3.049	0.114	377.5
58.5 AD	35.67	27.63	36.70	3.049	3.972	242.2
58.5 AD	35.49	27.50	37.01	3.048	4.066	239.7
58.5 AD	44.66	34.60	20.74	3.049	0.120	377.0
58.5 AD	44.41	34.40	21.19	3.049	0.207	378.6
58.5 AD	39.69	30.75	29.56	3.049	2.032	303.5
58.5 AH	29.50	22.85	47.65	3.049	7.974	169.4
58.5 AH						170.7
57 P	9.43	25.53	65.04	0.872	12.60	56.2
57 C	31.20	24.15	44.65	3.052	6.722	190.2
55 A	30.80	23.93	45.27	3.040	6.960	189.1
55 A	31.17	23.93	44.90	3.077	6.841	187.7
55 A	30.64	23.57	45.79	3.070	7.199	175.5
55 AD	33.83	26.03	40.14	3.070	5.082	223.2
55 AD	35.36	27.20	37.44	3.070	4.206	238.8
55 AD	43.87	33.75	22.38	3.070	0.435	370.3
52.5 A	29.66	23.90	46.44	2.931	7.340	171.2
52.5 A						174.5
52.5 A	29.76	23.22	47.02	3.027	7.677	175.1
52.5 A	29.68	22.94	47.38	3.056	7.862	169.9
52.5 AD	32.57	26.12	41.31	3.056	5.054	215.0
52.5 AD	35.32	27.30	37.38	3.056	4.181	234.0
52 P	7.49	24.86	67.65	0.712	13.67	44.5
52 A	30.44	24.12	45.44	2.981	6.978	183.2
52 B	29.97	23.42	46.61	3.023	7.497	175.2
52 C	31.43	23.97	44.60	3.097	6.739	189.6
47 P	8.64	22.45	68.91	.909	15.32	52.3
47 P	11.41	21.57	67.02	1.249	15.18	67.7
47 A	30.37	23.50	46.13	3.052	7.325	174.6
47 B	29.63	23.26	47.11	3.009	7.697	172.2
47 C	30.34	23.94	45.72	2.993	7.102	183.1
42 A	30.12	23.52	46.36	3.025	7.394	177.3
42 B	29.74	22.71	47.55	3.093	7.975	169.9
42 C	30.07	23.47	46.46	3.026	7.438	176.8
37 C	31.00	24.05	44.95	3.045	6.835	186.6

[a] Corrected for water equivalent to MgO to form $Mg(OH)_2$.

[b] 74.3, etc., equals original percent of $MgCl_2 \cdot 6H_2O$ by weight in the solution from which the sample was obtained. A, Precipitated from clear metastable solution of MgO in $MgCl_2$ solution. Washed with alcohol and ether. B, Reaction product of $Mg(OH)_2$ and $MgCl_2$ solution. Washed with alcohol and ether. C, Precipitate A placed in fresh $MgCl_2$ solution containing no dissolved MgO. Washed with alcohol and ether. P, Precipitated as in A. $MgCl_2$ solution removed by pressure. Precipitate not washed. D, Partially dehydrated. H, Equilibrated over saturated solution of $Na_2Cr_2O_7$.

[c] Average of four determinations. Standard deviation of individual test for MgO = ±0.027 percent, for $MgCl_2$ = ±0.032 percent.

The second condition would be caused (under the conditions of drying) by inadequate washing so that the sample retained magnesium chloride solution. The observed heats of solution were corrected using 26.88 kcal/mole [12] for the heat of solution of excess $Mg(OH)_2$ and 1.65 kcal/mole (determined in this work) for the heat of solution of $MgCl_2 \cdot 6H_2O$. The total water was corrected for that in the $MgCl_2 \cdot 6H_2O$ or $Mg(OH)_2$ and the corrected value taken as n in

the formula $3Mg(OH)_2 \cdot MgCl_2 \cdot nH_2O$ for the oxychloride.

The calculated heats of solution for the oxychloride samples are shown in figure 3 where they are plotted in kilocalories per mole of $MgCl_2$ (equivalent to per mole of $3Mg(OH)_2 \cdot MgCl_2 \cdot nH_2O$) against the value of n. The standard deviations of the individual tests calculated from the relatively few replicate measurements are ± 0.48 kcal/mole for the heat of solution and ± 0.026 for the value of n.

The straight lines in figure 3 were calculated by the method of least squares from the data in the range of values of n from 0 to 4 for one line and from 4 to 8 for the other. Values near $n=4$ were used for both lines. The data as a whole could be represented by a single curved line. However, the grouping shown would be explained if the samples were composed of three oxychlorides containing 8, 4, and 0 moles of water respectively per mole of $MgCl_2$. In the dehydration experiments there was evidence of a hydrate containing four molecules of water, since the material heated at 110° C tended to reach and remain at that composition, as did material heated at 45° C. A washed sample of magnesium oxychloride kept over saturated solution of $MgCl_2$ (relative humidity 33 percent [9]) attained the composition $3Mg(OH)_2 \cdot MgCl_2 \cdot 7.859H_2O$. When the sample was transferred to a desiccator containing a saturated solution of $Na_2Cr_2O_7$ (relative humidity 52% [13]) the composition became $3Mg(OH)_2 \cdot MgCl_2 \cdot 7.974H_2O$.

It should be pointed out that the dehydration of certain samples was arbitrarily stopped when the composition reached approximately 5 and 2 molecules of water per mole of $3Mg(OH)_2 \cdot MgCl_2$ in order to secure the heats of solution of samples containing those amounts of water. On the other hand, the composition at 4 molecules of water was reached in 1 day by samples heated at 110° C whereas further heating at that temperature for several days resulted in very little further loss of water. The dehydration of $3Mg(OH)_2 \cdot MgCl_2 \cdot 8H_2O$ over KOH and magnesium perchlorate did not show with certainty the existence of other hydrates.

The author believes that the oxychloride as precipitated contains 8 molecules of water in agreement with the composition $2MgO \cdot HCl \cdot 5H_2O$ (equivalent to $3Mg(OH)_2 \cdot MgCl_2 \cdot 8H_2O$) given by Robinson and Waggaman [1] from analyses of unwashed precipitates and of the solutions in which they formed. (Their reported composition $3MgO \cdot MgCl_2 \cdot 10H_2O$ seems to be erroneously converted from their determined composition of $2.02MgO \cdot HCl \cdot 5.04H_2O$.) Part of this water is removed when the precipitated material is prepared for analysis, and samples are obtained containing from 7 to 8 molecules of water as given in table 3. Feitknecht and Held [6] prepared materials containing 7, 5.14, 3.4, or 0.15 molecules of water per mole of $3Mg(OH)_2 \cdot MgCl_2$ by drying the precipitated oxychloride. Wehner [14], who also concluded that the precipitated form contained 8 molecules of water, found that an air-dried sample originally containing 10 molecules of water contained 7 after drying for 30 min at 80° C, 4.7 after drying at 120° C for 1 hr, and 3.1 molecules after 5 hrs at 120° C. After drying for 5 hrs at 200° C, the material was anhydrous. The differential thermal analysis [19] obtained in the present work and shown in figure 4 indicates the loss of water in three steps A, B, and C at 140°, 165°, and 210° C, respectively. The other deflections in this curve at higher temperatures represent the further stepwise decompositions of $3Mg(OH)_2 \cdot MgCl_2$ to the final solid product of MgO. If hydrates other than that containing four molecules of water were formed during the dehydration of the precipitated oxychloride, however, the heat-of-solution measurements shown in figure 3 were not precise enough to reveal their presence.

From the equations for the straight lines in figure 3, the following heats of solution in HCl, $26.61H_2O$ were calculated:

$3Mg(OH)_2 \cdot MgCl_2$, 103.96 kcal/mole;
$3Mg(OH)_2 \cdot MgCl_2 \cdot 4H_2O$, 81.43 kcal/mole;
$3Mg(OH)_2 \cdot MgCl_2 \cdot 7H_2O$, 72.54 kcal/mole;
$3Mg(OH)_2 \cdot MgCl_2 \cdot H_2O$, 69.61 kcal/mole.

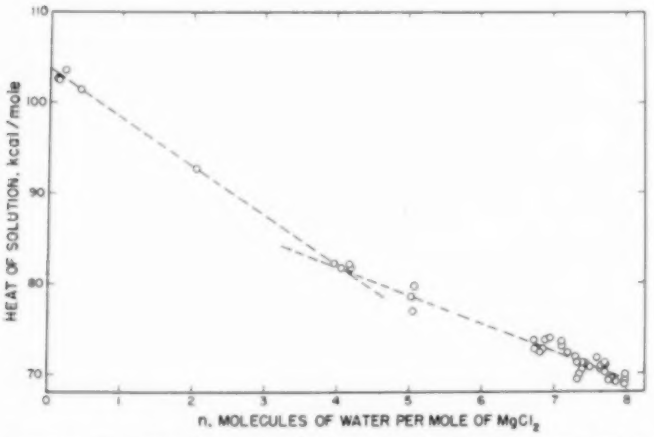

FIGURE 3. *The heat of solution of* $3Mg(OH)_2 \cdot MgCl_2 \cdot nH_2O$ *in* HCl. $26.61H_2O$ *at 25° C.*

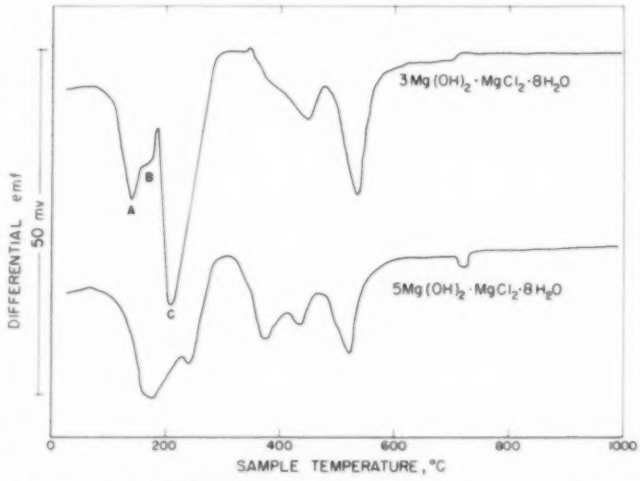

FIGURE 4. *Differential thermal analysis of magnesium oxychlorides.*

The heats of solution of the pressed samples, the crystals of which presumably were $3Mg(OH)_2 \cdot MgCl_2 \cdot 8H_2O$, agreed reasonably well with the value taken from figure 3. Corrected for the heat of dilution of the appropriate quantity of the $MgCl_2$ solution from which the precipitates were taken, heats of solution of 69.29, (72.96), 70.74, (72.96), 69.94, 70.04, 69.31, 69.07, 69.88, and 70.97 kcal/mole were obtained. Omitting those in parentheses which differed from the average of the others by more than four times their individual standard deviation, the average value is 69.90 kcal/mole.

b. $5Mg(OH)_2 \cdot MgCl_2 \cdot nH_2O$

The compound $5Mg(OH)_2 \cdot MgCl_2 \cdot nH_2O$ is metastable at 25° C in $MgCl_2$ solutions of all concentrations. It was obtained in the present work as the first precipitate from solutions containing 34 or 36 percent of $MgCl_2 \cdot 6H_2O$ respectively, and supersaturated with MgO. Most of the samples were obtained by pressing out the solution without washing, but some were obtained by washing the material with alcohol and acetone. The analyses and the heats of solution are given in table 4. The heats of solution were corrected for the heat of dilution of the $MgCl_2$ solution, or the heats of solution of $Mg(OH)_2$ or $MgCl_2 \cdot 6H_2O$, as indicated by the analysis and are given in the last column of the table, expressed as kilocalories per mole of the 5:1 compound. The value of n for the 7 samples of washed material varied only over the range 7.798 to 7.955. Over this short range, correlation was found between the heat of solution and the value of n. The heat of solution thus found for $n=8$ was 124.14 kcal/mole of $5Mg(OH)_2 \cdot MgCl_2 \cdot 8H_2O$. However, since in some cases differences were found in the X-ray patterns of samples before and after washing, the average value of the heats of solution of both the washed and the pressed samples was taken as the heat of solution in HCl, $26.61H_2O$ of the 5:1 compound. The value found was 125.94 kcal/mole. The standard deviation of the average was 0.30 kcal/mole. The associated value of n is considered to be 8 in the material as precipitated. Feitknecht and Held [6] found n to be for their preparation after washing and drying, but this value was not approached with the 5:1 compound in the present work

3.4. Heats of Formation

The heats of formation of the four magnesium oxychlorides were calculated from their heats of solution and the heats of solution of $MgCl_2.6H_2O$(c) and $Mg(OH)_2$. The samples were small (0.5 to 2.0 g) in comparison with the 600 g of HCl, $26.61H_2O$ used in the calorimeter. Heats of dilution and differences in final composition of the calorimeter solution from sample to sample were therefore in general neglected. The precision of the measurements did not warrant the labor of determination or calculation of the small corrections generated, for example, by the small deviations in the final concentrations caused by the use of differing small quantities of the various oxychloride preparations. The heats of reaction between $Mg(OH)_2$(c) (brucite), $MgCl_2 \cdot 6H_2O$ (c) and H_2O (l) to form the oxychlorides were calculated from the observed heats of solution and applied with the heats of formation of those reactants [8] to calculate the heats of formation of the oxychlorides. Pertinent data and the calculated results are included in table 5.

These heats of formation differ from those calculated [8] from the results of Andre's work [7]. He identified the compound obtained from 20.8 percent $MgCl_2$ solution (44.4 percent of $MgCl_2 \cdot 6H_2O$) as $MgO \cdot MgCl_2 \cdot 16H_2O$, a compound not reported elsewhere. The proportions given by the average of his

TABLE 4. *Heat of solution of* $5Mg(OH)_2 \cdot MgCl_2 \cdot 8H_2O$ *preparations in* HCl, $26.61H_2O$

Sample	Composition			Molar ratio		Heat of solution of sample	Calculated heat of solution of $5Mg(HO)_2 \cdot MgCl_2 \cdot 8H_2O$
	MgO	$MgCl_2$	H_2O	$Mg(OH)_2/MgCl_2$	[a]$H_2O/MgCl_2$		
	%	%	%			*cal/g*	*kcal/mole*
34P1[b]	13.88	17.27	68.85	1.898	19.18	87.9	127.4
34P1						88.2	127.9
34P2	14.31	16.91	68.78	1.999	19.50	89.5	125.8
34P3	10.03	16.89	73.08	1.403	21.47	64.0	128.2
34P4	12.95	16.83	70.22	1.817	20.24	80.7	125.4
34P5	17.97	17.58	64.45	2.414	16.96	111.7	125.2
34P6	16.98	17.54	65.48	2.287	17.45	104.4	123.7
34P7	12.92	16.91	70.17	1.805	20.13	81.7	127.2
34P8	13.10	18.38	68.52	1.683	18.02	82.6	126.8
36P1	13.88	17.50	68.62	1.873	18.86	88.6	128.4
36P2	12.50	17.67	69.83	1.671	19.22	77.0	123.8
36P3	15.62	18.76	65.62	1.967	16.52	97.1	125.0
36P4	11.07	17.06	71.87	1.533	20.74	69.2	125.5
36P5	14.16	17.73	68.11	1.886	18.42	86.8	123.6
36A1	37.85	18.06	44.09	4.950	7.955	234.3	124.8
36A2	38.30	17.93	43.77	5.045	7.859	238.4	125.4
36A3	39.16	17.51	43.33	5.282	7.799	247.0	126.8
36A4	37.95	18.18	43.97	4.931	7.825	237.4	126.1
36A5	38.70	17.78	43.52	5.141	7.798	242.6	126.2
36A6	38.07	18.09	43.84	4.971	7.839	238.0	125.9
36A7	38.33	17.93	43.74	5.049	7.846	239.0	125.6

[a] Corrected for water equivalent to MgO to form $Mg(OH)_2$.

[b] 34 and 36, Original percent of $MgCl_2.6H_2O$ by weight in the solution from which the sample was precipitated. A, Precipitated from clear solution of MgO in $MgCl_2$ solution. Washed with alcohol and acetone. P, Precipitated as in A. $MgCl_2$ solution removed by pressure. Precipitate not washed. 1, 2, etc., Preparation number.

TABLE 5. *Heats of solution and formation of magnesium oxychlorides*

Compound	ΔH_{298}	
	Heat of solution in $HCl26.6H_2O$	Heat of formation
	kcal/mole	*kcal/mole*
MgO (c)		−143.84[8]
MgO (c) finely divided		−142.95[8]
$Mg(OH)_2$ (c) brucite	−25.64[12]	−221.00[8]
$Mg(OH)_2$ (c) finely divided	−26.88[12]	
$MgCl_2$ (c)		−153.40[8]
$MgCl_2 \cdot 6H_2O$ (c)	−1.65	−597.42[8]
$MgCl_2 \cdot 20.69H_2O$ (soln.) [a]	−0.42	−188.12[8]
$MgCl_2 \cdot 43.25H_2O$ (soln.) [b]		−189.03[8]
H_2O (l)	−0.017[16]	−68.317[8]
$3Mg(OH)_2 \cdot MgCl_2 \cdot 8H_2O$ (c)	−69.61	−1409.05
$3Mg(OH)_2 \cdot MgCl_2 \cdot 4H_2O$ (c)	−81.43	−1123.90
$3Mg(OH)_2 \cdot MgCl_2$ (c)	−103.96	−828.04
$5Mg(OH)_2 \cdot MgCl_2 \cdot 8H_2O$ (c)	−125.94	−1848.00

[a] 22° B solution.
[b] Solution containing 10.69 percent of $MgCl_2$.

analyses are 0.94:1.00:15.8. Since his material was dried on paper it contained magnesium chloride solution in unknown amount, and because of his method of preparing the supersaturated solution of MgO in $MgCl_2$, of unknown concentration. Andre's description of his method of preparation is incomplete, because he did not give times of heating, but attempts were made to duplicate his procedure. When successful, these resulted in products which the X-ray patterns indicated were mixtures of the 5:1 and the 3:1 oxychlorides. The proportions varied with the time of standing before filtration, the 5:1 oxychloride predominating at short times. The heats of solution of these preparations were not determined.

3.5 Heat of Hardening of Magnesium Oxychloride Cement

The potential heat of hardening of magnesium oxychloride cement can be calculated from the heats of formation of the oxychlorides. As Rodt [17] and others have pointed out, the reaction of MgO and $MgCl_2$ solution is incomplete in a paste of a usable consistency because insufficient $MgCl_2$ solution is present. If the assumption is made that the concentration of the $MgCl_2$ solution does not fall below that given by Bury and Davies [4] as necessary to maintain the stability of the 3:1 oxychloride, 10.89 percent, the extent of the reaction can be calculated. Such a calculation was made for a paste made of 40 percent of MgO and 60 percent of 22° B $MgCl_2$ solution, a composition approximating those used in actual practice. The X-ray pattern of such a paste showed that at 254 days it consisted of the 5:1 oxychloride and $Mg(OH)_2$. The observed heat of hardening [18] was 235 cal/g MgO at 60 days. The potential heat of hardening calculated, based on the formation of $Mg(OH)_2$, the 5:1 oxychloride, and 10.89 percent $MgCl_2$ solution, was 265 cal/g of MgO. Only about one half of the MgO would be converted to the 5:1 compound under the conditions assumed, the rest would be present as $Mg(OH)_2$. Details of the calculation are shown in the appendix. As indicated there, by far the greater part of the heat evolved is due to the hydration of the magnesia to magnesium hydroxide.

The author gratefully acknowledges the assistance of Leonard P. Suffredini who prepared many of the samples of $5Mg(OH)_2 \cdot MgCl_2 \cdot 8H_2O$ and determined their heats of solution.

4. References

[1] W. O. Robinson and W. A. Waggaman, J. Phys. Chem. **13,** 673 (1909).
[2] H. S. Lukens, J. Am. Chem. Soc. **54,** 2372 (1932).
[3] L. Chassevent, Chimie & industrie **30,** 1020 (1933).
[4] C. R. Bury and E. R. H. Davies, J. Chem. Soc. (London) (a) **1932,** 2008; (b) **1933,** 701.
[5] W. Feitknecht, Helv. Chim. Acta **9,** 1018 (1926); **10,** 140 (1927); **13,** 1380 (1930).
[6] W. Feitknecht and F. Held, Helv. Chim. Acta **27,** 1480 (1944).
[7] G. Andre, Ann. chim. et phys. [6] **3,** 79 (1884).
[8] Selected Values of Chemical Thermodynamic Properties, Cir. NBS 500 (1952) (U. S. Government Printing Office Washington 25, D. C.).
[9] International Critical Tables, National Research Council (McGraw-Hill Book Co., Inc., New York, N. Y.).
[10] E. S. Newman and L. S. Wells, J. Research NBS **20,** 825 (1938) RP1107.
[11] W. P. White, The Modern Calorimeter (The Chemical Catalog Co., New York, N. Y., 1928).
[12] K. Taylor and L. S. Wells, J. Research NBS **21,** 133 (1938) RP1121.
[13] Handbook of Chemistry and Physics (Chemical Rubber Publishing Co., Cleveland, Ohio, 1939).
[14] G. Wehner, Z. anorg. u. allgem. Chem. **272,** 201 (1953).
[15] E. T. Carlson, R. B. Peppler, and L. S. Wells, J. Research NBS **51,** 179 (1953) RP2448.
[16] F. D. Rossini, BS J. Research **9,** 679 (1932) RP499.
[17] V. Rodt, Zement **26,** 597 (1937).
[18] E. S. Newman, J. V. Gilfrich, and L. S. Wells, J. Research NBS **49,** 377 (1952) RP2375.
[19] E. S. Newman and L. S. Wells, J. Research NBS **36,** 137 (1946) RP1696.
[20] F. R. Bichowsky and F. D. Rossini, The Thermochemistry of the Chemical Substances (Reinhold Publishing Corp., New York, N. Y., 1936).

5. Appendix

Calculation of the composition and potential heat of hardening of a paste consisting of 40 g MgO and 60 g of 22° B $MgCl_2$ solution ($MgCl_2$,20.69H_2O).

Products: $5Mg(OH)_2 \cdot MgCl_2 \cdot 8H_2O$, $Mg(OH)_2$, and 10.89 percent $MgCl_2$ solution ($MgCl_2$,43.254H_2O).

Basis: 100 g of paste

$$0.9921\ MgO + 0.1282\ (MgCl_2,20.69H_2O) = X\ Mg(OH)_2 + Y(5Mg(OH)_2 \cdot MgCl_2 \cdot 8H_2O) + Z(MgCl_2,43.254H_2O)$$

$$MgO = 0.9921 = X + 5Y,$$

$$MgCl_2 = 0.1282 = Y + Z,$$

$$H_2O = 2.65246 = X + 13Y + 43.254Z.$$

Solving; X=0.4411, Y=0.1102, Z=0.01801

Therefore the desired equation is:

$$0.9921MgO(c) + 0.1282(MgCl_2,20.69H_2O)(soln.) = 0.4411\ Mg(OH)_2(c) + 0.1102\ (5Mg(OH)_2 \cdot MgCl_2 \cdot 8H_2O)(c) + 0.01801(MgCl_2,43.254H_2O)(soln.) + \Delta H. \quad (A)$$

This equation is the sum of the following equations:

$0.9921MgO(c, \text{finely divided}) + 0.9921H_2O(l) = 0.9921Mg(OH)_2(c)$, $\Delta H_1 = -9.656$ kcal

$0.5510Mg(OH)_2(c) + 0.1102(MgCl_2 \cdot 6H_2O)(c) + 0.2204H_2O(l) = 0.1102(5Mg(OH)_2 \cdot MgCl_2 \cdot 8H_2O)(c)$, $\Delta H_2 = -0.986$ kcal

$0.1102MgCl_2(c) + 0.6612H_2O(l) = 0.1102(MgCl_2 \cdot 6H_2O.(c)$, $\Delta H_3 = -3.760$ kcal

$0.1102(MgCl_2 \cdot 20.69H_2O)(\text{soln.}) = 0.1102MgCl_2(c) + 2.2800H_2O(l)$, $\Delta H_4 = +3.826$ kcal.

$0.01801(MgCl_2 \cdot 20.69H_2O)(\text{soln.}) + 0.4063H_2O = 01801(MgCl_2 \cdot 43.25H_2O)(\text{soln.})$, $\Delta H_5 = -0.016$ kcal.

The ΔH of eq (A) is the sum of the five ΔH's shown. These have been calculated in the usual manner [20] from the data in table 5.

The ΔH of eq (A) is found to be -10.59 kcal or 265 cal/g MgO.

WASHINGTON, November 5, 1954.

Journal of Research of the National Bureau of Standards Vol. 54, No. 6, June 1955 Research Paper 2598

Dielectric Relaxation for Spherical Molecules in a Crystalline Field: Theory for Two Simple Models

John D. Hoffman and Benjamin M. Axilrod

A theory of dielectric relaxation is given for two simple models where the dipoles may occupy orientational sites arranged in three dimensions. In the first model, the dipole may point toward the corners of a regular tetrahedron, and in the second, toward the faces of a cube. Both models are simplified to the extent that only one of the sites can differ in energy from all the others.

The calculations show that these models lead to a discrete set of dielectric relaxation times when the sites are not equivalent. The effect of the set of relaxation times on the characteristics of the dielectric relaxation spectrum is examined. The relaxation times are always sufficiently close together so that the dielectric loss is confined to a single region. However, the separation of the relaxation times is sufficient to cause the dielectric loss peak to be considerably broader than that predicted by the Debye equations. In addition, it is found that the loss maximum will frequently be asymmetrical. The variation of the dielectric constant with temperature, and the breadth and asymmetry of the loss peaks are discussed.

1. Introduction

Our basic viewpoint is that an anisotropy in the crystalline field hindering the rotation of a dipole in a lattice can be the source of a set of discrete dielectric relaxation times. This viewpoint has already been explored in some detail for a single-axis rotator.[1,2] The main objective of this paper is to show how one type of calculation used with the single-axis rotator can be extended to include two simple models where each dipole in the lattice, by turning about a lattice point, can occupy orientational sites arranged in three dimensions. A model permitting such orientations in space may be a reasonable representation for certain molecular crystals composed of polar molecules that are approximately spherical.

The theory presented here and in the papers mentioned above may be regarded as an extension of Debye's two-position model.[3] The two-position model gives only a single[1,3,4] relaxation time; however, a set of relaxation times frequently appears for a single-axis rotator when more than two sites are involved.[1,2] We have also modified Debye's theory to the extent that transition probabilities of the elementary process for dipole reorientation have been defined along the lines proposed by Kauzmann.[5]

2. Tetrahedral Model With One Stable Site

2.1. Model

In this model the dipole possesses four equilibrium orientations (sites) designated 1 through 4 which are arranged in a tetrahedral manner (fig. 1). The permanent dipole moment has the magnitude μ.

[1] J. D. Hoffman and H. G. Pfeiffer, J. Chem. Phys. **22**, 132 (1954).
[2] J. D. Hoffman, ibid. (in press).
[3] P. Debye, Polar Molecules, p. 104 (Dover Publications, New York, 1945).
[4] H. Fröhlich, Theory of Dielectrics, p. 83 (Oxford University Press, 1949).
[5] W. Kauzmann, Rev. Mod. Phys. **14**, 12 (1942).

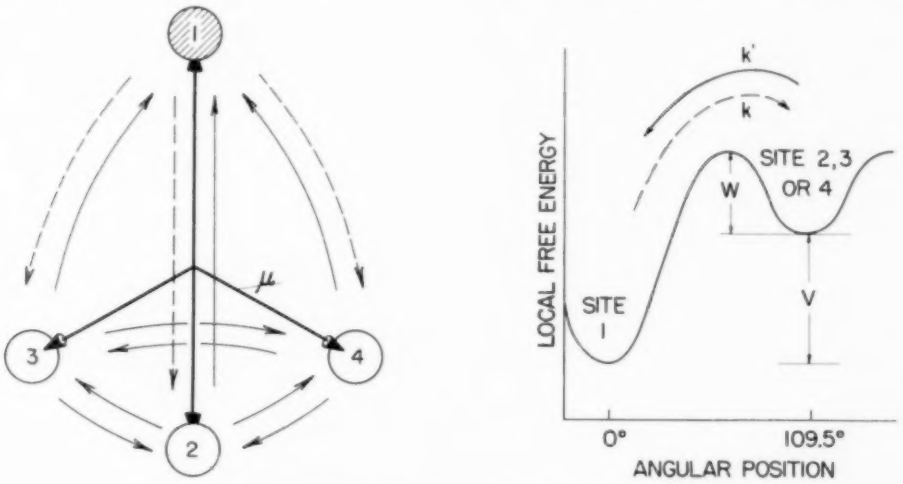

FIGURE 1. *Elementary processes for the tetrahedral model.*

Left diagram: Heavy straight arrows indicate equilibrium dipole orientations, light curved arrows the elementary processes k (- - →) and k' (——→). Site 1 is the stable orientation. Right diagram: Details of the barrier system for site 1 relative to sites 2, 3, and 4. The barrier between sites 2, 3, and 4 (not shown) is W, and the corresponding transition probability is k'.

Sites 2, 3, and 4 are equivalent; site 1 is unique, and may be more stable than the others.

The dipole can turn in a single jump (elementary process) from site 1 to either site 2, 3, or 4 by surmounting a local free energy of activation barrier $W+V$. W and V are shown in figure 1 (right diagram). The barrier system is considered to be the result of the crystalline field imposed on the dipole by its neighbors in the lattice. It is assumed in this simplified treatment that there is no correlation with the motion of neighboring dipoles.

The probability that a dipole will jump from site 1 to either site 2, 3, or 4 is given by

$$k=B\,e^{-(W+V)/kT} \tag{1}$$

where B is a frequency factor, k is Boltzmann's constant, and T the absolute temperature. The dipole must surmount an activation barrier W in order to turn from either site 2, 3, or 4 back to site 1, and the corresponding probability is

$$k'=B\,e^{-W/kT}. \tag{2}$$

The barrier between any pair of the sites 2, 3, and 4 is also W so that the probability of the reorientations $2\rightleftarrows3$, $3\rightleftarrows4$, and $2\rightleftarrows4$ is k'. It is readily seen that when $V>0$, so that site 1 is relatively stable, we have $k'>k$. The assigned transition probabilities for reorientations between the various sites are shown in figure 1 (left diagram.)

2.2. Rate Equations

The molecular relaxation times associated with the model are calculated by constructing and solving the differential equations that describe the rate at which dipoles enter and leave each site in terms of the elementary process transition probabilities given by eq (1) and (2). The number of dipoles leaving a site i and entering another designated j is the product of the probability of the transition $i\rightarrow j$ and the population, N_i, of site i. In our problem each k represents the probability that a dipole will leave a site in a specified direction and turn to an adjacent site (*single-jump hypothesis, S–J*).[1,2]

Consider the net rate at which dipoles enter and leave site 1. According to our hypothesis the number per second leaving site 1 and entering site 2 is kN_1; the total number leaving to enter sites 2, 3, and 4 is $3kN_1$. Similarly, the number returning from site 2 to site 1 is $k'N_2$. The corresponding numbers leaving sites 3 and 4 to enter site 1 are $k'N_3$ and $k'N_4$. Hence the net rate for site 1 is given by $dN_1/dt=-$(number leaving)$+$(number entering)$=-3kN_1+k'(N_2+N_3+N_4)$. Similar reasoning leads to the differential equations for the net rates for the other sites. Thus we find

$$\left.\begin{aligned} dN_1/dt&=-3kN_1+k'(N_2+N_3+N_4)\\ dN_2/dt&=kN_1-3k'N_2+k'(N_3+N_4)\\ dN_3/dt&=kN_1+k'N_2-3k'N_3+k'N_4\\ dN_4/dt&=kN_1+k'(N_2+N_3)-3k'N_4.\end{aligned}\right\} \tag{3}$$

[1] Ince, Ordinary Differential Equations, p. 144 (Dover Publications, New York, 1944).

The solutions of eq (3) will provide the molecular (intrinsic) relaxation times, τ_β, where β is the mode of decay, and will also give considerable information regarding the nature of the modes of decay.

2.3. Relaxation Times and Modes of Decay

Solutions of the equations of the type illustrated in eq (3) are of the form[1,2,6]

$$N_i=\sum_\beta C_{i\beta}\psi_\beta;\quad i=1,2,\cdots\Omega, \tag{4}$$

where i refers to a particular site, Ω is the number of sites, β is the mode of decay, and ψ_β is a decay function of the form

$$\psi_\beta=e^{f_\beta(k,k')t}. \tag{5}$$

The set of discrete relaxation times is given by

$$\tau_\beta=-1/f_\beta(k,k'). \tag{6}$$

The solutions of eq (3) are obtained by forming the characteristic determinant of the differential equations, and solving for eigenvalues of the operator $\mathbf{D}=d/dt$. These eigenvalues, which are always found to be negative or zero, are the $f_\beta(k,k')$. One of the $f_\beta(k,k')$ is always zero, and this mode is designated by $\beta=1$; the corresponding C_{i1} are the equilibrium values of the N_i. The relationships between the $C_{i\beta}$ for each mode where $\beta\geqq2$ are determined by substituting each solution $C_{i\beta}\psi_\beta$ into eq (3). On carrying out the above steps we find that the solutions of eq (3) may be written[7]

$$\left.\begin{aligned} N_1&=C_{11}+3C_{22}\psi_2+0\\ N_2&=C_{21}-C_{22}\psi_2+C_{23}\psi_3\\ N_3&=C_{31}-C_{22}\psi_2+C_{33}\psi_3\\ N_4&=C_{41}-C_{22}\psi_2+C_{43}\psi_3\end{aligned}\right\} \tag{7}$$

(Mode 2 / Mode 3)

where $\psi_2=\exp[-(k'+3k)t]$ and $\psi_3=\exp(-4k't)$. Also, we may note that $C_{21}=C_{31}=C_{41}=C_{11}\exp(-V/kT)$, and that $C_{23}+C_{33}+C_{43}=0$.

Equation (7) describes the rate at which equilibrium is established after the abrupt removal of a disturbance at $t=0$. In the present case the displacement from equilibrium at $t\leqq0$ will be assumed to be the result of a static electric field. The quantities C_{i2} and C_{i3} in eq (7) represent the (small) number of dipoles that are displaced from their equilibrium orientations by the field.

If we form the vectors $\vec{C}_{i2}$ where each $\vec{C}_{i2}$ has the direction of a dipole in the ith site and the magnitude

[6] The eigenvalue of the characteristic determinant $\mathbf{D}=-4k'$ occurs twice. In the case of such doubly degenerate roots we actually have $N_i=C_{i1}+C_{i2}\psi_2+C_{i3}t_3+tC_{i3}\psi_2$. However, it is found by substituting this solution into the original differential equations that the C_{i3} are identically zero.

C_{i2}, the sum of the $\vec{C}_{i2}$ is a measure of the polarization associated with mode 2. A similar relation applies to mode 3. Thus, eq (7) indicates that, owing to the return of the displaced dipoles to their equilibrium orientations, the polarization will decay with time according to

$$P(t)=P_2e^{-(k'+3k)t}+P_3e^{-4k't}. \tag{8}$$

P_2 and P_3 are the polarizations associated with modes 2 and 3 at $t=0$. The actual values of P_2 and P_3 are calculated in a following section. Since the dielectric relaxation time is defined as the time the polarization takes to fall to $1/e$ times its original value, it is seen that the molecular relaxation times are

$$\left.\begin{aligned}\tau_2&=1/(k'+3k)\\ \tau_3&=1/4k'\end{aligned}\right\} \tag{9}$$

in accord with eq (6).

Information regarding the nature of the modes of decay can also be obtained from the solutions. The constants C_{i2} in eq (7) show that mode 2 promotes the attainment of equilibrium by permitting a flow of dipoles from site 1 equally to sites 2, 3, and 4 (or vice versa). Similarly, it is seen that mode 3 involves reorientations among the equivalent sites only; site 1 is not involved. The uncertainty (which is removed when we place an electric field on the system) regarding the exact nature of the motions for mode 3 is a result of the fact that this mode is degenerate.

2.4. Polarization and Orientational Polarizability Associated With the Relaxation Times

It is desirable to know the polarization and polarizability associated with each mode of decay. This means that we must evaluate the $C_{i\beta}$ in eq (7) for $\beta \geqq 2$. To do this we first calculate the new equilibrium number of dipoles, C_{i1}^F, in each site when a static electric field $\vec{F}$ is present, where F is the magnitude of the field.

According to the Boltzmann distribution law we may write

$$C_{i1}^F/C_{11}^F=C_{i1}e^{(\overrightarrow{\mu\cdot F})_i/kT}/C_{11}e^{(\overrightarrow{\mu\cdot F})_1/kT} \tag{10}$$

where C_{i1}^F is the equilibrium number of dipoles in site i in the presence of the field $\vec{F}$, and C_{11}^F is the corresponding number for site 1. The quantity $\overrightarrow{\mu\cdot F}$ is given by

$$\begin{aligned}\left(\overrightarrow{\mu\cdot F}\right)_i=\mu F[&\sin\xi_i'\cos\theta_i'\sin\xi\cos\theta+\\ &\sin\xi_i'\sin\theta_i'\sin\xi\sin\theta+\cos\xi_i'\cos\theta].\end{aligned} \tag{11}$$

The angles ξ_i' and θ_i' define the angular position of the ith site, while ξ and θ define the field direction (fig. 2). After calculating the ratio C_{i1}^F/C_{11}^F for $i=2$, 3, and 4, and applying the condition $\sum_i C_{i1}^F=N$ where N is the total number of dipoles in the lattice, we obtain

$$\left.\begin{aligned}C_{11}^F&=C_{11}+4C_{11}C_{21}\mu F\cos\xi/NkT\\ C_{21}^F&=C_{21}-4C_{11}C_{21}\mu F\cos\xi/3NkT-\\ &\quad C_{21}\mu F\sin\lambda\sin\xi(\cos\theta+\sqrt{3}\sin\theta)/2kT\\ C_{31}^F&=C_{21}-4C_{11}C_{21}\mu F\cos\xi/3NkT-\\ &\quad C_{21}\mu F\sin\lambda\sin\xi(\cos\theta-\sqrt{3}\sin\theta)/2kT\\ C_{41}^F&=C_{21}-4C_{11}C_{21}\mu F\cos\xi/3NkT+\\ &\quad C_{21}\mu F\sin\lambda\sin\xi\cos\theta/kT\end{aligned}\right\} \tag{12}$$

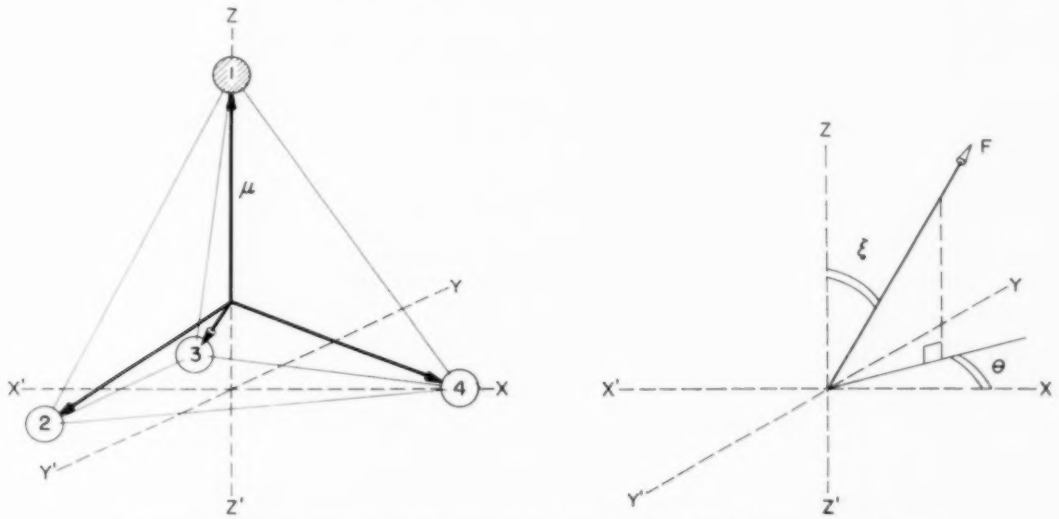

FIGURE 2. *Arrangements of the sites and field direction for the tetrahedral model.*

Left diagram: Heavy arrows represent the equilibrium dipole orientations. Right diagram: Polar coordinates used to define the field direction. The same angles with the notation ξ_i' and θ_i' are used to define the equilibrium dipole orientations.

to an excellent approximation.[8] λ is the tetrahedral angle.

The actual number of dipoles displaced by the field into each site for each mode is readily obtained if we note, as implied in sections 2, 3, that

$$\left.\begin{aligned} N_i &= C_{i1}^{\nu} \text{ at } t=0 \\ N_i &= C_{i1} \text{ at } t=\infty . \end{aligned}\right\} \tag{13}$$

With the C_{i1}^{ν} given in eq (12), application of these boundary conditions to eq (7) yields

$$\left.\begin{aligned} C_{12} &= 4\ C_{11}\ C_{21}\ \mu\ F \cos\xi/3\ N\ \boldsymbol{k}T \\ C_{23} &= -C_{21}\ \mu\ F \sin\lambda \sin\xi\ (\cos\theta+\sqrt{3}\sin\theta)/2\ \boldsymbol{k}T \\ C_{33} &= C_{21}\ \mu\ F \sin\lambda \sin\xi\ (\sqrt{3}\sin\theta-\cos\theta)/2\ \boldsymbol{k}T \\ C_{43} &= C_{21}\ \mu\ F \sin\lambda \sin\xi \cos\theta/\boldsymbol{k}T \end{aligned}\right\} \tag{14}$$

Now that the coefficients $C_{i\beta}$ have been evaluated for the case of an applied electric field, the polarization and polarizability associated with each mode at $t=0$ may be calculated. For each mode we obtain the components of the polarization in the x, y, and z directions with

$$\left.\begin{aligned} P_x &= \mu \sum N_i \sin\xi_i' \cos\theta_i' \\ P_y &= \mu \sum N_i \sin\xi_i' \sin\theta_i' \\ P_z &= \mu \sum N_i \cos\xi_i' \end{aligned}\right\} \tag{15}$$

where the N_i (at $t=0$) are given by eq (7) after relations (14) have been inserted. To obtain P_x, P_y, and P_z for a given mode, only the part of the N_i involving that mode is employed. The components of P_x, P_y, and P_z in the field direction are

$$\left.\begin{aligned} P_{(x,F)} &= P_x \sin\xi \cos\theta \\ P_{(y,F)} &= P_y \sin\xi \sin\theta \\ P_{(z,F)} &= P_z \cos\xi . \end{aligned}\right\} \tag{16}$$

The average value of the polarization for all orientations of the applied field is given by

$$P_\beta = \overline{P}_{(x,F)} + \overline{P}_{(y,F)} + \overline{P}_{(z,F)} . \tag{17}$$

The averaging over all orientations of the applied field implies that the sample is polycrystalline.

Following the above procedure we obtain for mode 2

$$P_2 = \left(\frac{16C_{11}C_{21}}{3N}\right)\left(\frac{\mu^2 F}{3\boldsymbol{k}T}\right), \tag{18a}$$

and for mode 3

$$P_3 = \left(\frac{8C_{21}}{3}\right)\left(\frac{\mu^2 F}{3\boldsymbol{k}T}\right). \tag{18b}$$

These are the polarizations referred to in eq (8). Using the defining relation $P_\beta = N\alpha_\beta F$, we find the molecular orientational polarizabilities to be

$$\alpha_2 = \left(\frac{16C_{11}C_{21}}{3N^2}\right)\left(\frac{\mu^2}{3\boldsymbol{k}T}\right) = \frac{16}{3}\left[\frac{k\,k'}{(k'+3k)^2}\right]\left(\frac{\mu^2}{3\boldsymbol{k}T}\right), \tag{18c}$$

$$\alpha_3 = \left(\frac{8C_{21}}{3N}\right)\left(\frac{\mu^2}{3\boldsymbol{k}T}\right) = \frac{8}{3}\left[\frac{k}{(k'+3k)}\right]\left(\frac{\mu^2}{3\boldsymbol{k}T}\right) \tag{18d}$$

where we have made use of the fact that $C_{11}/N = k'/(k'+3k)$ and $C_{21}/N = k/(k'+3k)$. The total polarizability, α_{total}, is given by $[8k(k'+k)/(k'+3k)^2]\,(\mu^2/3\boldsymbol{k}T)$ or $[8g(1+g)/(1+3g)^2]\,(\mu^2/3\boldsymbol{k}T)$ where $g=k/k'$.

2.5. Characteristics of the Dielectric Relaxation Spectrum

So far, we have given our results in terms of quantities that describe how the polarization will decay with time after the abrupt removal of a static field. It should be noted that the relaxation times and polarizabilities which describe the rate of decay, as well as the relative magnitude of each decay process, are expressed in terms of molecular properties. It is desirable to apply these results to macroscopic systems where the measuring field is sinusoidal so that we may learn something of the shape of the regions of loss in the dielectric relaxation spectrum.

If the polarization of a macroscopic system decays after the abrupt removal of a static field with time according to [cf. eq (8)][9]

$$P(t) = \sum_\beta P_\beta \epsilon^{-t/\mathrm{T}_\beta}, \tag{19a}$$

where T_β is the macroscopic relaxation time for the βth mode of decay, we may write (assuming linear superposition) for sinusoidal fields

$$\epsilon''(\omega) = \sum_\beta \Delta\epsilon_\beta \omega \mathrm{T}_\beta/(1+\omega^2\mathrm{T}_\beta^2). \tag{19b}$$

$\epsilon''(\omega)$ is the dielectric loss factor, ω the angular frequency, and $\Delta\epsilon_\beta$ the increment of dielectric constant associated with the βth mode of decay. Equation (19b) reduces to the form of the Debye equation[10] for $\epsilon''(\omega)$ when there is only one relaxation time. For an Onsager-like internal field, it has been suggested by Powles [11] that $\mathrm{T}_\beta \cong \tau_\beta$, and we will employ this approximation. Also, for this field it is reasonable for the purposes of an approximate analysis to assume that $\Delta\epsilon_\beta \cong K\cdot\alpha_\beta$ where K is a con-

[8] In applying eq (10), the exponentials have been expanded and terms $O(\overrightarrow{\mu\cdot F}/\boldsymbol{k}T)^2$ and higher dropped. This is permissible since for ordinary field strengths $\overrightarrow{\mu\cdot F}/\boldsymbol{k}T \ll 1$.

[9] The macroscopic relaxation time exceeds the molecular relaxation time owing to the tendency of the internal field to maintain itself, and the magnitude of the effect is proportional to the difference between the applied field E and the internal field F.

[10] See p. 94 of reference in footnote 3.

[11] J. G. Powles, J. Chem. Phys. **21**, 633 (1953).

stant.[12] With these approximations we have the working equation,[12,2]

$$\epsilon''(\omega) \simeq K \cdot \sum_{\beta} \alpha_\beta \omega \tau_\beta / (1 + \omega^2 \tau_\beta^2). \qquad (20)$$

This equation, together with eq (9) and (18) can be used to predict the general characteristics of the dielectric relaxation spectrum for the tetrahedral model. For the present, we will restrict the discussion to the nature of a plot of ϵ'' against log ω. This discussion will be facilitated by reference to table 1 where the ratios α_2/α_3 and τ_2/τ_3 are given, together with values for the total orientational polarizability, α_{total}, for various values of k/k'. It is convenient to discuss the results in terms of what happens as the ratio k/k' goes from zero to unity.

When site 1 is relatively stable so that k/k' is small compared to unity, it is seen from the table that the relaxation times are moderately far apart, and that the polarizabilities are unequal but still of comparable magnitude. Under these conditions the dielectric loss peak calculated with eq (20) is not only broader than that predicted by the Debye equation with a single relaxation time, but is also slightly asymmetrical. Since the longer relaxation time, τ_2, is associated with the larger polarizability, α_2, the loss peak is somewhat steeper on the low frequency side (fig. 3, curve A). Since the total polarizability is rather low when k/k' is small, that part of the dielectric constant resulting from orientation of dipoles will be small.

If we now raise k/k' to the value one-third, the relaxation times are somewhat closer together than before, and the polarizabilities are equal. The calculated loss maximum is still somewhat broader than one would predict from the Debye equation, and is also symmetrical (fig. 3, curve B).

TABLE 1. *Properties of the tetrahedral model*

$g=k/k'$	Ratio of the relaxation times τ_2/τ_3	Ratio of the polarizabilities α_2/α_3	Total polarizability α_{total} in units of $\mu^2/3kT$
0	4	2	0
1/100	3.88	1.94	.08
1/10	3.07	1.54	.52
1/3	2	1	.89
1/2	1.60	.80	.96
3/4	1.23	.62	.99
1	1	.50	1

As k/k' is increased above a value of one-third, the relaxation times continue to converge so that the loss maximum becomes even narrower. The polarizabilities are again unequal so that the loss maximum again becomes asymmetrical, but owing to the close spacing of the relaxation times the effect will hardly be noticeable. It should be observed that this slight asymmetry is of a type opposite to that found for values of $k/k' < 1/3$.

[12] These approximations are probably fairly accurate, especially in the case where the dielectric constant is low.

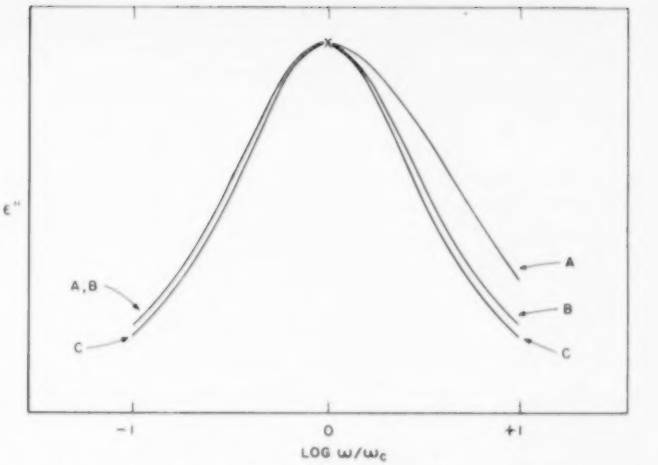

FIGURE 3. *Shape of the dielectric loss peaks for the tetrahedral model.*

Curve A, asymmetrical and broadened peak calculated for $g \cong 0$; curve B, broadened but symmetrical peak calculated for $g = 1/3$; curve C, narrow and symmetrical peak for $g = 1$ (single relaxation time). ω is the measuring frequency, and ω_c is the frequency where ϵ'' is a maximum. For convenience in comparing the shape of the curves, the maximum value for the loss has been matched at X.

Finally, as the ratio k/k' tends to unity, the total polarizability reaches the full value $\mu^2/3kT$, and only a single relaxation time $\tau_2 = \tau_3 = 1/4k$ remains. Thus, the Debye equation for $\epsilon''(\omega)$ holds (fig. 3, curve C). It must be emphasized that, although the polarizability becomes $\mu^2/3kT$, the value for a free rotator, we are dealing with hindered rotation inasmuch as barriers still exist between the sites. Hence, the observed mean relaxation time for the model will always considerably exceed that of a free rotator.

The dependence of the shape, breadth, and magnitude of the loss maximum with increase of temperature is easily obtained if we note that

$$g = k/k' = e^{-V/kT}. \qquad (21)$$

It is clear from this expression that the ratio k/k' will increase with rising temperature even if V is a constant. Therefore, the previous discussion of the changes in the dielectric relaxation spectrum for the case of increasing values of k/k' also holds for the case of rising temperature. Thus, for the tetrahedral model it is seen that the loss maximum will generally tend to become narrower with rising temperature. The loss peak will be steeper on the low frequency side if k/k' is between zero and one-third; i. e., if V/kT lies between ∞ and 1.1. Hence, for a very large range of temperature one should expect to find some asymmetry, and this asymmetry should tend to diminish as the temperature is increased. An analysis shows that the total polarizability, and hence the dielectric constant, will rise up to a temperature where $T \simeq V/1.95k$. Above this temperature the $1/T$ term in the polarizability begins to predominate so that the total polarizability will fall with further increase of temperature.

3. Six-position Model With One Stable Site

The details of the model are shown in figure 4. The dipole in any lattice point may lie in either direction along each of the Cartesian axes, x, y, and z. Site 1 is unique; all the other sites are equivalent and may be unstable with respect to site 1. The model might correspond, for instance, to the case where the central dipole in a body-centered cubic lattice prefers to point toward one face of the cube, but may also point toward any of the five remaining faces.

The S–J hypothesis is assumed. A dipole can turn from site 1 to any of the adjacent sites (2, 3, 4, or 5) with a probability k where k is defined as in eq (1). All other reorientations to adjacent sites occur with a probability k' [eq (2)]. The assigned probabilities for the various elementary processes are shown in figure 4. It should be observed that the double jumps 1→6, 2→4, and 3→5 (or the reverse processes) are forbidden as elementary processes by the S–J hypothesis.

The rate equations are

$$\left.\begin{aligned}
dN_1/dt &= -4kN_1+k'(N_2+N_3+N_4+N_5)\\
dN_2/dt &= kN_1-4k'N_2+k'(N_3+N_5+N_6)\\
dN_3/dt &= kN_1+k'N_2-4k'N_3+k'(N_4+N_6)\\
dN_4/dt &= kN_1+k'N_3-4k'N_4+k'(N_5+N_6)\\
dN_5/dt &= kN_1+k'(N_2+N_4)-4k'N_5+k'N_6\\
dN_6/dt &= k'(N_2+N_3+N_4+N_5)-4k'N_6.
\end{aligned}\right\} \quad (22)$$

The solutions may be written in the form

$$N_i = C_{i1}+C_{i2}\psi_2+C_{i3}\psi_3+C_{i4}\psi_4+C_{i5}\psi_5; \quad (23)$$

$$\psi_2 = e^{-4k't},$$

$$\psi_3 = e^{-6k't},$$

$$\psi_4 = e^{-(2k+3k'-Q)t},$$

$$\psi_5 = e^{-(2k+3k'+Q)t},$$

$$Q = \sqrt{4k^2-8kk'+5k'^2}.$$

Substitution of the solutions $C_{i\beta}\psi_\beta$ for $\beta \geqq 2$ in the differential equations yields the following:[13]

Mode 2.

$$\left.\begin{aligned}
C_{12} &= C_{62}=0\\
C_{22} &= -C_{42}\\
C_{32} &= -C_{52}.
\end{aligned}\right\} \quad (24)$$

This mode of decay thus involves only those dipoles reorienting in sites 2, 3, 4, and 5. The mode is active in the dielectric relaxation spectrum.

[13] Mode 2 is doubly degenerate, and is handled in the same manner as modes 3 and 4 for the tetrahedral model.

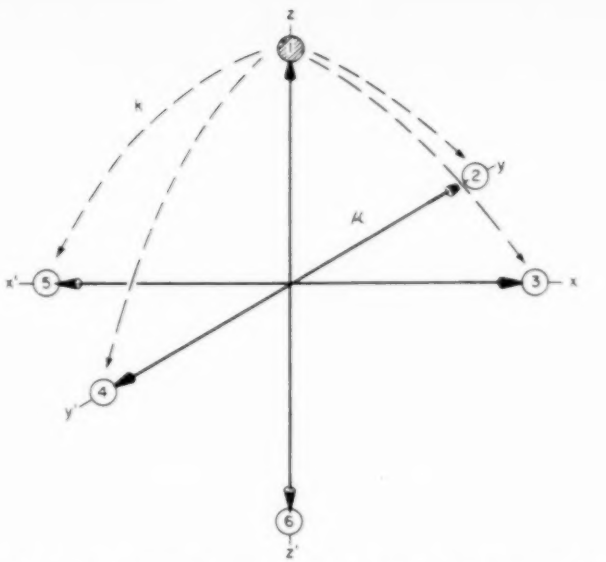

FIGURE 4. *Six-position model with a single stable orientation (site 1).*

Heavy straight arrows indicate the equilibrium dipole orientations. Light dashed arrows indicate elementary processes which take place with a probability k. All other jumps to adjacent sites (such as 2→1 or 2→3) take place with a probability k'. Jumps of the type 1→6 or 5→3 are forbidden as elementary processes. The coordinates used to denote the field direction and orientations of the sites are the same as those given in figure 2 (right diagram).

Mode 3.

$$\left.\begin{aligned}
C_{13} &= C_{63}=0\\
C_{23} &= -C_{33}=C_{43}=-C_{53}.
\end{aligned}\right\} \quad (25)$$

Again, only dipoles in the plane containing sites 2, 3, 4, and 5 are involved. This mode of decay is inactive in the dielectric relaxation spectrum owing to a compensatory motion of the dipoles; the sum of the vectors $\vec{C}_{i3}$ is zero, so no polarization results. A similar situation arises for the single-axis rotator with four equivalent sites.[1]

Mode 4.

$$\left.\begin{aligned}
C_{24} &= C_{34}=C_{44}=C_{54}\\
C_{14} &= -4(1-1/H)C_{24}\\
C_{64} &= -4C_{24}/H
\end{aligned}\right\} \quad (26)$$

where $H=2g-1-q$, $q=Q/k'$, and $g=k/k'$.

Mode 5.

$$\left.\begin{aligned}
C_{25} &= C_{35}=C_{45}=C_{55}\\
C_{15} &= -4(1-1/H')C_{25}\\
C_{65} &= -4C_{25}/H'
\end{aligned}\right\} \quad (27)$$

where $H'=2g-1+q$. Both modes 4 and 5 are complicated and involve dipoles in all of the sites.

The polarizability associated with each mode of decay is readily calculated in the same manner as for the tetrahedral model. We summarize the

results below together with the relaxation times.

$$\left.\begin{aligned} \alpha_2&=\left(\frac{4g}{1+5g}\right)\left(\frac{\mu^2}{3\boldsymbol{k}T}\right), & \tau_2&=1/4k';\\ \alpha_3&=0, & \tau_3&=1/6k';\end{aligned}\right\} \tag{28}$$

$$\alpha_4=\frac{g(q+3-2g)[(2g-1+q)(2g+1)-2(g-1)]}{(1+5g)^2q}\left(\frac{\mu^2}{3\boldsymbol{k}T}\right),$$

$$\tau_4=1/(2k+3k'-Q);$$

$$\alpha_5=\frac{g(2g-3+q)[(2g-1-q)(2g+1)-2(g-1)]}{(1+5g)^2q}\left(\frac{\mu^2}{3\boldsymbol{k}T}\right),$$

$$\tau_5=1/(2k+3k'+Q).$$

The total polarizability is given by $[12g(1+2g)/(1+5g)^2](\mu^2/3\boldsymbol{k}T)$. Since the results are rather complicated, we resort to calculation of the polarizabilities and relaxation times numerically for various values of k/k'. The results are given in table 2.

It is convenient to discuss the results in terms of what happens as k/k' goes from zero to unity. It is seen in table 2 that the maximum separation of the relaxation times occurs when k/k' tends toward zero. We then have $\tau_4/\tau_5\simeq 6.85$. The two most important relaxation times, τ_2 and τ_4, tend to converge as k/k' increases, with the result that the corresponding dielectric loss maximum will at first be somewhat broader than a Debye type peak, but becomes more narrow as k/k' increases, and finally assumes the simple Debye form when $k=k'$. The total polarizability always increases with increasing k/k'.

As in the case of the tetrahedral model, the loss peaks will be noticeably asymmetrical for low values of k/k'. Owing to the fact that the longest relaxation time is associated with the largest polarizability when $k/k'<0.2$, the loss maximum will be steeper on the low frequency side in this region. At about $k/k'=0.2$ the peak will be slightly broadened but nearly symmetrical since the dominant polarizabilities are equal. A slight asymmetry again appears when k/k' exceeds ~ 0.2, but it will not be particularly noticeable owing to the closeness of the relaxation times. It should be observed that the slight asymmetry that appears in this region is such that the loss peaks will be steeper on the high frequency side. The asymmetry completely disappears when $k=k'$.

TABLE 2.—*Properties of the six-position model*

$g=k/k'$	Relaxation times (in units of $1/k'$)			Polarizabilities (in units of $\mu^2/3\boldsymbol{k}T$)			
	τ_2	τ_4	τ_5	α_2	α_4	α_5	α_{total}
0	0.25	1.31	0.191	0	0	0	0
1/100	.25	1.25	.191	.038	.069	.004	.111
1/10	.25	.88	.190	.267	.347	.026	.640
1/5	.25	.66	.189	.400	.404	.036	.840
1/2	.25	.39	.185	.571	.377	.031	.979
1	.25	.25	.167	.666	.333	0	1

The expression $k/k'=\exp(-V/\boldsymbol{k}T)$, where V is the energy difference between site 1 and each of the other sites, gives the dependence of k/k' on temperature. It follows that k/k' will increase with rising temperature, so the discussion given above in terms of growing values of k/k' also holds for the case of increasing temperature. The dielectric behavior of this model is qualitatively similar to that of the tetrahedral model. The total polarizability rises up to the temperature $T\simeq V/2.17\boldsymbol{k}$, but falls as the temperature is increased further.

4. Discussion

It is clear from the results cited above that an anisotropy in the crystalline field can lead to the existence of a set of discrete dielectric relaxation times for polar molecules that possess orientational sites arranged in three dimensions. The separation of the relaxation times is a maximum when the crystalline field is highly anisotropic. The relaxation times tend to merge as the temperature is increased.

The following experimental predictions hold for both models: (1) The regions of loss in the dielectric relaxation spectrum will become narrower with increasing temperature. (2) At low temperatures the dielectric loss peak will be steeper on the low frequency side. This asymmetry will decrease as the temperature is raised, and practically completely disappear somewhat before the loss peak assumes the simple Debye form. At high temperatures the Debye equations will be a good approximation. (3) The dielectric constant will be small when the temperature is low, and will increase as the temperature is raised; at temperatures above $T\sim V/2\boldsymbol{k}$, the dielectric constant will decrease with rising temperature. It should be noted that no real substance should be expected to show the entire range of behavior mentioned above since melting or transition phenomena may intervene.

It should be observed that the effect of a set of (discrete) active relaxation times on the shape of the loss regions is virtually indistinguishable from the effect of a suitably chosen continuous "distribution" of relaxation times. Also, it should be noted that the effects that have been predicted for the case of rising temperature with V constant will occur in a more marked way if V decreases with rising temperature, as is often assumed for the case of cooperative interaction.

The models treated here are obviously rather specialized, and do not necessarily correspond closely to any real crystal. For instance, one might expect the anisotropy of the crystalline field to be such that more than two transition probabilities are required to represent the system. More general models are being studied.

WASHINGTON, January 5, 1955.

INDEX TO VOLUME 54

January to June 1955—Research Papers 2559 to 2598

A

Page

Absorption of radiant energy by solid particles in suspension, RP2563 ... 41
Algorithm for solving the transportation problem, RP2583 ... 213
Alloy, nickel-copper, effect of temperature on tensile properties, RP2561 ... 21
Alloys, corrosion-resistant enthalpy and specific heat at high temperatures, RP2560 ... 15
Alloys, mixed carbide, X-ray study, RP2584 ... 217
An improved method of measuring efficiencies of ultra-high-frequency and microwave bolometer mounts, RP2594 ... 321
Appel, W. D., R. Schaffer, F. H. Forziati, Reactions at wet-dry interfaces on fibrous materials, RP2570 ... 103
Asphalt, fractionation into distinctive groups of components, RP2577 ... 163
Astigmatism of skew pencils in optical systems containing toric surfaces, RP2586 ... 251
Azrikrod, B. M., J. D. Hoffman, Dielectric relaxation for spherical molecules in a crystalline field: Theory for two simple models, RP2598 ... 357

B

Beatty, R. W., F. Reggia, An improved method of measuring efficiencies of ultra-high-frequency and microwave bolometer mounts, RP2594 ... 321
Beryllium carbide, X-ray study of, RP2584 ... 217
Block designs, partially balanced incomplete, RP2579 ... 177
Bolometer mounts, ultra-high-frequency and microwave, efficiencies of, RP2594 ... 321
Branching ratio in the decay of polonium-210, RP2564 ... 47
Bremsstrahlung, low-energy, scintillation spectrometry of, RP2571 ... 103
Bromophthalein magenta E, as indicator in nonaqueous acid-base titrations, RP2593 ... 309
Burdick, M. D., H. S. Parker, R. S. Roth, E. L. McGandy, An X-ray study of the system uranium monocarbide-uranium dicarbide-beryllium carbide, RP2584 ... 217

C

Calcium-strontium aluminate and strontium aluminate solid solutions, study of some, RP2595 ... 329
Carbides, uranium and beryllium, X-ray study of, RP2584 ... 217
Carlson, E. T., A study of some strontium aluminates and calcium-strontium aluminate solid solutions, RP2595 ... 329
Carwile, N. L., G. W. Geil, Effect of low temperatures on the mechanical properties of a commercially pure titanium, RP2569 ... 91
Chromatographic method for the fractionation of asphalt into distinctive groups of components, RP2577 ... 163
Clatworthy, W. H., Partially balanced incomplete block designs with two associate classes and two treatments per block, RP2579 ... 177
Collagen and leather, pore-size distribution in, RP2567 ... 73
Collagen pores determined by electron microscopy, RP2568 ... 83
Computers, automatic, a numerical method of integration for, RP2572 ... 119
Copper-nickel alloys, effect of temperatures on tensile properties, RP2561 ... 21
Corrosion and its prevention, geometric factors in electrical measurements relating to, RP2566 ... 61
Corrosion resistant alloys, enthalpy and specific heat at high temperatures, RP2560 ... 15
Coughanour, L. W., R. S. Roth, S. Marzullo, F. E. Sennett Solid-state reactions and dielectric properties in the system magnesia-lime-tin oxide-titania, RP2576 ... 149
—, —, —, —, Solid-state reactions and dielectric properties in the systems magnesia-zirconia-titania and lime-zirconia-titania, RP2580 ... 191
Crystalline field, dielectric relaxation for spherical molecules in; theory of two simple models, RP2598 ... 357
Cyanohydrin synthesis of 2-C^{14}-labeled sugars, RP2581 ... 201

D

Darling-Dennison and Fermi resonance, effect of, on thermodynamic functions, RP2592 ... 299
Davis, M. M., H. B. Hetzer, Titrations of bases with diphenyl phosphate in some aqueous and nonaqueous solvents, RP2593 ... 309
Denison, I. A., W. H. Schwerdtfeger, Geometric factors in electrical measurements relating to corrosion and its prevention, RP2566 ... 61
Dever, J. L., T. B. Douglas, Enthalpy and specific heat of four corrosion-resistant alloys at high temperatures, RP2560 ... 15
de Vogelaere, R., A method for the numerical integration of differential equations of second order without explicit first derivatives, RP2572 ... 119
Dibeler, V. H., R. M. Reese, Selected positive and negative ions in the mass spectra of the monohalomethanes, RP2573 ... 127
Dielectric properties in the system magnesia-lime-tin oxide-titania, RP 2576 ... 149
Dielectric properties in the systems magnesia-zirconia-titania and lime-zirconia-titania, RP2580 ... 191
Dielectric relaxation for spherical molecules in a crystalline field: Theory for two simple models, RP2598 ... 357
Differential equations of second order without explicit first derivatives, numerical integration of, RP2572 ... 119
Digges, T. G., W. D. Jenkins, C. R. Johnson, Effect of temperature on the tensile properties of a commercial and a high-purity 70-percent nickel-30-percent copper alloy, RP2561 ... 21
Diphenyl phosphate as a titrant for bases in aqueous and nonaqueous solutions, RP2593 ... 309
Diphenyl phosphate, purification and properties, RP2593 ... 309
Distortion, variation in, with magnification, RP2574 ... 135
Douglas, T. B., J. L. Dever, Enthalpy and specific heat of four corrosion-resistant alloys at high temperatures, RP2560 ... 15

E

Effect of low temperatures on the mechanical properties of a commercially pure titanium, RP2569 ... 91
Ehrlich, M., Scintillation spectrometry of low-energy bremsstrahlung, RP2571 ... 103
Electrical measurements relating to corrosion and its prevention, geometric factors in, RP2566 ... 61
Electron microscopy, collagen pores determined by, RP2568 ... 83
Engel, O. G., Mechanism of high-speed-waterdrop erosion of methyl methacrylate plastic, RP2565 ... 51
—, Waterdrop collisions with solid surfaces, RP2591 ... 281
Enthalpy and specific heat of four corrosion-resistant alloys at high temperatures, RP2560 ... 15
Erosion of methyl methacrylate plastic by high-speed waterdrop:
RP2565 ... 51
RP2591 ... 281

F

Fading range in radio transmission, analysis of, RP2585 ... 231
Fermi and Darling-Dennison resonance, effect of, on thermodynamic functions, RP2592 ... 299
Fibers, properties and behavior of, when impacted at high velocities:
RP2589 ... 269
RP2590 ... 277
Fibrous materials, reactions at wet-dry interfaces, RP2570 ... 103
Florman, E. F., A measurement of the velocity of propagation of VHF radio waves at the surface of the earth, RP2596 ... 335
Forziati, F. H., W. D. Appel, R. Schaffer, Reactions at wet-dry interfaces on fibrous materials, RP2570 ... 103
Fox, G., W. K. Stone, H. F. Schiefer, Stress-strain relationships in yarns subjected to rapid impact loading: 1. Equipment, testing procedure, and typical results, RP2589 ... 269
Fractionation of asphalt into distinctive groups of components, chromatographic method for, RP2577 ... 163
Fraser, F. M., E. J. Prosen, Heats of combustion and isomerization of six pentadienes and spiropentane, RP2575 ... 143
Frush, H. L., H. S. Isbell, Macromethods for reducing aldonic lactones to sugars; the preparation of L-glucose, RP2588 ... 267
—, *R. Schaffer, H. S. Isbell,* The synthesis of α-D-glucose-2-C^{14}, α-D-mannose-2-C^{14}, and α-D-galactose-2-C^{14}, RP2581 ... 201

G

D-Galactose-2-C^{14}, synthesis of, RP2581 ... 201
Geil, G. W., N. L. Carwile, Effect of low temperatures on the mechanical properties of a commercially pure titanium, RP2569 ... 91
Geometric factors in electrical measurements relating to corrosion and its prevention, RP2566 ... 61
Gleyzal, A., An algorithm for solving the transportation problem, RP2583 ... 213
D-Glucose-2-C^{14}, synthesis of, RP2581 ... 201

H

Hayward, R. W., D. D. Hoppes, W. B. Mann, Branching ratio in the decay of polonium-210, RP2564 ... 47
Heat of formation of magnesium oxychloride, RP2597 ... 347
Heats of combustion and isomerization of six pentadienes and spiropentane, RP2575 ... 143
Hetzer, H. B., M. M. Davis, Titrations of bases with diphenyl phosphate in some aqueous and nonaqueous solvents, RP2593 ... 309
High-speed-waterdrop erosion of methyl methacrylate plastic, mechanism of:
RP2565 ... 51
RP2591 ... 281
Hoffman, J. D., B. M. Azrikrod, Dielectric relaxation for spherical molecules in a crystalline field: Theory for two simple models, RP2598 ... 357
Hoppes, D. D., R. W. Hayward, W. B. Mann, Branching ratio in the decay of polonium 210, RP2564 ... 47

I

Page

Indicators, acid-base, for titrations with diphenyl phosphate in nonaqueous solutions, RP2593 309
Infrared spectra absorption by solid particles in suspension, RP2563 41
Interfaces on fibrous materials, reactions at wet-dry, RP2570 103
Interpolation, osculatory, in the complex plane, RP2587 263
Ions, positive and negative, in mass spectra of the monohalomethanes, RP2573 127
Isbell, H. S., H. L. Frush, Marcomethods for reducing aldonic lactones to sugars; the preparation of L-glucose, RP2588 267
—, —, *R. Schaffer*, The synthesis of α-D-glucose-2-C^{14}, α-D-mannose-2-C^{14}, and α-D-galactose-2-C^{14}, RP2581 201
Isomerization and heats of combustion of six pentadienes and spiropentane, RP2575 143
Isoprene, heats of combustion and isomerization, RP2575 143

J

Janes, H. B., An analysis of within-the-hour fading in 100- to 1,000-Mc transmissions, RP2585 231
Jenkins, W. D., T. G. Digges, C. R. Johnson, Effect of temperature on the tensile properties of a commercial and a high-purity 70-percent nickel-30-percent copper alloy, RP2561 21
Johnson, C. R., W. D. Jenkins, T. G. Digges, Effect of temperature on the tensile properties of a commercial and a high-purity 70-percent-nickel-30-percent copper alloy, RP2561 21

K

Kleinschmidt, L. R., Chromatographic method for the fractionation of asphalt into distinctive groups of components, RP2577 163

L

Lactones, reduction of, RP2588 267
Leather and collagen, pore-size distribution in, RP2567 73
Length standards, calibration of NBS, RP2559 1
Lenses, variation in, distortion in image introduced by, RP2574 135
Lime, silica, water, the system, RP2582 205
Lime-water system at 21° C and high pressures, RP2562 37
Lime-zirconia-titania system, solid-state reactions and dielectric properties in, RP2580 191
Line standards of length, calibration of National Bureau of Standards, RP2559 1

M

Macromethods for reducing aldonic lactones to sugars; the preparation of L-glucose, RP2588 267
Magill, A. A., Variation in distortion with magnification, RP2574 135
Magnesia-lime-tin oxide-titania system, solid-state reactions and dielectric properties in, RP2576 149
Magnesia-zirconia-titania system, solid-state reactions and dielectric properties in, RP2580 191
Magnesium oxychloride, heat of formation, RP2597 347
Magnification, variation in distortion with, RP2574 135
Mandelkern, L., D. E. Roberts, Nature of stark rubber, RP2578 167
Mann, W. B., R. W. Hayward, D. D. Hoppes, Branching ratio in the decay of polonium-210, RP2564 47
D-Mannose-2-C^{14}, synthesis of, RP2581 201
Marzullo, S., L. W. Coughanour, R. S. Roth, F. E. Sennett, Solid-state reactions and dielectric properties in the system magnesia-lime-tin oxide-titania, RP2576 149
—, —, —, —, Solid-state reactions and dielectric properties in the systems magnesia-zirconia-titania and lime-zirconia-titania, RP2580 191
Mass spectra of the monohalomethanes, selected positive and negative ions in, RP2573 127
McCrackin, F. L., H. F. Schiefer, J. C. Smith, W. K. Stone, Stress-strain relationships in yarns subjected to rapid impact loading: 2. Breaking velocities, strain energies, and theory neglecting wave propagation, RP2590 277
McGandy, E. L., M. D. Burdick, H. S. Parker, R. S. Roth, An X-ray study of the system uranium monocarbide-uranium dicarbide-beryllium carbide, RP2584 217
Mechanical properties of a commercially pure titanium, effect of low temperatures on, RP2569 91
Mechanism of high-speed-waterdrop erosion of methyl methacrylate plastic: RP2565 51
RP2591 281
Meter bars, calibration of NBS standard, RP2559 1
Methyl methacrylate plastic, mechanism of high-speed-waterdrop erosion of: RP2565 51
RP2591 281
Microscopy, electron, collagen pores determined by, RP2568 83
Molecules, spherical, in a crystalline field, dielectric relaxation for; theory of two simple models, RP2598 357
Monohalomethanes, selected positive and negative ions in the mass spectra of, RP2573 127

N

NBS line standards of length, calibration, RP2559 1
Newman, E. S., A study of the system magnesium oxide-magnesium chloride-water and the heat formation of magnesium oxychloride, RP2597 347
Nickel-copper alloy, effect of temperature on tensile properties, RP2561 21
Numerical analysis:
Numerical integration of differential equations of second order without explicit first derivatives, RP2572 119

O

Page

Optical systems containing toric surfaces, astigmatism of skew pencils in, RP2586 251
Osculatory interpolation in the complex plane, RP2587 263

P

Page, R. L., Calibration of meter line standards of length at the National Bureau of Standards, RP2559 1
Parker, H. S., M. D. Burdick, R. S. Roth, E. L. McGandy, An X-ray study of the system uranium monocarbide-uranium dicarbide-beryllium carbide, RP2584 217
Pentadienes and spiropentane, heats of combustion and isomerization, RP2575 143
Peppler, R. B., The system of lime, silica, and water at 180° C, RP2582 205
Plastic, methyl methacrylate, high-speed waterdrop erosion: RP2565 51
RP2591 281
Polonium-210, branching ratio in the decay of, RP2564 47
Pore-size distribution in collagen and leather by the porosimeter method, RP2567 73
Pores, collagen, determination by electron microscopy, RP2568 83
Porosimeter method for measuring pore-size distribution in leather and collagen, RP2567 73
Power measurements, ultra-high-frequency and microwave, method for determining efficiency of bolometer mounts use for, RP2594 321
Propagation of radio waves, velocity of, RP2596 335
Prosen, E. J., F. M. Fraser, Heats of combustion and isomerization of six pentadienes and spiropentane, RP2575 143

R

Radiant energy, absorption of, by solid particles in suspension, RP2563 41
Radio propagation measurements, analysis of fading range, RP2585 231
Radio transmission, analysis of fading range, RP2585 231
Radio waves, velocity of propagation, RP2596 335
Reactions at wet-dry interfaces on fibrous materials, RP2570 103
Reese, F. M., V. H. Dibeler, Selected positive and negative ions in the mass spectra of the monohalomethanes, RP2573 127
Reggia, F., R. W. Featly, An improved method of measuring efficiencies of ultra-high-frequency and microwave bolometer mounts, RP2594 321
Roberts, D. E., L. Mandelkern, Nature of stark rubber, RP2578 167
Roth, R. S., M. D. Burdick, H. S. Parker, E. L. McGandy, An X-ray study of the system uranium monocarbide-uranium dicarbide-beryllium carbide, RP2584 217
—, *L. W. Coughanour, S. Marzullo, F. E. Sennett*, Solid-state reactions and dielectric properties in the system magnesia-lime-tin oxide-titania, RP2578 149
—, —, —, —, Solid-state reactions and dielectric properties in the systems magnesia-zirconia-titania and lime-zirconia-titania, RP2580 191
Rubber, stark, nature of, RP2578 167

S

Salzer, H. E., Osculatory interpolation in the complex plane, RP2587 263
Schaffer, R., W. D. Appel, F. H. Forziati, Reactions at wet-dry interfaces on fibrous materials, RP2570 103
—, *H. S. Isbell, H. L. Frush*, The synthesis of α-D-glucose-2-C^{14}, α-D-mannose-2-C^{14}, and α-D-glactose-2-C^{14}, RP2581 201
Schiefer, H. F., F. L. McCrackin, J. C. Smith, W. K. Stone, Stress-strain relationships in yarns subjected to rapid impact loading: 2. Breaking velocities, strain energies, and theory neglecting wave propagation, RP2590 277
—, *W. K. Stone, G. Fox*, Stress-strain relationships in yarns subjected to rapid impact loading: 1. Equipment, testing procedure, and typical results, RP2589 269
Schwerdtfeger, W. J., I. A. Denison, Geometric factors in electrical measurements relating to corrosion and its prevention, RP2566 61
Scintillation spectrometry of low-energy bremsstrahlung, RP2571 103
Selected positive and negative ions in the mass spectra of the monohalomethanes, RP2573 127
Sennett, F. E., L. W. Coughanour, R. S. Roth, S. Marzullo, Solid-state reactions and dielectric properties in the system magnesia-lime-tin oxide-titania, RP2576 149
—, —, —, —, Solid-state reactions and dielectric properties in the systems magnesia-zirconia-titania and lime-zirconia-titania, RP2580 191
Silica, lime, water, the system, RP2582 205
Skew pencils, astigmatism of, in optical systems containing toric surfaces, RP2586 251
Smith, J. C., F. L. McCrackin, H. F. Schiefer, W. K. Stone, Stress-strain relationships in yarns subjected to rapid impact loading: 2. Breaking velocities, strain energies, and theory neglecting wave propagation, RP2590 277
Sodium amalgam reduction of lactones to sugars, RP2588 267
Sodium acid oxalate, use as buffer in sodium amalgam reductions, RP2588 267
Solid-state reactions and dielectric properties in the system magnesia-lime-tin oxide-titania, RP2576 149
Solid-state reactions and dielectric properties in the systems magnesia-zirconia-titania and lime-zirconia-titania, RP2580 191
Specific heat and enthalpy of four corrosion-resistant alloys at high temperatures, RP2560 15
Spectra, mass, of the monohalomethanes, selected positive and negative ions in, RP2573 127
Spectrometry, scintillation, of low-energy bremsstrahalung, RP2571 103
Spiropentane and pentadienes, heats of combustion and isomerization, RP2575 143
Standards of length, calibration of NBS, RP2559 1
Stark rubber, nature of, RP2578 167
Statistics, partially balanced incomplete block design, RP2579 177
Stewart, J. E., Absorption of radiant energy by solid particles in suspension, RP2563 41

Page

Stone, W. K., F. L. McCrackin, H. F. Schiefer, J. C. Smith, Stress-strain relationships in yarns subjected to rapid impact loading: 2. Breaking velocities, strain energies, and theory neglecting wave propagation, RP2590 ... 277
—, H. F. Schiefer, G. Fox, Stress-strain relationships in yarns subjected to rapid impact loading: 1. Equipment, testing procedure, and typical results, RP2589 ... 269
Strength of yarns when impacted at high velocities:
RP2589 ... 269
RP2590 ... 277
Stress-strain relationships in yarns subjected to rapid impact loading: 1. Equipment, testing procedure, and typical results, RP2589 ... 269
Stress-strain relationships in yarns subjected to rapid impact loading: 2. Breaking velocities, strain energies, and theory neglecting wave propagation RP2590 ... 277
Stromberg, P. R., M. Swerdlow, Collagen pores determined by electron microscopy, RP2568 ... 83
—, Pore-size distribution in collagen and leather by the porosimeter method, RP2567 ... 73
Strontium aluminates and calcium-strontium aluminate solid solutions, a study of, RP2595 ... 329
Sugars, preparation of, by sodium amalgam reduction, RP2588 ... 267
Swerdlow, M., P. R. Stromberg, Collagen pores determined by electron microscopy, RP2568 ... 83
Synthesis of α-D-glucose-2-C^{14}, α-D-mannose-2-C^{14}, and α-D-galactose-2-C^{14}, RP2581 ... 201
System of lime, silica, and water at 180° C, RP2582 ... 205
System lime-water at 21° C and high pressures, RP2562 ... 37
System magnesium oxide-magnesium chloride-water and heat of formation of magnesium oxychloride, study of, RP2597 ... 347
System magnesia-zirconia-titania and lime-zirconia-titania, solid-state reactions and dielectric properties in, RP2580 ... 191

T

Temperature, low, effect on mechanical properties of titanium, RP2569 ... 91
Tensile properties of a commercial and a high-purity 70-percent-nickel-30-percent-copper alloy, effect of temperature on, RP 2561 ... 21
Textile yarns, rapid impact testing of:
RP2589 ... 269
RP2590 ... 277
Thermodynamic functions, effect of Darling-Dennison and Fermi-resonance on, RP2592 ... 299
Titanium, commercially pure, effect of low temperatures on the mechanical properties of, RP2569 ... 91
Titrations, acid-base, aqueous and nonaqueous, RP2593 ... 309
Transportation problem, an algorithm for solving the, RP2583 ... 213

U

Ultra-high frequency and microwave bolometer mounts, an improved method of measuring efficiencies, RP2594 ... 321
Uranium carbides, X-ray study of, RP2584 ... 217

V

Variation in distortion with magnification, RP2574 ... 135
Velocity of propagation of VHF radio waves at the surface of the earth, a measurement of, RP2596 ... 335

W

Water, lime, silica, the system, RP2582 ... 205
Waterdrop collisions with solid surfaces:
RP2565 ... 51
RP2591 ... 281
Waterdrop erosion of methyl methacrylate plastic:
RP2565 ... 51
RP2591 ... 281
Weinstein, W., Astigmatism of skew pencils in optical systems containing toric surfaces, RP2586 ... 251
Weir, C. E., The system lime-water at 21° C and high pressures, RP2562 ... 37
Wooltey, H. W., Effect of Darling-Dennison and Fermi resonance on the thermodynamic functions, RP2592 ... 299

X

X-ray study of mixed carbide alloys, RP2584 ... 217

Y

Yarns, stress-strain relationships in:
RP2589 ... 269
RP2590 ... 277